SURFACE FLUXES OVER NATURAL LANDSCAPES USING SCINTILLOMETRY

W.M.L. MEIJNINGER

Surface fluxes over natural landscapes

using scintillometry

Promotor:

> Prof. dr. A.A.M. Holtslag
>
> Hoogleraar in de meteorologie en luchtkwaliteit

Co-promotor:

> dr. H.A.R. de Bruin
>
> Universitair hoofddocent bij de leerstoelgroep meteorologie en luchtkwaliteit, Wageningen Universiteit

Samenstelling promotiecommissie:

> dr. F. Beyrich – German Weather Service (DWD), Lindenberg, Germany
>
> dr. W. Kohsiek – Koninklijk Meteorologisch Nederlands Instituut (KNMI), De Bilt
>
> Prof. dr. P.A.A. Troch – Wageningen Universiteit
>
> Prof. dr. W.G.M. Bastiaanssen – WaterWatch, Wageningen

Surface fluxes over natural landscapes

using scintillometry

W.M.L. Meijninger

PROEFSCHRIFT

ter verkrijging van de graad van doctor
op gezag van de rector magnificus
van Wageningen Universiteit
prof. dr. ir. L. Speelman,
in het openbaar te verdedigen
op woensdag 1 oktober 2003
des namiddags te vier uur in de aula

Voorwoord

Eindelijk kan ik nu ook zeggen, "het is gelukt". Na veel avonden en weekenden zwoegen is eindelijk dit boekje af. Al ben ik zeer benieuwd naar het leven na de promotie, de afgelopen 6 jaar zijn voor mij onvergetelijk. Het schrijven van het voorwoord is dan ook een mooi moment om eens terug te kijken en te denken aan diegenen die hebben bijgedragen aan de totstandkoming van dit boekje.

Allereerst wil ik mijn co-promotor Henk de Bruin bedanken. Al tijdens mijn studie tijd heb je me enthousiast gemaakt voor de experimentele kant van de meteorologie. Jij was het die begin 1997 vroeg of ik interesse had in een promotie baan. Nog voordat ik goed en wel aan mijn OIO baan begon werd me duidelijk dat jij in je drukke en af en toe hectische werk vrij to-the-point bent: binnen 10 minuten was mijn baan geregeld. Niet alleen je enthousiasme voor het vak maar ook je inventiviteit in het schrijven van onderzoeksvoorstellen en het regelen van tijdelijke aanstellingen op nog aanwezige geldpotjes heeft een grote indruk op mij gemaakt. Ik moet echter wel bekennen dat ik al vrij snel het overzicht kwijtraakte op welke project of potje ik nu tijdelijk weer was aangesteld. Henk bedankt voor alles!

Halverwege mijn promotie kwam mijn promotor Bert Holtslag ten tonele. Je interesse en frisse kijk op mijn onderzoek waardeer ik enorm. Nog voordat ik een concept van mijn artikel op je bureau had neergelegd was de titel al grondig aangepast. Tot slot kan ik zeggen dat de jazz muziek, regelmatig te horen in de hal, zeker heeft bijgedragen aan dit boekje. Bert bedankt!

Er is nog iemand die enorm heeft geholpen aan dit boekje, die ik daarvoor speciaal wil bedanken: Wim Kohsiek. Van het begin af aan was je 1 dag per week op de vakgroep aanwezig. Ik ben ontzettend blij dat ik jou ook als extra 'leermeester' had. Op al mijn vragen, al dan niet over scintillometers, had je wel een duidelijk antwoord klaar en tijdens de vele veldexperimenten was je altijd van de partij. Ik hoop dat we in de toekomst nog vaak samen kunnen werken.

Al vrij kort na mijn aanstelling in 1997 verschenen de hydrologen Bas en Reinder op de vakgroep. Ik moet zeggen dat het toch wel geruststellend was om niet meer het enige 'groentje' te zijn tussen de ervaren OIO's Job, Berenice, Bert (Heusinkveld), Joost (Nieveen) en Rushdi. Job, jouw korte beschrijving van de levensloop van een gemiddeld OIO kwam aardig overeen met die van mij. Misschien kan je onze weddenschap ook nog wel herinneren. Gaandeweg in 1998 kreeg ik er meer collega's bij, Oscar, Arnold en Arjan en de mensen van de voormalige luchtkwaliteitgroep. Om iedereen te kunnen huisvesten werd de vakgroep opnieuw ingedeeld. Er werd besloten dat de 'experimentele' groep beneden ging zitten. Zo zie je maar weer, experimenteel werk is de basis van alle wetenschappelijk onderzoek. Jongens, allemaal bedankt voor de gezellige sfeer!

Het jaar 1998 was voor mij het jaar van de veldexperimenten. Na enkele 'sightseeing' trips met Wim en Henk werd besloten om in Flevoland het belangrijkste meetexperiment van mijn promotieonderzoek uit te voeren. Voor het uitvoeren van de meetexperimenten was de technische ondersteuning van Willy, Teun en Frits onmisbaar. Dankjewel! Tot deze groep behoren ook Bert (Heusinkveld) en Oscar. Bert, ik heb je geduld menigmaal op de proef gesteld met al mijn vragen over de LAS en eddy correlatie systemen. Ook je klim- en

klauterinspanningen in de windturbines waren onmisbaar. Oscar, ik ben blij dat jij er tijdens Flevoland bij was (weer een idee van Henk). We vormden samen een uitstekend team. Maar ook daarna konden we goed met elkaar samenwerken. Bedankt voor alles.

Tijdens het Flevoland experiment mochten we meetmasten opzetten in een aantal veldjes en scintillometers plaatsen in 2 windturbines. Ik ben dhr. Pollemans, dhr. Meijnders, dhr Haverman en dhr. Maarsingh zeer dankbaar voor hun medewerking en vertrouwen in een toen nog langharig en ongeschoren figuur. Samen met Oscar, Bas en de studenten Roos Zuurbier en Joost Hoedjes was het Flevoland tijdperk onvergetelijk. Uiteindelijk heeft jullie enthousiasme en inzet gedurende 8 weken bivakkeren op een camping wel wat opgeleverd, 2 artikelen en een foto van ons tentenkamp in de RCN campinggids. During the Flevoland experiment I had the opportunity to borrow a radio wave scintillometer from Alan Green (Horticultural Research Institute, New Zealand). Alan, thanks for your corporation and the long email discussions together with Wim about the derivation of the structure parameters.

In het jaar 1998 ging ik ook nog naar Turkije en Duitsland, waar we deelnamen aan andere veldexperimenten. Hoe dit mogelijk is? Eigenlijk heel eenvoudig. Gewoon een kwestie van een beetje plannen maar bovenal de medewerking van Peter Droogers (IWMI), Kees van den Dries, Frank Beyrich (DWD) en de studenten Francine Engelsman en Hans Schipper. Met name Kees ben ik veel dank verschuldigd. Zowel voor de gezellige en leuke sfeer tijdens de Italië en Duitsland meetcampagnes, maar ook op de vakgroep. Altijd en op ieder moment van de dag was je beschikbaar voor een praatje of schoot je meteen te hulp bij allerlei al dan niet computer gerelateerde problemen.

Na de vele meetcampagnes begon dan uiteindelijk de data-analyse. En dan is het goed dat collega's met een frisse blik de nodige suggesties en commentaar (en foutenbalkjes) aanleveren. Arnold en Arjan mijn dank daarvoor! Daarnaast, geloof het of niet, hebben jullie indirect ervoor gezorgd dat dit boekje redelijk op tijd af is.

De afgelopen jaren heb ik met veel plezier gewerkt op de vakgroep meteorologie. Naast de al eerder genoemde personen was het met Anne-Wim, Adrie, Allessandro, Dirk, Floris, Jeff, Jordi, Jon, Leo, Mara, Miau, Michaël, Peter en Sjaak en de mensen van de Alterra groep Bart, Cor, Eddy, Herbert, Jan, Ronald, Celso en Helma een gezellige boel. Een persoon heb ik nog niet genoemd. Gerrie, jou wil ik speciaal bedanken. Jouw hulp, variërend van het regelen van reisverzekeringen tot aan GSM abonnementen, is onmisbaar geweest. Ik heb grote waardering voor je werk en de manier waarop jij je staande weet te houden in dit 'mannen' bolwerk. De vakgroep is bij jou in goede handen. Dankjewel voor je hulp.

In de laatste fase van mijn promotie heb ik mij op een geheel nieuw onderwerp gestort: remote sensing. Daarbij was de steun van de experts Wim Bastiaanssen (voor het beschikbaar stellen van SEBAL) en Ambro Gieske onmisbaar. Mede dankzij hen heb ik samen met student Remco van de Beek SEBAL aardig onder de knie gekregen. Ambro, ik ben je heel dankbaar voor het processen van de vele Turkije beelden. Ik hoop dat we in de toekomst weer kunnen samenwerken.

Uiteindelijk hebben de mensen van de promotiecommissie, Prof. dr. Peter Troch, Prof. dr. Wim Bastiaanssen, Dr. Wim Kohsiek en Dr. Frank Beyrich, dit boekje bekeken en beoordeeld. Ik wil jullie daarvoor hartelijk danken.

Sinds enige tijd werk ik parttime bij het bedrijf Kipp & Zonen in Delft. Ik kan wel zeggen dat dit STW promotieonderzoek op 2 manieren is geslaagd. Ten eerste door dit boekje en ten tweede door de commercialisering van de LAS door Kipp & Zonen.

Dan resten mij nog mijn (schoon)familie en mijn vele vrienden. Ik wil jullie allemaal bedanken voor jullie interesse in mijn werk en de steeds terugkerende vragen "Hoe gaat ie?" en "Ben je al bijna klaar?". Speciaal wil ik Henk & Jannie, Jan-Evert & Stasha en de kids en Judith & Frank bedanken. Maar bovenal pa en ma, volgens mij kan ik wel zeggen dat jullie wijze woorden ('hard werken en studeren') en vertrouwen in mij maar ook in zus Astrid (dierenarts) en broer Bart (AIO) hun vruchten hebben afgeworpen. En niet te vergeten jullie steun, liefde en geduld, ….. heel veel geduld. Dat geldt tevens voor jullie, Astrid, Bart en Kees. De filmavondjes in Wageningen en schuurfeesten waren af en toe een goede afleiding. En Bart, ik weet zeker dat het jou ook zal lukken. Als je nog wijze raad nodig hebt, dan hoor ik het wel. Kees, jouw enthousiasme voor het motorrijden heeft er voor gezorgd dat ik nu ook een nieuwe hobby erbij heb, en deze staat hoog op het 'na-de-promotie-doe-lijstje'.

Tenslotte kom ik bij jou Jantien. Naast jouw steun en liefde heb jij mij laten zien dat er ook nog andere leuke dingen (.nl) zijn in het leven dan alleen promoveren. Skaten heb ik al aardig onder de knie, maar salsa zal vrees ik nog een probleem worden.

Dan wil ik nog maar 1 ding zeggen, zoals mijn oma altijd zei: "houd de zonzijde!"

Contents

Chapter 1

General introduction

1.1 Background

In the lowest part of the atmospheric boundary layer (ABL) known as the surface layer (SL), interaction between the atmosphere and the earth's surface takes place in the form of turbulent exchange of energy and mass. The surface-atmosphere exchange can be described as follows (see e.g. Stull, 1988)

$$R_n = H + L_v E + G_s .$$
<div align="right">(1.1)</div>

In the surface energy balance equation R_n represents the amount of energy (or net radiation) available for various different land surface processes. One of these processes is the warming of the air by the underlying surface, known as the sensible heat flux density H (or shortly sensible heat flux). Part of the net radiation will be used to evaporate water present at the surface and is symbolised by $L_v E$, the water vapour flux or latent heat flux density (shortly latent heat flux, or evaporation). Another portion of R_n is transferred into the soil defined by the soil heat flux density G_s. In most cases advection and heat storage within the vegetation layer are thought to be small and therefore ignored in the surface energy balance equation. The evaporative term shows the linkage of the energy balance to the hydrological water balance. Both atmospheric and surface properties (such as surface type and status) determine the size of each flux: in dry areas H and G_s consume most of the available energy, while in wet areas $L_v E$ is dominant. It is well known now that the atmosphere-surface interactions, which take place at various scales, play an important role in atmospheric processes such as the growth of the ABL, terrestrial and atmospheric moisture content, cloud formation, and consequently precipitation patterns. But also in other scientific fields such as agriculture, bioclimatology and hydrology these interactions are of importance.

A large part of our knowledge of these processes in the ABL is based on observations conducted at the surface and also higher in the atmosphere. Early studies were mainly focussed on ideal (uniform and flat) surfaces, because in such conditions the surface forcings are easiest to understand (see e.g. Businger et al., 1971). Nowadays, science is able to model the atmospheric processes over homogenous area using deduced semi-empirical relations based on similarity theories. Traditional measurement techniques are based also on these semi-empirical relations and therefore restricted to homogeneous areas. Moreover, the physical design of these instruments (i.e. point instruments) limits their application to homogeneous areas.

Nowadays, our interest is focussed more on determining surface fluxes associated with natural landscapes. When we look outside (Figure 1.1) we can see why, the natural landscape is far from homogeneous. Both photos show that the natural landscape consists of many different elements, such as forests, lakes, agricultural fields, villages etc. The various surface elements differ in surface characteristics (e.g. moisture content, vegetation, etc) and all of them affect the atmosphere in a different way. In order to determine representative surface fluxes over natural landscapes the fluxes of the individual elements need to be spatially aggregated (see e.g. Mahrt et al., 2001).

Figure 1.1: Typical examples of natural landscapes (left: the Lindenberg area (Germany); right: the Flevoland polder (The Netherlands)).

As such there is more effort on developing new (ground-based) measurement techniques that are able to provide reliable area-averaged fluxes over natural areas (and thus heterogeneous) ranging between field to catchment scale or even continental scale. These techniques are important for the future development of new surface parameterisation schemes designed for

2

heterogeneous areas (see e.g. Beljaars and Holtslag, 1991). Furthermore, many validation studies (e.g. of meteorological and hydrological models and remote sensing techniques, etc) require large-scale observations because most of these models and satellite imagers have a grid box size or a pixel resolution, respectively, of several kilometres (Carlson et al., 1995). Examples of recent projects are LITFASS-1998 (Lindenberg Inhomogeneous Terrain − Fluxes between Atmosphere and Surface: a long-term Study; see e.g. Müller et al., 1995; Beyrich et al., 2002b) and EVA_GRIPS-2003 (Regional EVAporation at Grid/Pixel Scale over heterogeneous land surfaces; http://w3.gkss.de/KSH/EVA_GRIPS). These projects have been initiated to measure and parameterise surface fluxes over heterogeneous areas at a grid box scale (~ 10 km). In the next Sections some measurement techniques that can provide area-averaged fluxes will be discussed and one in particular.

1.2 Current measurement techniques

In this Section some measurement techniques will be discussed briefly that can provide area-averaged surface fluxes. These methods range from ground based (in-situ) sensors mounted on towers to space-born satellite remote sensing techniques. Some of their advantages and disadvantages will be discussed showing the relevance of further exploration to new methods and techniques. An overview of the methods is given in Table 1.1.

a. Network of tower flux measurements

One way to obtain area-averaged surface fluxes is to construct them from a number of locally measured fluxes (i.e. point observations, or in-situ), such as the eddy covariance method (EC method) (Mahrt, 1998; Mahrt et al., 2001). The EC method measures the turbulent fluxes directly and is regarded as the best method available at this moment. Nowadays, a variety of robust and reliable instruments are available for continuous measurements of the three wind components and scalars (e.g. temperature, water vapour and carbon dioxide). Nevertheless, one must recognize its errors and restrictions. Due to the physical limitations of the sensor size and response, set-up and data analysis techniques, which can result in flux loss, a number of corrections must be applied in order to reduce the systematic underestimation of the turbulent fluxes (van Dijk, 2001; Finnigan et al., 2003). Usually an averaging period of 30-

minutes is taken to increase the sample size of the large eddies. Although this reduces the random flux error additional non-stationary (and heterogeneity) events can occur, caused by the diurnal trend, meso-scale motions and the passage of clouds (Mahrt, 1998). Also the field of view (or source area) of tower-based measurements is relatively small, which questions the representativeness of the measurements, even over homogeneous areas (Horst and Weil, 1992; 1994). When constructing area-averaged fluxes from a significant number of point measurements, there is always the problem that data is missing or unreliable during certain periods from at least one point (Mahrt, 1998). Furthermore, surface fluxes of heterogeneous landscapes are usually not a simple mean value of the fluxes from each of all land cover types, due to the non-linear turbulent response of the atmospheric flow to step changes in land cover.

b. Turbulent aircraft measurements

Today, small-specialised airplanes and helicopters equipped with modern and fast response sensors (EC instruments) have increased the capabilities and greatly reduced the costs of airborne flux measurements. In this way it is possible to perform reliable measurements in remote areas, where ground based measurements are difficult to conduct. Furthermore, airborne measurements provide information on the spatial variability of the land surface (Mahrt, 1998). The derivation of fluxes is however complicated since the separation of time and spatial dependencies requires special attention. In order to obtain reliable turbulent statistics, the flight path has to be repeated several times. Problem is that the meteorological conditions can change during the period it takes to perform a flight program. Furthermore, it is advised to fly as low as possible and as often as possible the same flight track when comparing airborne based fluxes to ground measurements in order to avoid significant flux divergence between the surface and the aircraft level (Shuttleworth, 1991; Mahrt, 1998).

c. Boundary-layer budget method

The basic idea behind this method is that the convective boundary layer (or mixed-layer z_i, $h = z_i +$ entrainment layer, where h is the height of the boundary layer) grows during the day in response to the regional surface flux (see e.g. Stull, 1998). A typical mixed-layer growth

(except for early mornings) is controlled by the surface heat flux, the temperature profile, the friction velocity, horizontal advection and large-scale subsidence. Under summer daytime convective conditions z_i primarily depends on the lapse rate and the integrated surface heat flux. Various models have been proposed to diagnose or predict z_i based on these parameters (Batchvarova and Gryning, 1991; 1994; Seibert et al., 2000). When the evolution of the mixed-layer is known, e.g. based on a sequence of frequent radio soundings (or LIDAR and SODAR observations), an inverse performance of a mixed-layer growth-model can provide an estimate of the regional sensible heat flux (see e.g. Gryning and Batchvarova, 1999). Although nowadays the quality of radio sounding observations is good, the interpretation of the data is not always straightforward (Seibert et al., 2000). Furthermore, on days with significant advection and cloud formation the method does not work.

d. Satellite based remote sensing techniques

With the launch of a number of satellites (polar orbiting and geo-stationary) with onboard imagers that can measure reflected solar and thermal radiation an important source of meteorological and climate data is available. Geo-stationary satellites provide a continuous view of the earth disc from an apparently stationary position in space (temporal scale ~ 30 minutes; spatial scale > 1 km). The imagers on polar orbiting satellites, flying at a much lower altitude, provide more precise details although with a less frequent global coverage (temporal scale ~ 1 – 14 days; spatial scale ≤ 1 km). An example of a polar orbiting satellite is the NOAA satellite series with the onboard AVHRR (Advanced Very High Resolution Radiometer) imager, which has a global resolution of 4 km and a limited cover resolution of approximately 1 km, has provided a data record of more than 20 years. Imager data can provide estimates of land surface characteristics such as surface albedo, vegetation cover (e.g. NDVI (Normalised Difference Vegetation Index)) and surface temperature. Next these characteristics can be used to estimate surface fluxes indirectly using physical and/or empirical algorithms. However, delicate steps must be taken (e.g., cloud removal, sensor calibration and degradation, sun/satellite angle effects and atmospheric corrections), which finally determine the accuracy of the derived fluxes (Carlson et al., 1995). Examples of remote sensing algorithms are SEBI (Menenti and Choudhury, 1993), S-SEBI (Roerink et al., 2000) and SEBAL (Bastiaanssen et al., 1998). A review of remote sensing algorithms is given in Bastiaanssen et al. (1999) and Li and Lyons (1999).

Table 1.1: Overview of various methods.

Method	Flux	Spatial scale	Temporal scale
Tower turbulent fluxes	direct	0.5 - 5 km (~ field scale)	large (24 h day^{-1})
Airborne turbulent fluxes	direct	~ 100 km (large scale)	small (1 to 2 times day^{-1})
Satellite remote sensing techniques	indirect	field scale to continental scale	small to moderate (1 time day^{-1} to 24 h day^{-1})
Boundary-layer budget method	indirect	~ 100 km (large scale)	small (1 time day^{-1})

1.3 Objective of this study

The main objective of this study (sponsored by STW, project WMO4133[1]) is to develop and to test a ground based measurement technique that can provide reliable area-averaged fluxes of sensible (H) and latent heat (L_vE) on a routine basis and with a limited amount of additional meteorological data (e.g. standard observations of air pressure (P), wind speed (u) and air temperature (T)). In summary it must hold to the following requirements:

- Robust, low power consumption, no obstacle in the field
- Easy to maintain and user friendly
- Relatively cheap
- Provide area-average surface fluxes (H and L_vE)

This study embraces three aspects: **technical-instrumental** aspects, **practical-operational** aspects and **application** aspects. The **technical-instrumental** part consists of designing an instrument that is robust and user-friendly and can withstand a wide range of weather conditions. To make the installation requirements more flexible a small and relative cheap data acquisition unit is added. Finally, the data provided by the instrument has to be checked and once reliable processed to fluxes using a user-friendly software program. The evaluation and area-representativeness of the sensible heat fluxes and also the water vapour fluxes provided by the method over non-homogeneous areas is part of the **practical-operational** aspects. Finally, the **applicability** of the LAS in different scientific fields such as meteorology, hydrology, remote sensing and water management studies is investigated. Although this thesis is mainly focussed on the **practical-operational** and **application** aspects

---

[1] Dutch Technology Foundation (STW) project number WMO4133 (www.stw.nl).

of the method, some **technical-instrumental** aspects are discussed in the Section 1.5 and Appendix B.

1.4 The scintillation method

The method investigated in this study is known as the scintillation method. Research studies of e.g. Wesely (1976b), Green et al. (1997), De Bruin et al. (1995; 1996), Hill (1997) and many others have demonstrated that the scintillation technique is a reliable and suitable method and therefore a potential candidate that might satisfy the criteria given above. In the following Sections the scintillation phenomenon and the technique (i.e. the derivation of surface fluxes) will be discussed briefly. In Appendix A the theoretical background of the scintillation technique is discussed comprehensively and step by step: The relationship between the propagation statistics of EM radiation and the 'turbulent behaviour' of the atmosphere, expressed as the structure parameter of the refractive index of air C_n^2 for the different scintillometers; The saturation phenomenon; Inferring the structure parameters of temperature (C_T^2) and humidity (C_Q^2) from C_n^2; The derivation of the surface fluxes of sensible heat (H) and latent heat flux (L_vE) using MOST and additional wind speed data; And finally a summary of the differences and restrictions of the various scintillometer types (such as the SAS, LAS, XLAS and RWS).

a. Scintillation phenomenon

When electromagnetic (EM) radiation propagates through the atmosphere it is distorted by a number of processes that can influence its characteristics, e.g. its intensity or amplitude (by far the most important), polarization and phase. Two of these processes are scattering and absorption by constituent gases and atmospheric particles. These processes remove energy from the beam and lead to signal attenuation (i.e. the intensity). The most serious mechanism however that influences the propagation of EM radiation are small fluctuations in the refractive index of air (n). These turbulent refractive index fluctuations in the atmosphere lead to intensity fluctuations and are known as scintillations (Andrews et al., 2001; Tatarskii, 1961). Some examples that clearly show the distortion of wave propagation by the turbulent

atmosphere that can be seen regularly by the human eye are the twinkling of stars, image dancing and image blurring above a hot surface.

In most cases the atmosphere behaves turbulent. Turbulence is described as three-dimensional air motions (known as eddies), which have sizes ranging between millimetres to tens of metres. Turbulence in the atmosphere is the most effective transport mechanism for many scalar quantities, such as sensible heat (H) and water vapour (L_vE). The refractive index of air is a function of the temperature and to a lesser degree the humidity of the air, i.e. the density of the air. As these eddies transport both heat and water vapour their refractive indices are different from their surroundings, resulting in refractive index fluctuations and thus scintillations.

b. Measurement principle

A scintillometer is an instrument, consisting of a transmitter and a receiver part, that can measure the 'amount' of scintillations by emitting a beam of light over a horizontal path. The scintillations 'seen' by a scintillometer can be expressed as the structure parameter of the refractive index of air $C_n{}^2$ (see e.g. Wang et al., 1978). The structure parameter is a representation of the 'turbulent strength' of the atmosphere. In turn the turbulent strength describes the ability of the atmosphere of transporting e.g. sensible heat and water vapour. Because the scintillometer integrates over its optical path the structure parameter is actually a path-averaged[2] value. Path-averaging is the most important advantage of the scintillation method compared to traditional (point) measurement techniques. A following advantage of path-averaging is that it can provide statistically reliable information over short time intervals, which can be of advantage e.g. during stable and/or non-steady atmospheric conditions (see e.g. De Bruin et al., 2002; Hartogensis et al., 2002).

As mentioned before, scintillations are primarily the result of both turbulent temperature and humidity fluctuations (as the influence of pressure fluctuations can be neglected). The relative

---

[2] A scintillometer essentially provides path-averaged information. Because the air that passes the beam has originated from an upwind area carrying its characteristics, the path-averaged $C_n{}^2$ is in fact an area-averaged representative.

contribution of the temperature and humidity fluctuations to the refractive index fluctuations is wavelength dependant (see e.g. Hill et al., 1980; 1988; Andreas, 1989). At visible and near-infrared wavelengths primarily temperature fluctuations are dominant. As the wavelength increases towards radio wavelengths the contribution of humidity fluctuations increases. This means that by selecting a specific wavelength, the observed scintillations are either produced more by temperature fluctuations (i.e. C_T^2) or humidity fluctuations (i.e. C_Q^2) (Andreas, 1989). Finally, it is possible to derive sensible heat and water vapour fluxes from the structure parameter of temperature and humidity, respectively, using Monin-Obukhov Similarity Theory (MOST) (see e.g. Wyngaard et al., 1971). In the latter step (see Figure 1.2) information about the friction velocity (u_*) is required, which in this study will be derived from additional wind speed data (other methods for deriving u_* are given in Appendix A and C).
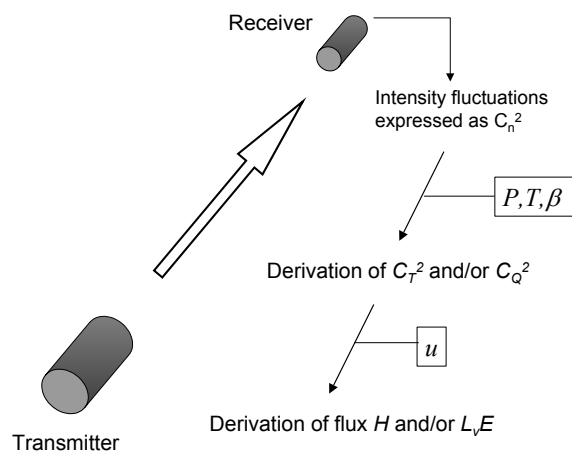
Figure 1.2: Schematic overview of the scintillation method and the derivation of the surface fluxes. Additional data required in the steps are also shown (wind speed (u), air temperature (T), air pressure (P) and Bowen ratio (β)).

In this study a near-infrared scintillometer is used. This Large Aperture Scintillometer (further denoted as LAS) has an aperture size of 0.15 m, which makes it possible to measure the structure parameter and in turn the sensible heat flux over path lengths up to 5 km. Small aperture scintillometers (SAS) or point source/detector scintillometer (or laser scintillometer) operating at a similar wavelength are restricted to much shorter path lengths (~ 250 m). The reason is that over longer path lengths the signal of the SAS becomes saturated and the method fails (see Appendix A). By increasing the aperture size the saturation limit can be altered such that the path length can be extended to several kilometres (Wang et al., 1978). In

Figure 1.3 some scintillometers are shown (XLAS, LAS and a laser scintillometer). The XLAS is 2× larger than the LAS and can be used over distances of 10 km (Kohsiek et al., 2002a,b).

Figure 1.3: From left to right the transmitter and receiver unit of the XLAS, the LAS and the laser scintillometer from Scintec (SLS20, Scintec, Atmosphärenmesstechnik GmbH, Germany).

c. History

The scintillation method is a fairly new measurement technique in the meteorology. In the 1950s theoretical research began to investigate the influence the turbulent atmosphere had on the propagation of EM waves, which in the astronomy was known as scintillation phenomena (Tatarskii, 1961). In the 1960s the meteorological community also became interested in scintillation phenomena with the idea that this 'remote sensing' technique could provide turbulent information of the atmosphere. With the invention of the laser (also in the 1960s) experimental studies followed. Impressive progress was made in 1970s when the experimentally observed saturation phenomenon was better understood and the agreement between modelled and measured data significantly improved. Now we reached a point that we can remotely measure the turbulent atmosphere, using the scintillation method. An excellent compilation of classical papers can be found in Andreas (1990). Also Hill (1992) published a good historic overview of the scintillation method.

1.5 Technical-instrumental aspects

The LAS developed and built by the Meteorology and Air Quality Group of the Wageningen University is based on the theory conceived by Wang et al. (1978). The LAS is similar to the one developed at the NOAA wave propagation laboratory (Ochs and Wilson, 1993). However, the electronics have been re-designed (e.g. demodulation circuit) to improve the signal-to-noise ratio and the sensitivity of the det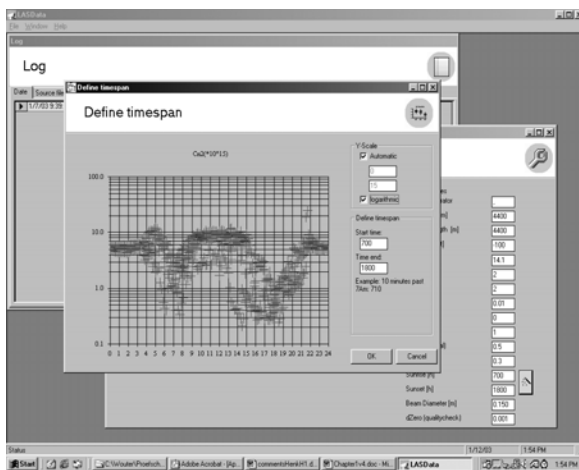ector allowing an optical path length of 5 km (see e.g. De Bruin et al., 1996; Beyrich et al., 2002a). A full description of the LAS is given in Appendix B. In order to make its installation requirements more flexible several LAS instruments have been equipped with a small internal data logger. The experiences with this data logger are however disappointing. Parallel to the LAS an extra large aperture scintillometer (XLAS) has been developed. The XLAS is identical to the LAS (i.e. LED, detector and electronics)

Figure 1.4: Software package for the LAS. Developed by Jan de Bruin of De Bruin IctInnovations.

except its aperture size is 0.31 m. Fresnel lenses are used instead of mirrors, primarily to keep the weight down and the size small. Due to its increased aperture, the XLAS can operate over distances up to 10 km (Kohsiek et al., 2002a,b). Detailed information on the XLAS can be found in Appendix B. Furthermore, a software package is developed in corporation with De Bruin Ictinnovations, which allows the user to compute relatively easy the surface fluxes from the LAS data (see Figure 1.4). In addition the software can validate the measurements based on the received signal intensity. Finally, an attempt has been made to develop a ULAS system, which is in fact a LAS that has a spatial filter (black stripes placed vertically) in front of its apertures. Churnside et al. (1988) have demonstrated that by adding these spatial filters it is possible to derive the average crosswind and its variance (see Appendix C), which are related to the friction velocity (u_*). Reason is that in the derivation of the sensible heat flux from the current LAS (and XLAS) additional wind speed data is required, which in most cases is a local representative. Although the wind speed dependency is small (~ 10% - 20%, see e.g. De Bruin et al., 1995), spatial filtering can be a solution.

1.6 Practical-operational aspects

In the last decades impressive progress has been made in the use of the scintillation method and derivation of turbulent statistics and surface fluxes (see Andreas (1989) and Hill (1992)). There are however still theoretical and practical-operational issues concerning this method that require further research. In this Section some of these issues will be discussed. The first two issues, namely surface heterogeneity and evaporation, will be further investigated in Chapter 2 and 3 of this thesis. In addition, some other aspects that are explored in parallel scintillometer studies are discussed briefly.

a. Surface heterogeneity - MOST restriction

In order to derive surface fluxes from the scintillometer obtained structure parameter the Monin-Obukhov Similarity Theory (MOST) is applied. According to MOST all dimensionless groups in the homogeneous surface layer, including the dimensionless made structure parameter (see Appendix A), depend on the dimensionless surface layer scaling parameter z/L_{Ob} (L_{Ob} is the Obukhov length and z is the height above the surface). It is however theoretically essential that the surface conditions are homogeneous and stationary for the dimensionless groups to follow MOST (Wyngaard et al., 1971; De Bruin et al., 1993). By extending the path length of the LAS to several kilometres over natural landscapes, which at these scales in most cases are heterogeneous as shown in Figure 1.1, it can be doubted whether the scintillation method can provide reliable fluxes. So far most studies dealing with MOST and non-homogeneous surfaces (including surface step-changes) were focussed on the derivation of fluxes from temperature- and wind-profiles and the turbulent variances of temperature, humidity and wind speed (see Beljaars, 1982; Beljaars et al., 1983; De Bruin et al., 1991). They show evidence that under certain conditions some of the MOST relations still can be used. Only recently, scintillometer experiments have been conducted over heterogeneous areas (Lagouarde et al., 1996; 2002; Chehbouni et al., 1999; 2000). However, these experiments took place over two adjacent fields and relatively close to the surface. In Chapter 2 and 3 the derivation of fluxes from scintillometer obtained structure parameters installed at two heights relatively high above a chessboard configuration of different crops are discussed. The results are analysed using a blending height approach (introduced by Wieringa, 1976), which is considered here as the height where the signatures of the different

crops start to blend due to turbulent mixing and a footprint model (Horst and Weil, 1992; 1994). In both Chapters the scintillometer fluxes are evaluated against aggregated EC measurements.

A similar scintillometer experiment was conducted in Lindenberg (Germany) as part of the LITFASS-98 project (see Beyrich et al., 2002a). Interesting of the Lindenberg area is that this area, compared to the Flevoland area (see Chapter 2 and 3), has also spatial variations in the surface roughness. One of the objectives of LITFASS-98 was to investigate the performance the LAS instrument (i.e. its long term operational capabilities) and to evaluate the surface fluxes. In Figure 1.5 the mean diurnal cycle of the sensible heat flux from the LAS is depicted together with the area-averaged flux aggregated from in-situ fluxes (also shown). Important to note is that this LAS, which was installed in April 1998, is still in operation. Beyrich et al. (2002a) have shown the results from a complete year. They found that approximately 70% of the daytime summer measurements are reliable for flux derivations. During winter less data is available, which in most cases is the result of stable stratification and poor visibility due to fog and rainfall.
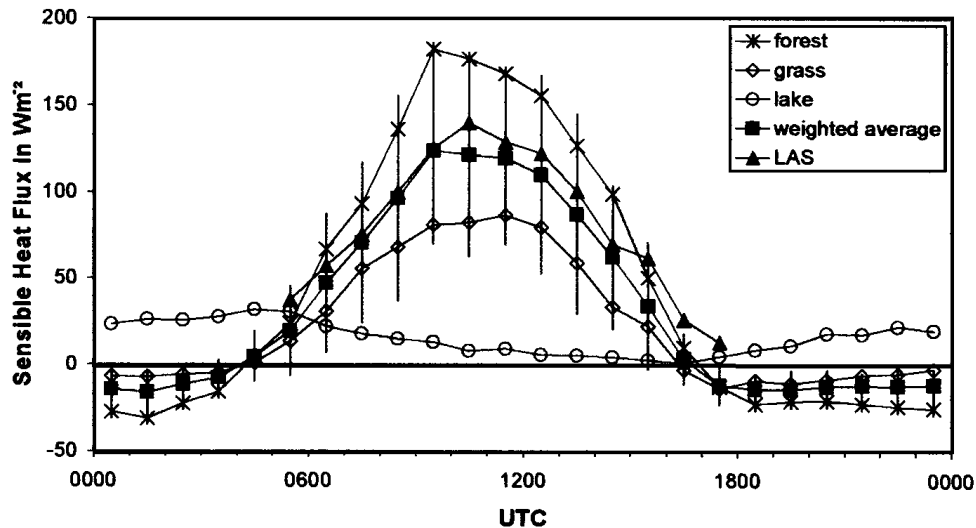
Figure 1.5: Mean diurnal cycle of sensible heat flux during the LITFASS-98 experiment over different land-use classes, as a land-use-weighted average and from LAS measurements (reproduced from Beyrich et al., 2002a).

In Figure 1.6 the vertical H-profile is shown (Helipod) together with the area-averaged surface fluxes based on the LAS and in-situ measurements. Note that these observations are also part of the LITFASS-98 project. The downward extrapolation of the Helipod

measurements (solid line) would suggest a surface flux of 100 W m^{-2}. This is in good agreement with the surface flux obtained with the LAS. Note that the low-level tower measurements show a large discrepancy compared to the other observations. Possible reasons responsible for this discrepancy is first, the non-representativeness of the low-level tower measurements and second, a substantial contribution of the heat flux from the forest (Beyrich, 2000).
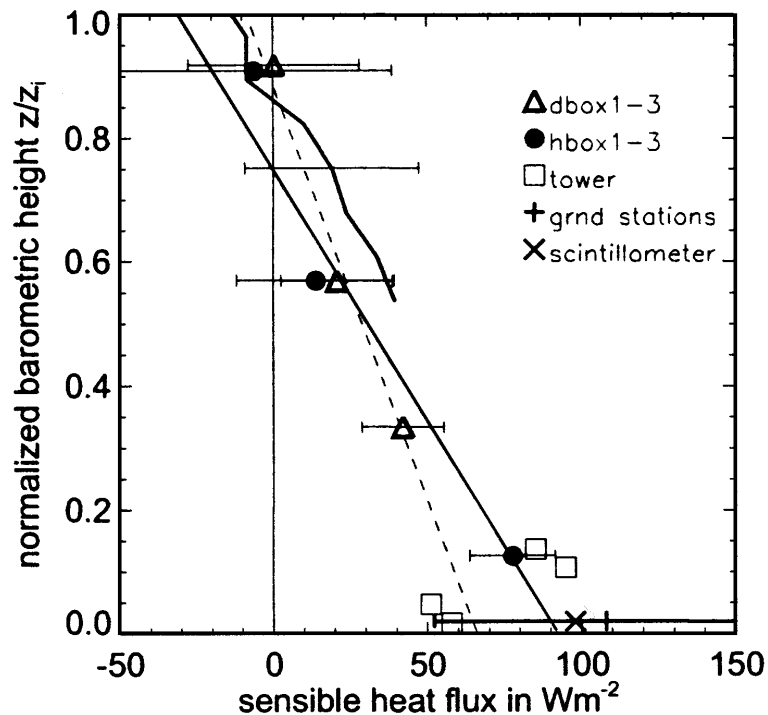
Figure 1.6: Vertical profile of *H* obtained with the Helipod (helicopter) (solid line) and the DO-128 (aircraft) (dashed line) together with the area-averaged surface flux derived from the LAS and by aggregating of the EC stations. The curve in the upper half of the *H*-profile represents the wind-profiler/RASS system measurements (reproduced from Bange et al., 2002).

b. Evaporation

To cope with the decreasing availability of fresh water for various consumers especially in arid and semi-arid regions, good management of the sparse water sources is essential. An important requirement of good water management is knowledge of the water balance, especially at large scales (e.g. catchment scale to continental scale). One of the terms of the water balance is the water vapour flux (L_vE). In this thesis two methods for deriving area-averaged water vapour fluxes will be discussed (see Chapter 3). The first method is entirely

based on the 'stand-alone' LAS and additional estimates of net radiation and soil heat flux densities based on global radiation data. Here, the water vapour flux is evaluated as the residual of the surface energy balance. In addition a second method is investigated as alternative. This method is based on a Radio Wave Scintillometer (RWS) in combination with a LAS and is known as the two-wavelength method (Andreas, 1989). The RWS operates at a radio wavelength (λ) of 11 mm. At this wavelength scintillations are caused primarily by turbulent water vapour fluctuations. Because a LAS (λ = 930 nm) is most sensitive to temperature fluctuations the combination of a LAS and a RWS is an ideal technique for deriving both the sensible heat and water vapour flux directly from the obtained structure parameters (C_T^2 and C_Q^2). In Chapter 3 both methods are evaluated (reliability and practical aspects) against spatially aggregated EC measurements. It must be noted that in many validation studies the non-closure problem of EC method is an important issue (Oncley et al., 2000). It is quite common for experimental data sets to have an energy balance closure of only 70% - 90% ($R_n \neq H + L_v E + G_s$). This disclosure problem has also further consequences in e.g. inter-comparison studies such as in Chapter 3.

c. Other aspects

In this section two other scintillometer studies are discussed briefly that are focussed on other scintillometer aspects. The first study is focussed on long-range scintillometry using extra large aperture scintillometers (XLAS) over path lengths of 10 km (Kohsiek et al., 2002a). A following issue that has to be considered is the saturation limit of the scintillometer (Kohsiek et al., 2002b). The second study is devoted to the applicability of the scintillation method during advective conditions (Hoedjes et al., 2002).

Long-range scintillometry and saturation

The basis of the scintillation technique, the EM wave propagation theory, is in fact a first-order scattering theory and valid to weak turbulent regimes only. This means that when the atmospheric turbulence becomes to intense, the signal 'saturates' and the scintillation method no longer functions properly. In this case the relationship between the variance of the received radiation and the structure parameter fails (see Appendix A). One way to overcome saturation is the use of large incoherent transmitter and receiver apertures, such as the LAS. Kohsiek at

al. (2002a,b) are the first who used an extra large aperture scintillometer (XLAS) over a distance of 10 km. They found a good agreement between the LAS fluxes and the EC measurements (Figure 1.7(left)) and aircraft based EC measurements (Figure 1.7(right)). The observed scatter in the left Figure might be the result of the following reasons: broken cloud cover, saturation, and intermittent behaviour of the local fluxes. A regression analysis yields: $H_{XLAS} = 0.9H_{EC}$, $R^2 = 0.87$. Possible effects of saturation have been further investigated by Kohsiek et al. (2002b). They found that based on the saturation criteria given by Frelich and Ochs (1990) saturation is likely to occur when the surface flux of sensible heat becomes higher than 50 W m^{-2}. Based on the analysis of Frehlich and Ochs, Kohsiek et al. performed a correction to the XLAS fluxes. A regression analysis of the corrected data yielded: $H_{XLAS\_cor} = 1.05H_{EC}$, $R^2 = 0.87$. The experimental data published in the few papers devoted to saturation show however significant variation of the saturation limit for the large aperture scintillometer (Wang et al., 1978; Ochs and Hill, 1982; Frehlich and Ochs, 1990). Furthermore, knowledge of the inner length sale is required when performing this correction (Frehlich and Ochs, 1990). Summarising, the indistinctness of the saturation limit, which has also consequences for the practical applicability of the LAS and XLAS, requires further research.
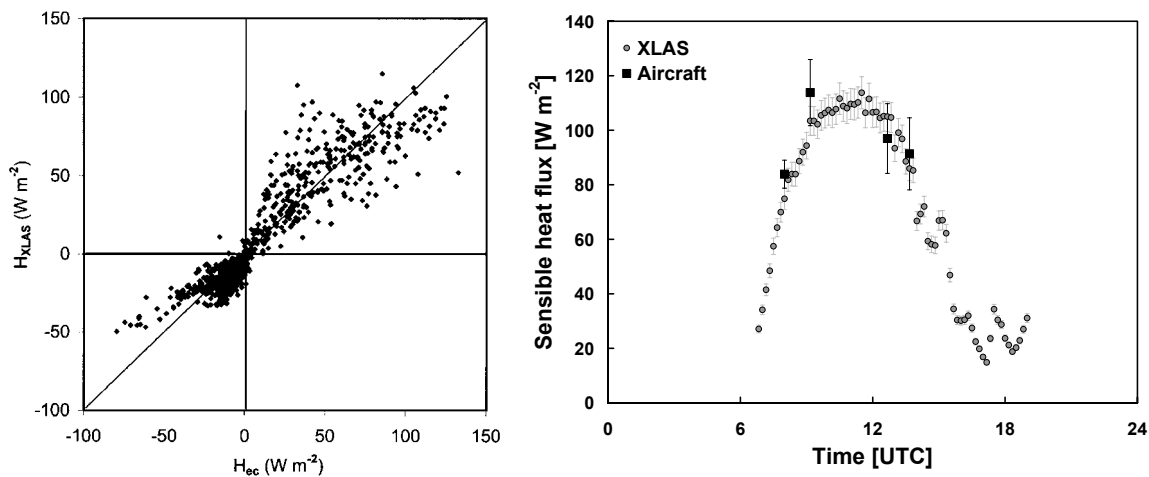
Figure 1.7 (left): Comparison of sensible heat flux measured by the XLAS and the EC method for the period August - September 2002 at Cabauw (The Netherlands) (reproduced from Kohsiek et al., 2002a); (right): Diurnal cycle of XLAS surface sensible heat flux compared to aircraft derived sensible heat flux (including flux divergence below 70 m) for July 27th (2002). The aircraft data are provided by Beniamino Gioli and Franco Miglietta of IATA-CNR (Italy) as part of the RECAB project.

In many arid and semi-arid areas agricultural activities involve the performance of irrigation. A regularly observed phenomenon during such irrigation events is the regional advection of dry air from areas surrounding the agricultural fields. This results in high water vapour fluxes and low or even negative sensible heat fluxes. Advection has also consequences on the performance of the scintillation method (i.e. the derivation of C_T^2 from C_n^2 and the applicability of MOST). Recently, Hoedjes et al. (2002) performed an intensive field experiment entirely focussed on this issue. They found a good agreement between the surface fluxes from the LAS and in-situ EC measurements during both irrigated and dry unstable conditions as well as during periods of advection.

1.7 The applicability of the scintillation method in other studies

Due to its path integrating capabilities over several kilometres the scintillation method can be considered as a method that can bridge the gap between the current availability of primarily point based observations and the demand for large-scale spatially averaged surface fluxes. This is recognised by many research studies, such as meteorological, hydrological, water-management, remote sensing studies and many others. The reason is that the spatial scale of the fluxes of the scintillation method is (almost) comparable to the spatial resolution of satellite imagers and the grid box size of meteorological and hydrological models. The method is therefore a useful tool for e.g. validation studies of all sorts of remote sensing methods and numerical models (see e.g. Carlson et al., 1995; Beyrich et al., 2002a; Kite and Droogers, 2000). In turn these studies are useful, directly or indirectly, to many agricultural, environmental, social, economical and political related issues, such as water balance monitoring, fresh water management, desertification combat activities, climate monitoring, irrigation productivity, crop yield prediction, land use planning etc.

In this context the usefulness and practical applicability of the scintillation method is investigated in Chapter 4 and 5 of this thesis. In Chapter 4 the operational performance of a LAS is demonstrated, which has been installed over a transect of a valley in the Gediz river basin (Turkey) that is partially irrigated for agricultural purposes. In Chapter 5 satellite based surface maps of surface fluxes produced by a satellite remote sensing method called SEBAL

(Bastiaanssen et al., 1998) are compared with ground-truth scintillometer observations. In this study a large amount of NOAA-14 AVHRR images are collected spanning an entire growing season. Similar studies using different remote sensing techniques and satellite images are performed by Hemakumara et al. (2002), Jia et al. (2003), Kite and Droogers (2000), Lagouarde et al. (2003), Roerink et al. (2000), Rosema et al. (2001) and Watts et al. (2000).
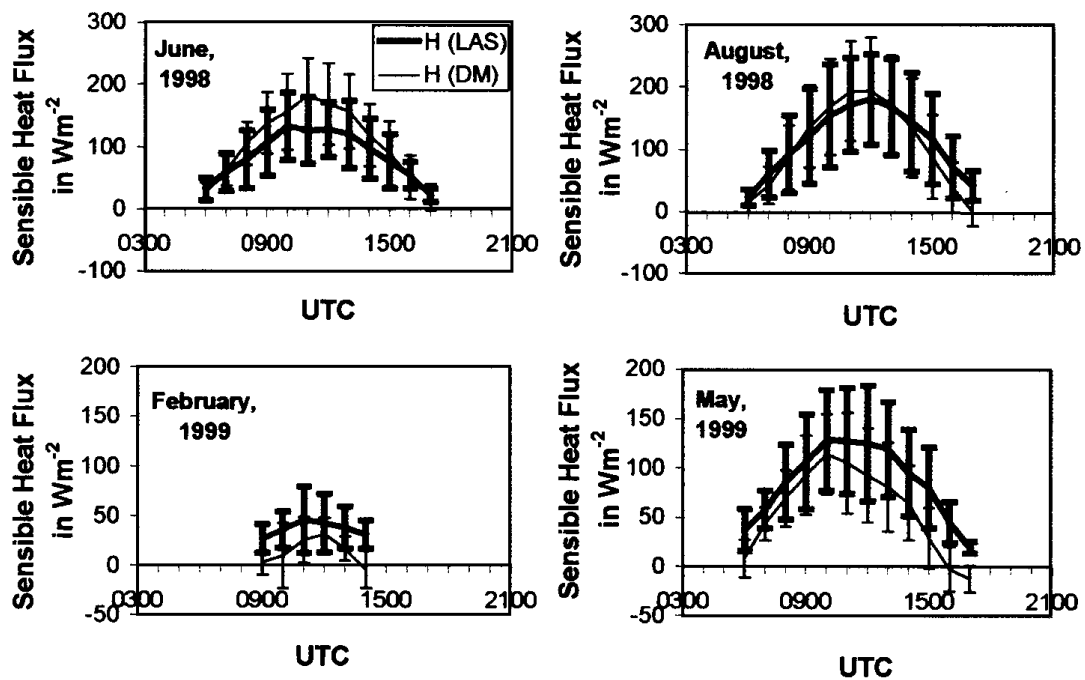
Figure 1.8: Mean daytime evolution of the sensible heat flux in the LITFASS area according to the NWP model and the LAS measurements for four different months (reproduced from Beyrich et al., 2002a).

Another interesting study is performed by Beyrich et al. (2002a) who did the first comparison between scintillometer obtained surface sensible heat fluxes and the output of a numerical weather prediction (NWP) model. Figure 1.8 shows the mean diurnal cycle of the sensible heat flux of the LAS and the NWP model of the DWD (German Weather Service) for four different months. This Figure indicates that in summer the model tends to give higher fluxes than the LAS, while in winter the opposite (see also Figure 6 in Beyrich et al., 2002a). Beyrich et al. (2002a) suggested that 'tuning' of the model in order to correctly predict the 2-m temperature had significantly effect on the discrepancy between both fluxes (as tuning lowered the evaporation rate resulting in higher sensible heat fluxes). In Table 1.2 an overview is given of recent published scintillometer studies focussed on different 'scintillometer' aspects, 'demonstration' experiments and validation studies using 'ground-truth' LAS observations.

18

Table 1.2: Overview of scintillometer studies including 'demonstration' projects.

Author	Subject	Scintillometer	Flux
Beyrich et al. (2002a)	Surface heterogeneity (MOST)	LAS	H
	Long term operational aspects		
	NWP model $\leftrightarrow$ LAS		
Cain et al. (2001)	EC $\leftrightarrow$ LAS	LAS	H
Chehbouni et al. (1999; 2000)	Surface Heterogeneity	LAS	H
De Bruin et al. (1996)	Long range scintillometry	LAS	H
Green et al. (2000; 2001)	Two-wavelength method	LAS, RWS	H, L_vE
	Water vapour flux		
Hemakumara et al. (2001)	Remote sensing (SEBAL$_{NOAA-14\ AVHRR}$) $\leftrightarrow$ LAS	LAS	L_vE
	Water vapour flux		
Hartogensis et al. (2003)	Effective height of the LAS over sloping terrain	LAS	H
Hoedjes et al. (2002)	Advection	LAS	H, L_vE
	Water vapour flux		
Jia et al. (2003)	Remote sensing (SEBS$_{ATSR2}$) $\leftrightarrow$ LAS	LAS	H
Kite and Droogers (2000)	Remote sensing techniques; hydrological models; field methods $\leftrightarrow$ LAS	LAS	H, L_vE
Kohsiek et al. (2002a; 2002b)	Long range scintillometry	XLAS	H
	Fresnel lenses		
	Saturation		
	Long term operational aspects		
Lagouarde et al. (1996; 2002)	Surface heterogeneity (MOST)	LAS	H
Lagouarde et al. (2003)	Remote sensing (SEBAL$_{aircraft\ INFRAMETRICS}$) $\leftrightarrow$ LAS	LAS	H
Meijninger and De Bruin (2000) (see also **Chapter 4**)	Long term operational aspects	LAS	H
Meijninger et al. (2002a) (see also **Chapter 2**)	Surface heterogeneity (MOST)	LAS	H
Meijninger et al. (2002b) (see also **Chapter 3**)	Surface heterogeneity (MOST)	LAS, RWS	H, L_vE
	Two-wavelength method		
	Water vapour flux		
Meijninger et al. (2003) (see also **Chapter 5**)	Remote sensing (SEBAL$_{NOAA-14\ AVHRR}$) $\leftrightarrow$ LAS	LAS	H
Nieveen et al. (1998)	Absorption related intensity fluctuations	LAS	H
Roerink et al. (2000)	Remote sensing (S-SEBI$_{LANDSAT-TM}$) $\leftrightarrow$ LAS	LAS	H
Rosema et al. (2001)	Remote sensing (EWBMS$_{METEOSAT}$) $\leftrightarrow$ LAS	LAS	H
Watts et al. (2000)	Remote sensing (NOAA-12 & 14 AVHRR) $\leftrightarrow$ LAS	LAS	H

1.8 Organisation of this thesis

In summary the following research questions and objectives are investigated in this thesis:

- How is the performance of a LAS over heterogeneous areas such as the Flevoland area?
- Can a 'stand-alone' LAS and/or a LAS-RWS combination provide reliable estimates of the water vapour flux over heterogeneous areas?
- How good is the operational performance and applicability of a LAS?
- How useful is a LAS in providing 'ground-truth' data for validation studies such as remote sensing?

These objectives and questions will be investigated in the following four Chapters. Chapter 2 deals with the aspects of surface heterogeneity and the performance of the scintillation method over such areas. For this purpose an intensive experiment was carried out in Flevoland (The Netherlands) in the summer of 1998. The spatial representativeness of the LAS' derived surface sensible heat fluxes are evaluated against spatial aggregated in-situ (EC) measurements. The experimental results and observed discrepancies are evaluated using a blending height approach and a footprint model.

In Chapter 3 water vapour flux estimates based on scintillation measurements over a heterogeneous landscape are evaluated. This study is also based on the scintillometer experiment that took place in Flevoland. Two methods are be explored. The first method is entirely based on a 'stand-alone' LAS, where L_vE is considered as the residual of the energy balance using estimates of the available energy based on global radiation data. The second method is known as the two-wavelength method and uses a radio wave scintillometer (RWS) in combination with a LAS to measure the water vapour flux directly.

In Chapter 4 the scintillometer results of an international experiment that took place in Turkey (1998) are presented. This experiment, which lasted an entire growing season, was initiated by the International Water Management Institute (IWMI). The main objective of this inter-comparison project was to compare the actual water vapour flux over irrigated areas using various remote sensing techniques, hydrological models and ground observations (Kite and

Droogers, 2000). Chapter 4 only deals with the scintillometer results and focuses on the operational aspects and the performance of the LAS.

Chapter 5 discusses an inter-comparison study between ground based surface fluxes obtained with a LAS and the so-called variance technique (or sigma-T method) installed at two different sites and surface flux maps generated by the SEBAL satellite remote sensing algorithm The data set used in this study is also based on the experiment that took place in Turkey. In this study a large amount of satellite images of the NOAA-14 AVHRR imager was collected spanning the entire growing season.

Finally the thesis is summarised in Chapter 6 followed by some perspectives in Chapter 7.

Chapter 2 and 3 are published in a special issue of Boundary-Layer Meteorology entirely devoted to scintillometry. Chapter 4 is published in a special issue of the Journal of Hydrology, wherein satellite, model and field based surface fluxes are compared. Chapter 5 is submitted to Int. J. Remote Sensing. In this thesis all papers are presented in the same form. As such, the scintillation technique is repeatedly explained in all four Chapters.

Chapter 2

Determination of area-averaged sensible heat fluxes with a large aperture scintillometer over a heterogeneous surface

Meijninger, W.M.L., Hartogensis, O.K., Kohsiek, W., Hoedjes, J.C.B., Zuurbier, R.M. and De Bruin, H.A.R.

2.1 Introduction

Surface fluxes at scales of 100 m to 5 km are required in many meteorological, hydrological and other related studies. In the last decades research has revealed that the scintillation method is one of the few methods that can obtain surface fluxes at these scales. Different scintillometer types have been developed, which can provide surface fluxes of momentum (τ), sensible heat (H) and latent heat (L_vE) using different wavelengths, aperture sizes and configurations (e.g., Wesely, 1976b; Kohsiek and Herben, 1983; Andreas, 1989; Hill et al., 1992a; Hill et al., 1992b; Thiermann and Grassl, 1992). For more information the reader is referred to Andreas (1990) and Hill (1992). L_v above is the latent heat flux of vaporisation.

It can be concluded from these studies that laser scintillometers (small aperture scintillometer, SAS) provide information on both the inner scale of turbulence (l_o) and the structure parameter of the refractive index of air (C_n^2), which can be obtained using different techniques (Hill et al., 1992a; Thiermann, 1992; Green et al., 1997). Once l_o and C_n^2 are known the fluxes of momentum and sensible heat can be derived. A disadvantage of this type of scintillometer is that saturation occurs at path lengths of about 250 m. As a consequence

the proportionality between $\sigma_{\ln A}{}^2$ and $C_n{}^2$ will fail. For a large aperture scintillometer (LAS) saturation occurs at much longer path lengths ($\approx$ 5 km, see e.g. De Bruin et al., 1996; Beyrich et al., 2002a). However this scintillometer only yields $C_n{}^2$.

In this study we will use a LAS similar to the design by NOAA (Ochs and Cartwright, 1980). This scintillometer has an aperture diameter of 0.15 m, uses an infrared light source (λ = 930 nm) and provides a path-averaged value of $C_n{}^2$ over distances up to 5 km. This scintillometer has been used recently by De Bruin et al. (1995, 1996), Chehbouni et al. (1999), Meijninger and De Bruin (2000), Cain et al. (2001) and Beyrich et al. (2002a).

In order to derive fluxes from the LAS signal one has to rely on the Monin-Obukhov Similarity Theory (MOST). Since MOST requires horizontal homogeneity the question arises whether the LAS can be applied at scales of 1 km, since usually the earth's surface is heterogeneous at that scale. Several authors have paid attention to the applicability of MOST over heterogeneous terrain. Beljaars (1982) discussed the flux of momentum and heat derived from profiles of wind and temperature over a perturbed area. Beljaars et al. (1983) also considered the relationship between turbulent variances of T and Q and the fluxes of heat and water vapour. De Bruin et al. (1991) focussed on the variance method, i.e. deriving fluxes from the variance of scalars using MOST within the so-called internal boundary layer (IBL) after a sudden dry to wet step change of the surface. However the relationships between fluxes and structure parameters over inhomogeneous areas have never been discussed.

An attempt to deal with the problems of surface heterogeneity introduces the concept of blending height, see Wieringa (1976). This concept is based on the idea that due to the turbulent mixing (i.e. blending) in the planetary boundary layer (PBL) internal boundary layers merge and the influence of individual surface elements begins to vanish at a level, called the blending height. The blending height mainly depends on the horizontal scale of the inhomogeneities (Mason, 1988). To a lesser degree the stability and also the considered quantity play a role (Wood and Mason, 1991; Mahrt, 1996; Ma and Daggupaty, 1998). If the blending height is low compared to the PBL depth (i.e. within the surface layer or constant flux layer) it is expected that above this height MOST is applicable.

Below the blending height the situation is more complicated as the flow is not in equilibrium with the local vertical gradient. As a result the conditions required for MOST are not satisfied. It is expected that a scintillometer, which is placed below the blending height, will 'see' the fluxes from the individual surfaces. Lagouarde et al., (1996) and Chehbouni et al. (1999) installed scintillometers over an area consisting of two adjacent fields with contrasting vegetation. They found a good resemblance between the scintillometer-derived sensible heat flux and the path weighted in-situ measured fluxes, which indicates that the violation of MOST is small.

To test the applicability of the LAS over heterogeneous terrain, and to study the blending height concept for the structure parameter of temperature and the sensible heat flux, an intensive field experiment in Flevoland (The Netherlands) was conducted. In this study also a footprint model (Horst and Weil, 1992) is used to estimate the relative contributions from the different terrains. The selected area is very flat and consists of rectangular patches of about 500 m × 250 m covered with different crops. This indicates that the Flevoland area can be classified as type A (Shuttleworth, 1988; De Bruin, 1989), i.e. the horizontal scale of the inhomogeneities are relatively small (< 10 km). In general four crops were grown, namely sugar beet, potatoes, wheat and onions. Eddy covariance instruments were installed over these crops to provide independent flux measurements. From these fluxes the area-averaged fluxes have been aggregated and will be compared with the fluxes derived from the scintillometers.

2.2 Theory

2.2.1 The scintillation method

The measurement principle of the scintillation method and the procedures to derive fluxes from the scintillometer signal are discussed in many papers (see e.g., Hill, 1992; 1997 and many others). Therefore we will only briefly focus on the theory of scintillometry and mention specific points, which are of importance in this study.

The LAS consists of a transmitter and receiver device installed at a certain height z_{LAS} above the surface and both with an aperture diameter D of 0.15 m. A known distance L, called the path length, separates the devices. The electromagnetic radiation emitted by the transmitter in the direction of the receiver is scattered by the turbulent atmosphere. The observed intensity fluctuations (or scintillations) are analysed at the receiver side ($\sigma_{\ln A}{}^2$), which can be expressed as the structure parameter of the refractive index of air $C_n{}^2$. Wang et al. (1978) found the following expression between the path averaged $\langle C_n^2 \rangle$ and the variance of the logarithm of amplitude fluctuations ($\sigma_{\ln A}{}^2$),

$$\langle C_n^2 \rangle = 4.48 \sigma_{\ln A}^2 D^{7/3} L^{-3} . \tag{2.1}$$

Wang et al. (1978) also showed that $\langle C_n^2 \rangle$ is path averaged according to a spatial weighting function ($W(x)$), which is bell-shaped. This means that scintillations produced by turbulence near the centre contribute more to the path-averaged $C_n{}^2$ than scintillations produced near the transmitter and receiver.

In general, both temperature (T) and humidity fluctuations (Q) produce fluctuations in the refractive index of air (n). Note that in this study the absolute humidity Q is expressed in kg m^{-3}. Therefore, strictly speaking, the measured $C_n{}^2$ value is related to the structure parameters of temperature ($C_T{}^2$), humidity ($C_Q{}^2$) and the covariant term (C_{TQ}). As a simplification, Wesely (1976a) showed that for a LAS, operating at a near-infrared wave length, $C_n{}^2$ is related to $C_T{}^2$ as follows

$$C_T^2 = C_n^2 \left(\frac{T^2}{-0.78 \times 10^{-6} P} \right)^2 \left(1 + \frac{0.03}{\beta} \right)^{-2} . \tag{2.2}$$

Here P is the atmospheric pressure, T the absolute air temperature and β the Bowen-ratio. Here we evaluate the Bowen-ratio value applying the iterative method proposed by Green and Hayashi (1998)

$$\beta = \frac{H_{LAS}}{\langle R_n \rangle - \langle G_s \rangle - H_{LAS}} , \tag{2.3}$$

26

where the net radiation (R_n) and the soil heat flux (G_s) are area-averaged values.

Using MOST the sensible heat flux can be derived from C_T^2 and additional wind speed (u) data, viz.

$$\frac{C_T^2 \left(z_{LAS} - d\right)^{2/3}}{T_*^2} = f_{TT}\left(\frac{z_{LAS} - d}{L_{Ob}}\right) \tag{2.4}$$

with the Obukhov length $L_{Ob} = \dfrac{u_*^2 T}{g \kappa_v T_*}$, $\quad T_* = \dfrac{-H}{\rho c_p u_*}$ and

$$u_* = \frac{\kappa_v u}{\ln\left(\dfrac{z-d}{z_o}\right) - \Psi_m\left(\dfrac{z-d}{L_{Ob}}\right)}, \tag{2.5}$$

where Ψ_m is the well-known Businger-Dyer correction, g the gravitational acceleration, κ_v the von Kármán constant, ρ the density of air, c_p the specific heat of air at constant pressure, u_* the friction velocity and T_* the temperature scale. The scintillometer is installed at the height z_{LAS}, the wind speed is measured at height z, d is the zero-displacement height and z_o the roughness length. In this study we will confine ourselves to unstable conditions and we will use the MOST relationship f_{TT} in Equation (2.4) given by De Bruin et al. (1993).

Due to the fact that in this experiment the LAS height is larger than 10 m it is expected under unstable conditions that the free convection approach is also a good approximation to H ($H \approx (C_T^2)^{3/4}$). This means that the influence of mechanically produced turbulence is small and therefore a crude estimate of u_* is sufficient. However, to avoid incidental uncertainties we will use the full set of equations and the area-averaged momentum flux ($-\langle \overline{u'w'} \rangle$) derived from eddy covariance measurements in this study. Here the area-averaged momentum flux is estimated as follows

$$-\langle \overline{u'w'} \rangle = \sum_i -f_i \left(\overline{u'w'}\right)_i \tag{2.6}$$

where f_i is the fractional area of each crop.

2.2.2 The concept of blending height applied to the LAS

Consider an area that consists of patches with different properties (e.g. surface roughness, surface temperature or soil moisture) as illustrated in Figure 2.1. As the air flows from one patch to another patch, an internal boundary layer (IBL) develops. As a result a number of IBLs develop within the surface layer (SL), assuming the horizontal extent of the patches is relatively small. It is expected that the top of each IBL becomes diffuse as the flow encounters new surface conditions. This means that the vertical extent of each IBL depends on the horizontal size of each patch. At a certain level (z_b) above the top of the IBLs, the signatures of the individual patches tend to merge due to turbulent mixing. As Mahrt (1996) noted, from a geometric point of view the IBLs should not extend above this certain height z_b. In the literature this height is often referred to as the blending height.
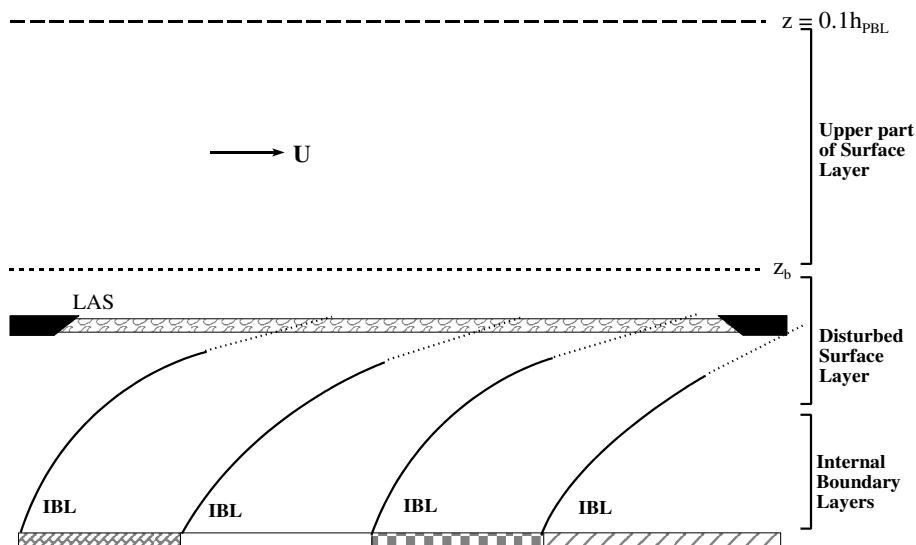
Figure 2.1: Schematic diagram of the various layers over a heterogeneous flat landscape, showing the heights of the top of the internal boundary layers, the top of the surface layer and the blending height.

Wieringa (1976) introduced the concept of blending height for the correction of wind speed data for small-scale exposure effects under neutral conditions. Other scientists have focused on the blending height concept and have formulated several definitions (Wieringa, 1986; Mason, 1988; Claussen, 1990; Wood and Mason, 1991; Schmid and Bünzli, 1995). In general

the blending height can be seen as a level where the influence of the patches or surface perturbations gradually decay. The overall agreement between the different approaches is that the blending height increases with increasing horizontal scale of heterogeneity (L_h) and instability. Also it must be noted that there are also indications that there are different blending heights for different quantities. Ma and Daggupaty (1998) found differences between the height scales for heat and momentum transfer, which agreed with the model results of Wood and Mason (1991).

In the case for type A landscapes (Shuttleworth, 1988; De Bruin, 1989) such as the Flevoland area where the horizontal scales of inhomogeneities are much smaller than roughly 10 km, primarily the lower part of the SL is affected by the inhomogeneities. In contrast, above the SL a uniform well-developed PBL will be formed, which 'sees' a single area-averaged surface flux of momentum, heat and water vapour. In this study the derivation of the sensible heat flux from scintillometer measurements (i.e. path-averaged C_T^2) that have been conducted above the blending height will be investigated.

Below the blending height, inside the disturbed surface layer, the situation is more complicated. A scintillometer, which is placed below the blending height, will 'see' the fluxes from the individual patches (see Figure 2.1). In this case turbulence is not in equilibrium with the local vertical gradients or structure parameters and MOST might be violated. Lagouarde et al. (1996) and Chehbouni et al. (1999) did scintillometer measurements relatively close to the surface over two adjacent surfaces with contrasting vegetation. Their results suggest that the violation of the MOST relationship between C_T^2 and H is fairly small.

In this study we will use as a working hypothesis the heuristic model proposed by Mason (1988) to evaluate the blending height as the level where the path-averaged C_T^2 is in equilibrium with the area-averaged surface flux of sensible heat. We used the extended model given by Wood and Mason (1991) to include the influence of stability.

$$z_b \cong 2 \left(\frac{u_*}{U} \right)^2 L_h .$$
(2.7)

Here U is the spatially averaged wind speed at the blending height and L_h the horizontal scale of heterogeneity.

2.2.3 The footprint concept applied to the LAS

If over heterogeneous terrain measurements are conducted below the blending height a portion of the surface upstream, called the source area (SA), influences the sensors. A useful tool to determine the SA for turbulent fluxes is a footprint model. Numerous versions of footprint models are described in the literature (Schuepp et al., 1990; Horst and Weil, 1992, 1994; Schmid, 1994; Horst, 1999) based on analytical solutions of the advection-diffusion equation. These models are very simple to use and can be applied in the SL where the wind flow is not disturbed by obstacles or topography and the surface is not too complicated (no 3 three-dimensional source/sink distributions).

The source weight or footprint function f relates the measured flux at height z_m, $F(x, y, z_m)$, to the spatial distribution of surface fluxes, $F(x, y, 0) \equiv F_0(x, y)$ (Horst and Weil, 1992), i.e.,

$$F(x, y, z_m) = \int\limits_{-\infty}^{\infty} \int\limits_{-\infty}^{x} F_0(x', y') f(x - x', y - y', z_m) dx' dy' . \tag{2.8}$$

The SA arises from the integration of the footprint or source weight function. This area can also be interpreted as the 'field of view' of the instrument. In our analysis we calculated the footprint function f using the model of Horst and Weil (1994)

$$\overline{f}^y(x, z_m) \cong \frac{d\overline{z}}{dx} \frac{z_m}{\overline{z}^2} \frac{\overline{u}(z_m)}{\overline{u}(c\overline{z})} A e^{-(z_m / b\overline{z})^r} , \tag{2.9}$$

where $\overline{z}$ is the mean plume height for diffusion from a surface source and $\overline{u}(z)$ the mean wind speed profile. The variables A, b and c are functions of the gamma functions of the shape parameter r. This model solely depends on the measurement height, surface roughness and the atmospheric stability and gives as output the contribution of any upwind surface flux to a 'measured' flux at some point downwind at height z_m. Again it must be noted that we assume that the violation of MOST is small.

In the case of a LAS one has to combine f with the spatial weighting function $W(x)$ of the LAS in order to estimate the SA. In Figure 2.2 an example is presented where the wind direction is perpendicular to the path of a LAS. The black diamonds stand for the transmitter

and receiver parts and the bars line represents the LAS's beam. In this case the path length is 2.2 km, with the LAS installed at a height of 11.6 m. The model predicted that 94% of the measured flux has originated from the first kilometre of the upwind area (z_o = 0.1 m, L_{Ob} = - 50 m and σ_v = 0.5 m s^{-1}). As the height of the scintillometer increases, e.g. to 20.4 m, the peak shifts from 132 to 220 m from the path of the LAS and only 90% of the flux has originated from the first kilometre upwind area (for the same atmospheric conditions).
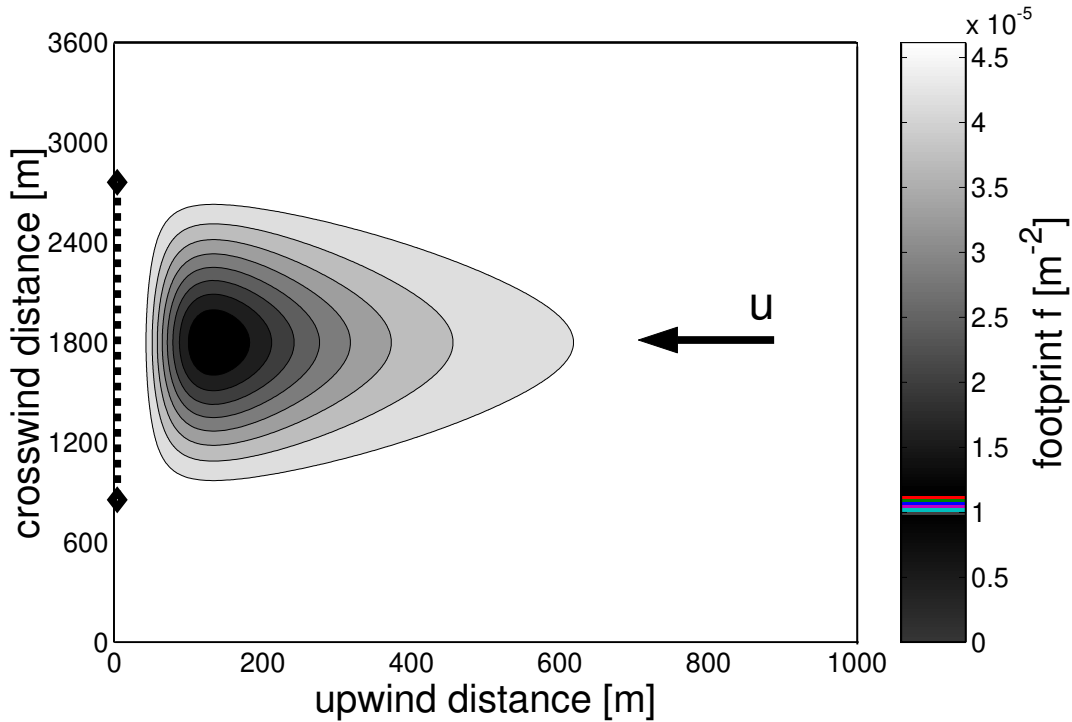

Figure 2.2: The footprint (plan view) of a LAS where the wind direction is perpendicular to its path. The bars line represents the beam of the scintillometer and the diamonds stand for the transmitter and receiver part.

When the wind is parallel to the path of the LAS, the SA lies approximately between the transmitter and receiver parts. An example is shown in Figure 2.3 with the same atmospheric conditions assumed as in Figure 2.2. It can be seen that the SA is larger when the wind direction is perpendicular to the LAS's path (SA$_\perp$ ≈ (2 km × 1 km)) than for parallel circumstances (SA$_{//}$ ≈ (2 km × 0.1 km)). In the latter case the lateral dispersion determines for a large part the size of SA.
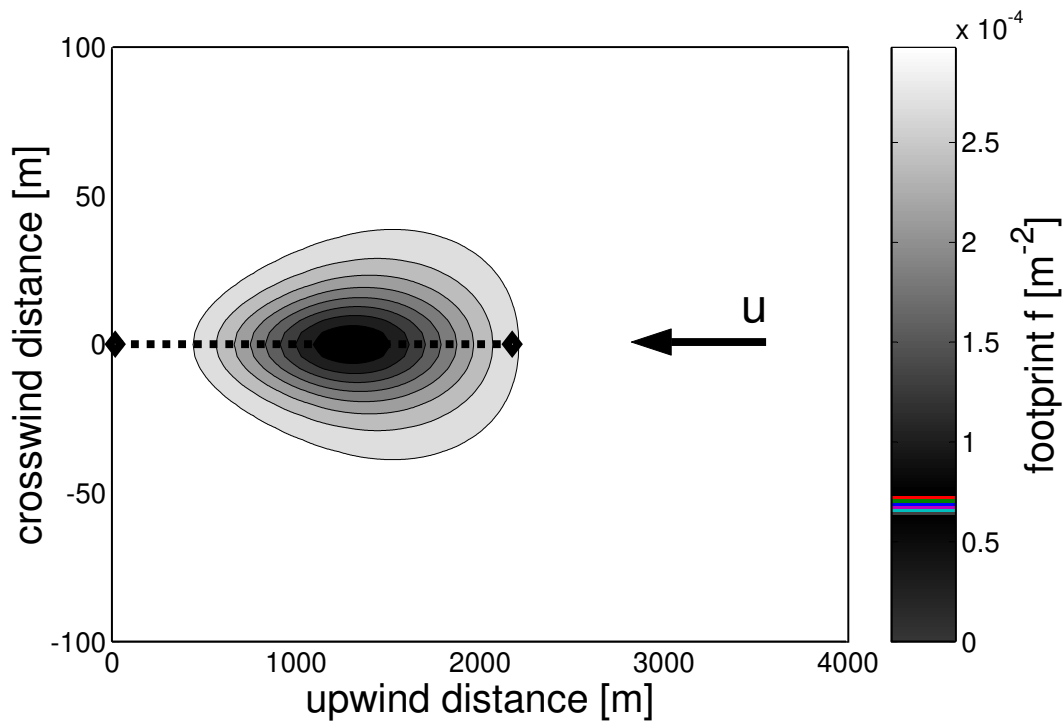
Figure 2.3: As Figure 2.2, except the wind direction is parallel to the LAS's path.

2.3 Experimental site and measurements

2.3.1 Site description and weather conditions

The experiment took place in the summer of 1998 in the southern part of Flevoland (The Netherlands, 52°22'51" N, 05°23'42" E), from 18th July until the 20th August. Flevoland is a vast expanse of reclaimed land created in the 1960s and is mainly used for agricultural purposes. The area consisted of rectangular fields of 0.5 km × 1 km, which were in turn divided into several smaller plots where different crops were grown. In general four crops were grown in the area (95%), namely sugar beet, potatoes, wheat and onions. The few farm buildings, some trees along the main road and the relatively large rectangular fields provided adequate fetch conditions. The area that we focus on is shown in Figure 2.4; note that the surrounding area (not presented in Figure 2.4) is similar, i.e., the same rectangular fields with the same crops.
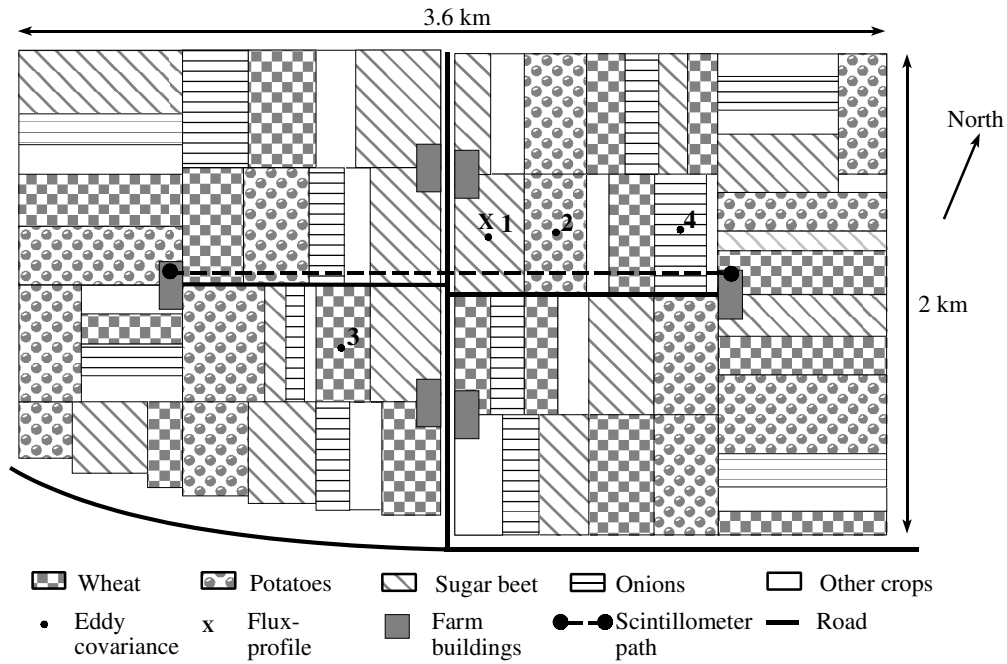
32

Figure 2.4: A plan of the Flevoland area showing the vegetable plots. The dashed line represents the beam of both scintillometers (LAS1 & LAS2) installed on the windmills. The numbered circles and X indicate the locations of the eddy covariance and profile systems.

The main reason this area was selected is that only four crops were grown within it. By measuring the surface fluxes over the four different crops, using eddy covariance (EC) equipment and assuming that all fields with the same crop behave similarly, the area-averaged fluxes can be obtained. It was found that the fractional area of each crop was as follows: sugar beet (26%), potatoes (25.4%), wheat (23%) and onions (25.6%), independent of the wind direction (i.e., isotropic conditions). The small percentage of other crops (carrots, peas and beans) was regarded as onions in this experiment since the crop characteristics were similar (crop height and leaf area index).

During the experiment the weather conditions were very wet and the clay soil was totally saturated by heavy rainfall before and during the experiment. This resulted in a high evaporation rate, making the Bowen-ratio correction (i.e. $\left(1+\dfrac{0.03}{\beta}\right)^{-2}$, see Equation (2.2)) quite significant (25%) for the entire period of the experiment.

2.3.2 Instrumentation and data processing

2.3.2.1 The Large Aperture Scintillometer (LAS)

The LAS used in this experiment was designed and built by the Meteorology and Air Quality Group (METAIR) at Wageningen University. This saturation-resistant optical scintillometer was conceived by Wang et al. (1978) and the electronics are similar to the design of Ochs and Wilson (1993). Two identical LAS instruments were used and placed on two windmills (see Figure 2.4). The first LAS was installed at a height of 11.6 m (denoted LAS1) and the second LAS at a height of 20.4 m (denoted LAS2). To avoid interference between the two scintillometers, the transmitter and receiver of the second LAS were installed in opposite directions. The path length was 2.2 km. Ten-minute averages from the output signal of the LAS were stored on a data logger (21X, Campbell Scientific Ltd., Shepshed, UK). To check whether windmill resonance was significant (primarily at high wind speeds), continuous half-hour spectra were collected with data loggers (CR23X, Campbell Scientific Ltd., Shepshed, UK). In this way less reliable data were rejected from further analysis. Especially for LAS2 many data points had to be removed since vibrations at a height of 20 m in the windmill became significant during windy conditions.

Besides the computation of the fluxes according to the theory (see Section 2.2.1), also the uncertainties (δ, defined as $\delta = 2\sigma$) in those fluxes were calculated. To do this, uncertainties in additional data (T, u, P, R_n, G_s and u_{ec*}) and other parameters (z_{LAS}, L, z_o and d) were measured or estimated. Then each δ_i in the flux due to the uncertainties in each input variable were calculated. Finally the total δ in the flux was derived from the geometric mean of all δ_is.

2.3.2.2 Eddy covariance and additional instruments

In the four crop fields eddy covariance (EC) systems were installed to measure the surface fluxes of heat, water vapour and momentum (see Figure 2.4). The EC systems consisted of a three-dimensional ultrasonic anemometer (Solent Research R2, Gill instruments Ltd., Lymington, UK), a rigid fast response thermocouple (manufactured at METAIR, Van Asselt

34

et al., 1991) and a krypton hygrometer (KH20, Campbell Scientific Ltd., Shepshed, UK). The EC-system in the onion field had no krypton hygrometer. The krypton hygrometers were calibrated before and after the experiment and all the signals were sampled at a rate of 20.8 Hz and collected on a portable computer for post-processing.

In the calculation of means, (co-)variances and fluxes together with their statistical error (Appendix 2A) for each half-hour, corrections for additive trends and misalignment (tilt corrections) were made; turbulent statistic involving the sonic temperature were corrected for humidity effects (Schotanus et al., 1983) and (co-)variances involving humidity were corrected for oxygen sensitivity. Limited sensor response, path averaging and sensor separation effects were accounted for by using frequency response corrections of Moore (1986). The Webb-correction was also applied (Webb et al., 1980). Finally footprint analyses for the EC flux measurements were done to investigate the fetch conditions (Horst and Weil, 1992).

At times the EC systems failed to function properly. To fill in the gaps in the data sets, fluxes of heat were interpolated using fluxes from crops that behaved similarly (e.g. potatoes and sugar beet, see Section 2.4) or by use of an interpolation-scheme using net radiation and soil heat flux data. The latter option was used to fill in the gaps in the onion and wheat data set. This gap-filling scheme was tested on the measured turbulent fluxes around the gaps. For wheat a regression analysis between the measured and simulated (H_{sim}) fluxes of sensible heat yielded: $H_{sim} = 0.98H$, $R^2 = 0.92$ and RMSD = 23 W m^{-2}. For onions the following regression was found: $H_{sim} = 0.97H$, $R^2 = 0.95$ and RMSD = 10 W m^{-2}.

At the same four locations net radiation was measured using three ventilated Schulze-Däke net radiometers (BDA065, Firma Walter Finck, Industrielle Fertigung mechanischer Kleinteile, Crinitz, Germany) and one Funk net radiometer (CN1, McVan Instruments Pty Ltd, Victoria, Australia). Also the soil heat flux was measured using heat flux sensor plates (WS31soil, TNO TPD, Delft, The Netherlands) placed just below the surface. The measured soil heat flux was corrected for differences in heat conductivity between the plate and the soil (Philip, 1961). At the sugar beet site profiles of wind speed, temperature and humidity were measured using cup anemometers (manufactured at METAIR) and psychrometers (radiation shielded and ventilated, manufactured at METAIR). All signals were recorded by data loggers

(CR10 and 21X, Campbell Scientific Ltd., Shepshed, UK). Table 2.1 gives an overview of all the instruments used during the experiment.

Table 2.1: Overview of instrumentation and the installed heights for each site.

Site	1: sugar beet	2: potatoes	3: wheat	4: onions
u,v,w and T_s	Solent R2 (4.8 m)	Solent R2 (3.5 m)	Solent R2 (3.5 m)	Solent R2 (2.8 m)
Temperature (T)	Thermocouple (4.8 m)	Thermocouple (3.5 m)	Thermocouple (3.5 m)	Thermocouple (2.8 m)
Humidity (q)	KH20 (4.8 m)	KH20 (3.5 m)	KH20 (3.5 m)	-
Net radiation (R_n)	Schulze-Däke (2.8 m)	Schulze-Däke (1.9 m)	Schulze-Däke (1.9 m)	Funk (1.6 m)
Soil heat flux (G_s)	WS31soil (0 cm)	WS31soil (0 cm)	WS31soil (0 cm)	Ws31soil (0 cm)
Wind speed (u)	Cup anemometers (3.9, 2.6 and 1.8 m)	-	-	-
Dry and wet bulb (T, T_w)	Psychrometers (3.1 and 1.8 m)	-	-	-

2.4 The eddy covariance results

Except for the observations in the onion field, the closure of the energy budgets of the eddy covariance data sets were analysed (unstable conditions only). For the sugar beet and potatoes data set it was found that the measured fluxes of heat, water vapour and the soil heat flux close 75% to 80% of the net radiation. In the case for the wheat data set a closure of about 90% was found. The results are shown in Table 2.2.

In general sugar beet and potatoes did not reach full cover until July, i.e. they were still in the vegetative stage at the beginning of the experiment. Wheat, which was sown earlier, was already at the end of its reproductive stage, and was in the stage of seed filling and ripening. This process can be seen in Figure 2.5. Figure 2.5b shows that the sensible heat fluxes measured over wheat were much higher than the fluxes observed over the sugar beet (ratio 3:1). Figure 2.5a and Figure 2.5c reveal that the potatoes and onions behaved similarly to the

sugar beet. All three crops had a much higher evaporation rate than wheat. Observed average Bowen-ratio values of sugar beat, potatoes and onions varied between 0.2 and 0.3, while for wheat values of about 1.2 were found.
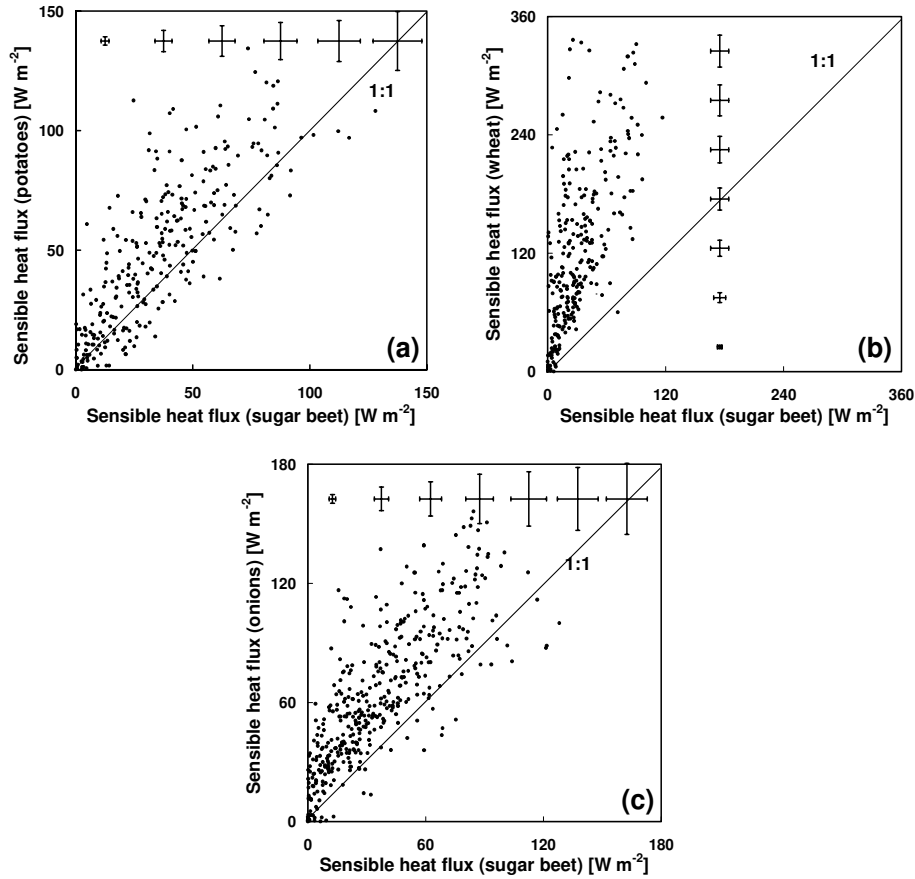

Figure 2.5: Comparison of the 30-minute average eddy covariance measurements over the four plots. (a): $H_{potatoes}$ versus $H_{sugar\ beet}$. (b): H_{wheat} versus $H_{sugar\ beet}$. (c): H_{onions} versus $H_{sugar\ beet}$. The error bars in all three sub-figures represent the average uncertainty of the measured fluxes for each 25 W m^{-2} interval (for (b): 50 W m^{-2}).

Shortly after the beginning of the experiment the potatoes and sugar beet reached their reproductive stage. This means that the development of leafs, stem and roots ceases, i.e. their aerodynamic roughness did not change significantly over the course of the experiment. For the onions a small increase in the roughness length was observed because the vegetative stage for this crop lasted longer. In Table 2.2 the derived roughness lengths are presented.

Table 2.2: Observed roughness lengths (derived from EC data), crop heights and energy balance closure of eddy covariance measurements ($y = H + L_vE + G_s$, $x = R_n$).

	z_o [m]	h_{crop} [m]	Energy balance closure
sugar beet	0.06	0.6 - 0.65	$y = 0.75x$, $R^2 = 0.84$
			RMSD = 106 W m^{-2}
potatoes	0.06	0.9 - 1.0	$y = 0.78x$, $R^2 = 0.86$
			RMSD = 89 W m^{-2}
wheat	0.06 (up to 10 August)	0.8 - 0.9 (up to 10 August)	$y = 0.91x$, $R^2 = 0.88$
	0.04 (after 11 August)	0 (after 11 August)	RMSD = 56 W m^{-2}
onions	0.05 - 0.06	05 - 0.65	-

The results, shown in Figure 2.5 and Table 2.2, reveal that the moderate heterogeneity in this area is primarily caused by differences in thermal properties between the crops. More specifically, contrasting sensible heat fluxes between wheat versus potatoes, sugar beet and onions were found. The area in general has a uniform aerodynamic roughness length. Note that all EC data represented here are the measured turbulent fluxes only; the interpolated fluxes to fill in the gaps are not included in Figure 2.5.

2.5 The scintillometer results

A first footprint analysis for both the LAS at 11.6 m and 20.4 m (Figure 2.2 and Figure 2.3 present examples) showed that under near-neutral conditions 80% and 60% of the measured LAS fluxes came from the area shown in Figure 2.4. This means that only 20% (for LAS1) to 40% (for LAS2) of the measured fluxes have originated from outside this area. During unstable conditions, the contribution of the area to the LAS fluxes increased to more than 95% for both scintillometers. Therefore, in our further analysis, we will focus on this particular area, further denoted as area A. The area-averaged surface fluxes of momentum (τ_A) and sensible heat (H_A) for area A are derived as follows

$$\phi_A = \sum_i f_i \phi_i \qquad (2.10)$$

with $\phi = H$, $-\overline{u'w'}$, R_n and G_s and where f_i is the fractional area of crop i inside area A.
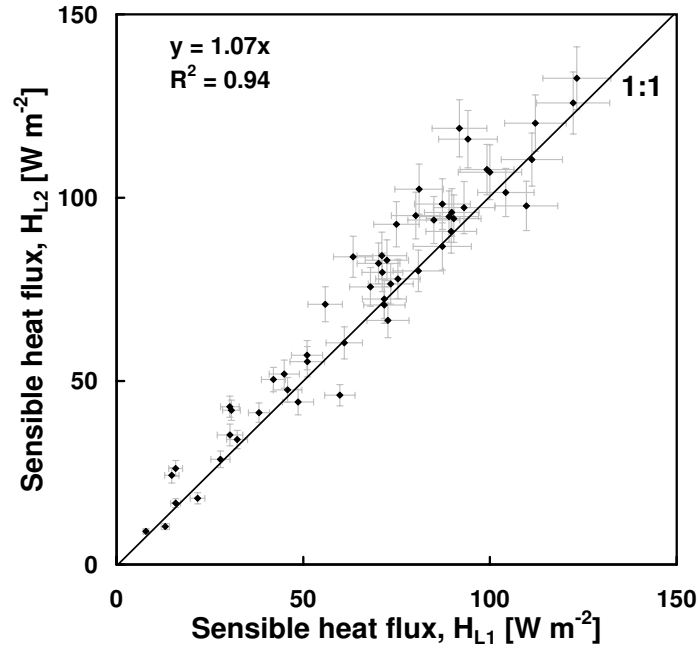

Figure 2.6: Comparison of 30-minute measurements of sensible heat flux derived from LAS1 (H_{L1}) and LAS2 (H_{L2}). Regression analysis $H_{L2} = 1.07H_{L1}$ ($R^2 = 0.94$, RMSD = 7.3 W m^{-2}). The error bars represent the uncertainties (δ) of the measured fluxes.

In Figure 2.6 the scintillometer results (30-minute averages) from both LAS1 and LAS2 are compared; a regression analysis yields: $H_{L2} = 1.07H_{L1}$, $R^2 = 0.94$, revealing that LAS1 gives approximately 7% lower values than LAS2. In Figure 2.7 and Figure 2.8 the results from scintillometers LAS2 and LAS1, respectively are plotted against the area-averaged fluxes (H_A) of area A. Although the uncertainties of most points straddle the 1:1 line, it can be seen that LAS1 slightly underestimates the area-averaged sensible heat flux, while LAS2 shows a 1:1 relation. Regression analysis for LAS2 yields: $H_{L2} = 0.99H_A$ and $R^2 = 0.93$; for LAS1 the following relationship is found: $H_{L1} = 0.86H_A$ and $R^2 = 0.80$.

Figure 2.7: Comparison of 30-minute fluxes of sensible heat derived from LAS2 (H_{L2}) and the area-averaged fluxes of sensible heat for area A (H_A) derived from eddy covariance measurements. Regression analysis $H_{L2} = 0.99 H_A$ ($R^2 = 0.93$, RMSD = 12.8 W m^{-2}). The error bars represent the uncertainties (δ) of the measured fluxes.
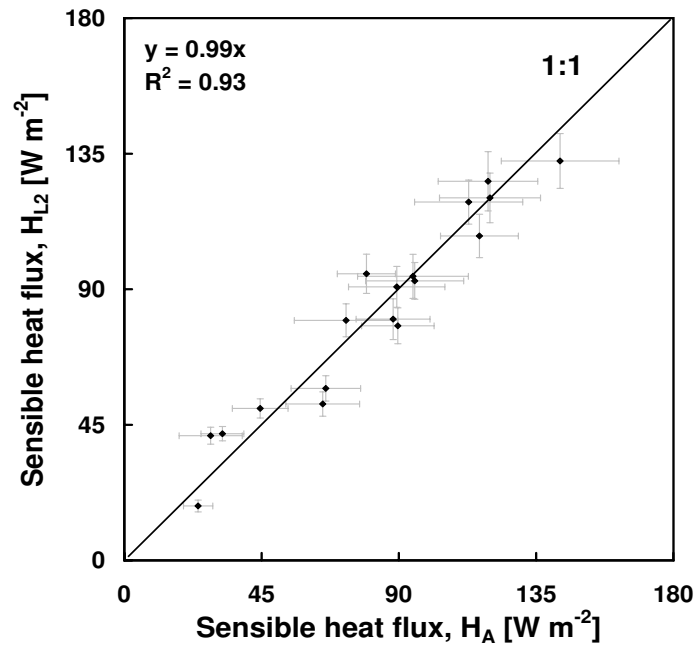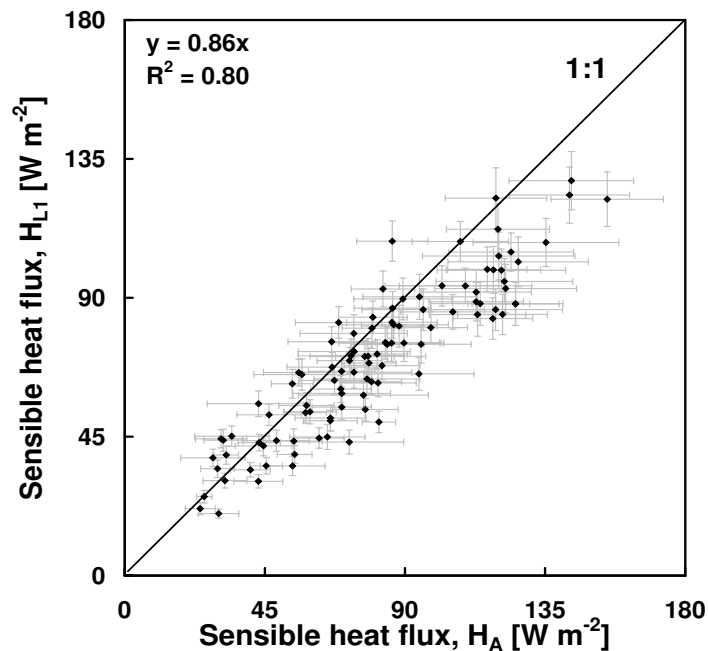

Figure 2.8: Comparison of 30-minute fluxes of sensible heat derived from LAS1 (H_{L1}) and the area-averaged fluxes of sensible heat for area A (H_A) derived from eddy covariance measurements. Regression analysis $H_{L1} = 0.86 H_A$ ($R^2 = 0.80$, RMSD = 10.4 W m^{-2}). The error bars represent the uncertainties (δ) of the measured fluxes.

It can be seen from Figure 2.4 that the patches in area A have a rectangular shape. For situations where the wind direction is perpendicular to the path of the scintillometers the patches have a horizontal size of 500 m. For parallel winds the size of the patches is between 200 m and 300 m. This resulted in a systematic difference in the estimated blending heights. For circumstances when the wind direction was parallel to the path of the LAS a blending height of approximately 5 m was found. For all other cases a blending height was found that varied between 9 and 14 m, implying that the local variations, caused by the individual patches, start to blend at a lower level for circumstances when the wind direction is parallel to the path of the LAS. Therefore it is reasonable to believe that this may affect the fluxes derived from the lower scintillometer. On the other hand the upper scintillometer is always above the blending height.
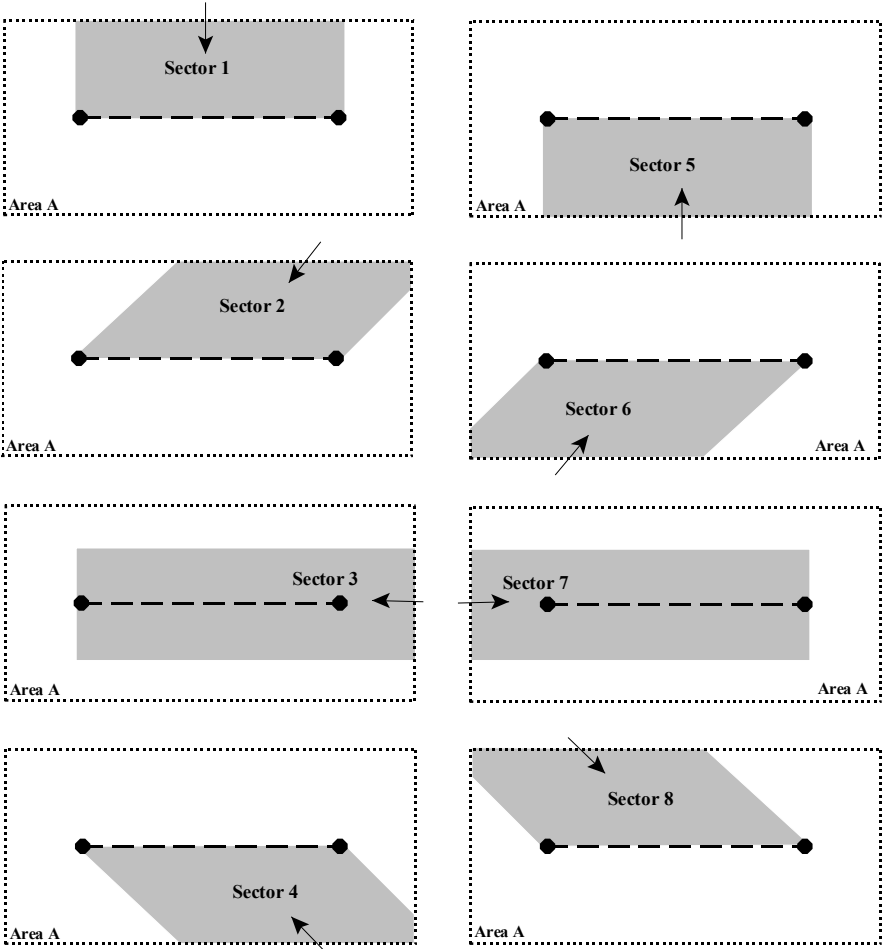

Figure 2.9: Division of area A into eight sectors based on three main wind directions, namely perpendicular, parallel and at an angle of 45 degrees to the path of the LAS. The arrows represent the wind direction. The shaded areas in area A are approximately the areas that influence LAS1, i.e. the source area lies in that particularly shaded area.

To investigate this possible effect, a more thorough footprint analysis was conducted to estimate the SA of the scintillometers. Since the size and location of the SA (which lies inside area A) depends on the atmospheric conditions and the wind direction, the LAS at a certain height area will 'see' areas wherein the relative contribution of the four crops will change constantly depending on the atmospheric conditions. The relative contribution of each crop (f_i), which depends on its fractional area and its orientation inside the SA, can be determined by combining the SA of the LAS with a digital map of area A. Once the relative crop contributions are known the area-averaged surface fluxes of the SA can be determined.

In order to determine the relative crop contributions area A was divided into eight sectors (Figure 2.9). For each sector the average source area was determined and combined with the digital map of area A. Note that this analysis was applied to the lower LAS, i.e. LAS1. The results in Figure 2.10(a) show large variations in the crops contributions (f_i) per sector. When the wind came from sectors 1, 2 and 8, sugar beet, which lies in the centre of the path of LAS1, contributed primarily to the scintillometer-derived sensible heat flux. For opposite wind directions (sectors 4, 5 and 6), wheat contributed more to the scintillometer flux. In general, fields located close to the centre of the path of LAS1 contribute significantly more to the LAS flux.
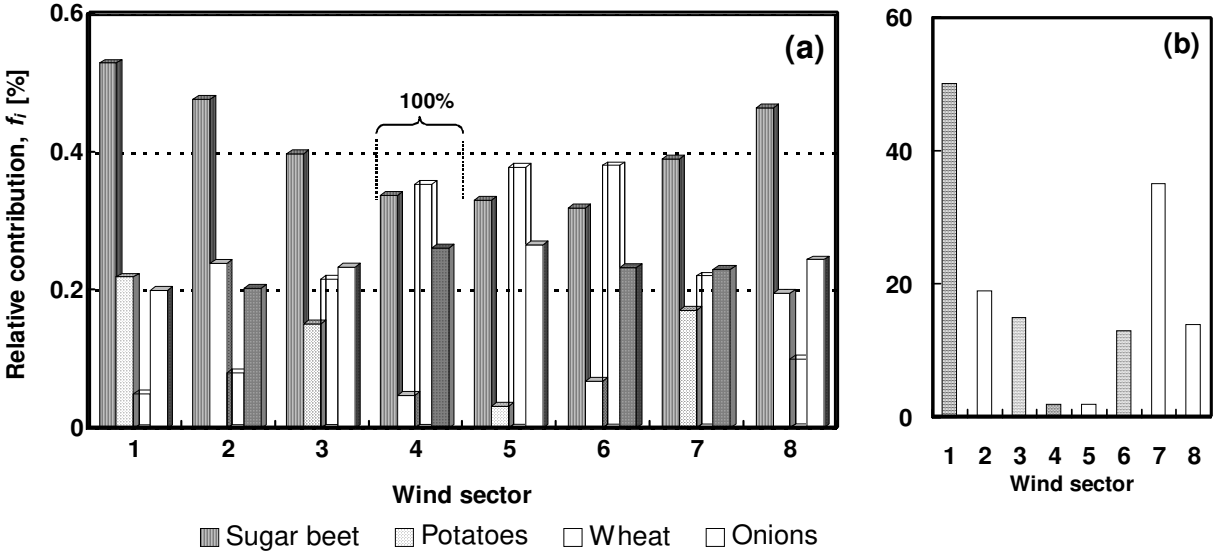

Figure 2.10: (a): The relative contribution of the four crops for each sector. The total contribution per sector is 100%. (b): Histogram of the observed wind direction during the experiment.

42

Based on the wind direction the area-averaged fluxes for area A and for the source areas were arranged. For sectors 3 and 7, when a lower blending height was observed, the area-averaged fluxes for area A were selected (i.e. H_A). For all other sectors, the area-averaged fluxes for the source areas (i.e. H_{SA}) were taken. In Figure 2.11 the 30-minute fluxes of sensible heat derived from LAS1 are plotted against the arranged area-averaged sensible heat fluxes. A regression analysis yields: $H_{L1} = 1.0(H_A \& H_{SA})$ and $R^2 = 0.65$. Although the correlation is less than the one found in Figure 2.8 the results are closer to the 1:1 line. The better agreement can be explained since for a large percentage of the analysed data the flow came from sector 8, 1 and 2 (see Figure 2.10b). In those sectors the contribution of the high evaporating crops (especially sugar beet) is large compared to the contribution of the low evaporating crops (i.e. wheat).
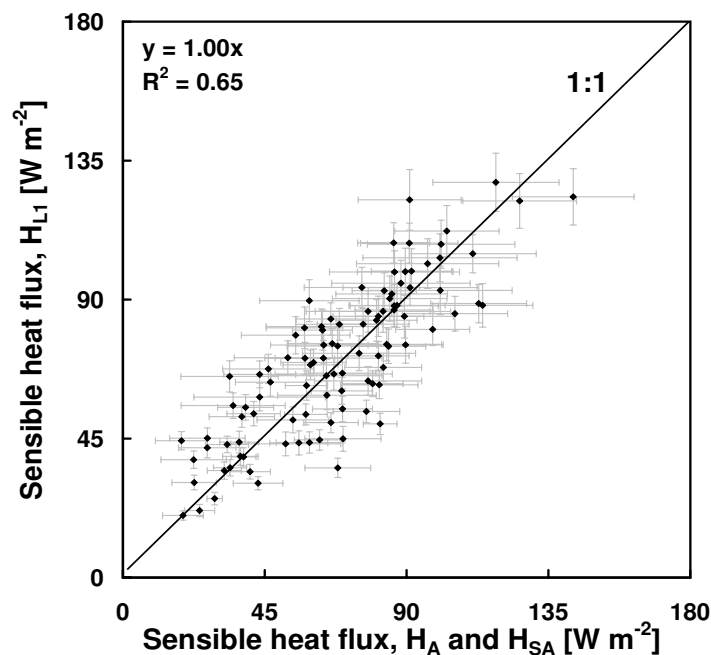

Figure 2.11: Comparison of 30-minute fluxes of sensible heat derived from LAS1 (H_{L1}) and the area-averaged heat fluxes for area A (H_A) and the estimated source area (H_{SA}). Regression analysis $H_{L1} = 1.0(H_A \& H_{SA})$ ($R^2 = 0.65$, RMSD = 12.8 W m^{-2}). The error bars represent the uncertainties (δ) of the measured fluxes.

2.6 Discussion

For the comparison between the sensible heat flux derived from the LAS and the area-averaged sensible heat flux, the fluxes from the individual patches have been aggregated according to Equation 2.10. However the relation between the structure parameter and the sensible heat flux is non-linear and will cause a systematic difference between the aggregated sensible heat flux of the individual patches and the sensible heat flux derived from the LAS (see Appendix 2B). It was found that for the Flevoland area this systematic difference is less than 4%, and therefore this non-linearity effect was ignored in the analysis.

The EC results have shown that sugar beet, potatoes and onions show comparable fluxes of heat, water vapour and momentum, whereas wheat has considerably larger heat fluxes. In the context of MOST, the distribution of the wheat fields that covered 25% of the area, and the considerable contrast in sensible heat flux (and likewise the buoyant production term in MOST), make this area heterogeneous.

Because the area had a uniform surface roughness no footprint analysis was applied for the momentum flux. This is justified by the fact that the LAS method is less dependent on the friction velocity. We have used the footprint model by Horst and Weil (1992), with a second footprint analysis conducted using the model of Schuepp et al. (1990). It was found that the results from the two models were comparable for our cases. A thorough test of the footprint model could not be done, due to the small amount of data points when the wind flow is coming from sectors 4, 5 and 6 (less than 12%, see Figure 2.10b) where wheat dominates and the heterogeneity is maximal.

Both in the studies of Hill and Ochs (1992) and Nieveen and Green (1999) systematic differences were found between two identical LAS instruments installed at the same height. Nieveen and Green found a difference of at least 5% between the 30-minute averaged values of C_T^2, which is close to the 4% difference found by Hill and Ochs. The only explanation Hill and Ochs could give is that a LAS can give enhanced C_n^2 values due to slightly non-uniform illumination of the transmitter and receiver aperture. Unfortunately, we cannot confirm any systematic differences since no comparison experiment took place between LAS1 and LAS2

at the same height. However we can exclude the possibility that tower vibration caused enhanced C_n^2 values since all data were carefully checked.

Using the surface characteristics of the experimental area (β and d) and the LAS set-up (z_{LAS}, D and L) the sensible heat flux (H_{sat}) was calculated taking into account when saturation sets in (assuming the free convection approach). We used the saturation criteria given by Frehlich and Ochs (1990). It was found that saturation occurs for the lower LAS when the area-averaged surface fluxes are larger than 230 W m^{-2}. For the upper LAS this saturation level was 400 W m^{-2}. The observed surface fluxes of sensible heat in the Flevoland area were all below these saturation levels.

2.7 Conclusions

This study has demonstrated that area-averaged fluxes of sensible heat can be derived from a LAS (large aperture scintillometer) that is installed over a heterogeneous area (type A). Two scintillometers were installed, LAS1 at 11.6 m height and LAS2 at 20.4 m height. The fluxes derived from the upper LAS (LAS2) compared well with the area-averaged surface fluxes obtained from in-situ eddy covariance measurements, when using the Monin-Obukhov Similarity Theory (MOST). The slight underestimation of the lower LAS (LAS1) could be assessed by using a blending height model and an analytical footprint model to estimate the source area. Also when the scintillometer was located below the blending height the results indicate that the violation of MOST is small and that reasonable fluxes can be obtained from path-averaged structure parameters after accounting for the spatial flux distribution in the source area.

A footprint analysis of the LAS revealed that the path of a scintillometer should be perpendicular to the main wind direction in order to have the maximum source area. In this way it is possible to obtain representative fluxes from a LAS at scales up to 5 km even when the LAS is located below the blending height. For parallel winds, the source area lies in a rather narrow region between the transmitter and receiver end. For such conditions the representativeness of the LAS is limited.

From the results of this study it follows that in validation experiments (e.g. of remote sensing techniques) using the scintillometer-derived surface fluxes as ground truth over heterogeneous areas, one should carefully check the position of the instruments with respect to the blending height. If the scintillometer is located below the blending height, the individual fluxes of the pixels located in the source area should be carefully weighted, especially when high-resolution images are used.

Appendix 2A. Estimation of tolerance levels for means and (co)variances

For the estimation of tolerance levels we used a method proposed by Van Dijk (2001, personal communication). We defined the tolerance level (δ, or level of uncertainty) of a quantity x as twice the standard deviation ($\delta(x) = 2\sigma(x)$). If quantity x is normally distributed this implies a 96% confidence interval. The tolerance level of the mean value $\bar{x}$ of a number of independent samples (N_{indep}) of quantity x is as follows (assuming the distribution is symmetrical)

$$\delta\left(\bar{x}\right) = \frac{1}{\sqrt{N_{indep}}}\delta\left(x\right) \tag{2A1}$$

where quantity x can be a mean, variance, or covariance.

The eddy covariance data are sampled with constant frequency (20.8 Hz). Since the time scale of turbulent fluctuations is generally larger than $(20.8)^{-1}$ s the samples will slightly overlap, meaning that the number of independent samples will be smaller than the total number of samples.

The number of independent samples can be estimated from the number of sign-changes (around the mean of the signal). It can be shown that the number of sign-changes ($N_{swap,indep}$) in a data set consisting of independent samples can be related to the number of independent samples as follows

$$N_{swap,indep} = N_{indep} p_{swap,indep} \text{ ,} \qquad\qquad (2A2)$$

where $p_{swap,indep}$ is the probability the sign will change.

In an oversampled signal the dependent samples will not alter the number of sign-changes. Therefore the number of sign-changes gives a good measure of the number of independent samples,

$$N_{swap} \cong N_{swap,indep} = p_{swap,indep} N_{indep} \text{ .} \qquad\qquad (2A3)$$

In the case of a non-skewed signal, where positive and negative fluctuations around the mean value (estimated from the same data) have an equal probability, the number of independent samples can be estimated as follows

$$N_{indep} = 2N_{swap} - 1 \text{ .} \qquad\qquad (2A4)$$

With this method uncertainties in the eddy covariance derived fluxes of about 10% were found.

Appendix 2B. Non-linearity between $C_T{}^2$ and H – Taylor approach

As is explained in Section 2.2.1 the LAS provides a path-averaged structure parameter of temperature $\langle C_T^2 \rangle$ (derived from $\langle C_n^2 \rangle$). Assuming for a moment that the LAS is measuring below the blending height, this means that the individual structure parameters of the underlying patches are spatially weighted instead of the fluxes (see also Figure 2.12). Inserting the free convection approach H_{fr} ($H_{fr} \sim c(C_T^2)^{3/4}$)) in the expression of the area-averaged sensible heat flux (Equation 2.10) gives the aggregated free convection flux for area A,

$$\overline{H}_{fc,A} = \sum_{i}^{n} f_i H_{fc,i} = c \sum_{i}^{n} f_i \left(C_{Ti}^2 \right)^{\frac{3}{4}} \qquad (2B1)$$

where C_{Ti}^2 is the C_T^2 value for each patch i at the LAS height. If $\left\langle C_T^2 \right\rangle$ is the value measured by the LAS and $C_{Ti}^2 = \left\langle C_T^2 \right\rangle + \varepsilon_i$, with $\sum_{i}^{n} f_i \varepsilon_i = 0$, Equation 2B1 can be written as follows

$$\overline{H}_{fc,A} = c \left\langle C_T^2 \right\rangle^{\frac{3}{4}} \sum_{i}^{n} f_i \left(1 + \frac{\varepsilon_i}{\left\langle C_T^2 \right\rangle} \right)^{\frac{3}{4}}. \qquad (2B2)$$

A Taylor expansion of Equation 2B2 gives

$$\overline{H}_{fc,A} \cong c \left\langle C_T^2 \right\rangle^{\frac{3}{4}} \sum_{i}^{n} f_i \left(1 + \frac{3}{4} \frac{\varepsilon_i}{\left\langle C_T^2 \right\rangle} - \frac{3}{32} \left(\frac{\varepsilon_i}{\left\langle C_T^2 \right\rangle} \right)^2 \right). \qquad (2B3)$$

Because $\sum_{i}^{n} f_i \varepsilon_i = 0$ this has the consequence that $\overline{H}_{fc,A}$ is smaller than the free convection flux derived from the LAS

$$\overline{H}_{fr,LAS} = c \left\langle C_T^2 \right\rangle^{\frac{3}{4}}. \qquad (2B4)$$

The overestimation of the LAS is systematic, assuming all patches have unstable atmospheric conditions and the violation of MOST in Equation 2B4 is negligible. A simple calculation shows that the overestimation decreases with increasing height of the LAS (Figure 2.13). For the Flevoland area, using eddy covariance data, it was found that the non-linearity causes about 4% difference between the area-averaged flux and the flux derived from a LAS.
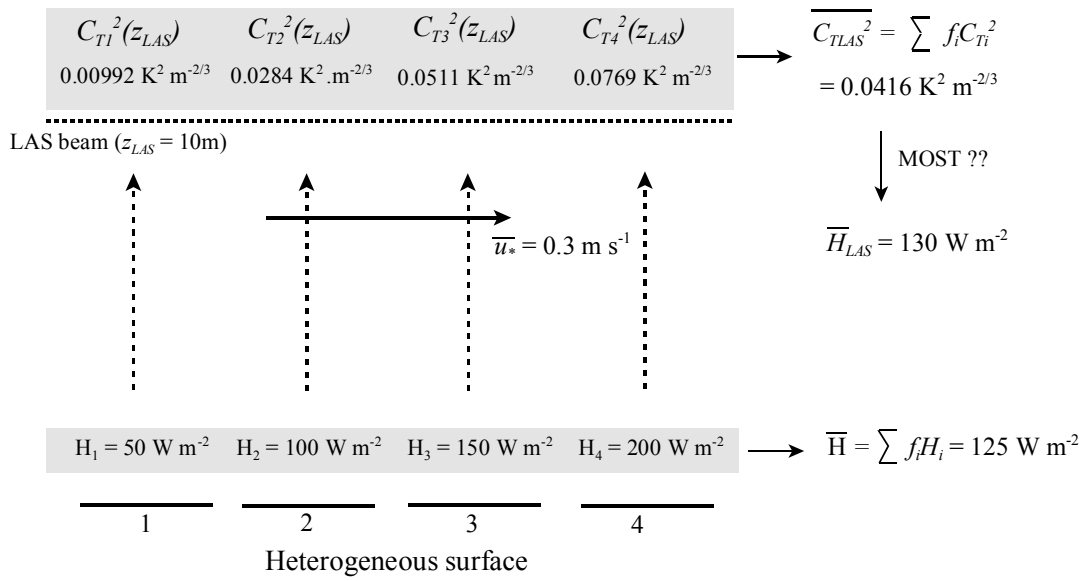
$C_{T1}^{2}(z_{LAS})$ $\quad$ $C_{T2}^{2}(z_{LAS})$ $\quad$ $C_{T3}^{2}(z_{LAS})$ $\quad$ $C_{T4}^{2}(z_{LAS})$ $\qquad \longrightarrow \qquad$ $\overline{C_{TLAS}^{2}} = \sum f_i C_{Ti}^{2}$

0.00992 K^2 m$^{-2/3}$ $\quad$ 0.0284 K^2.m$^{-2/3}$ $\quad$ 0.0511 K^2 m$^{-2/3}$ $\quad$ 0.0769 K^2 m$^{-2/3}$ $\qquad$ = 0.0416 K^2 m$^{-2/3}$

LAS beam (z_{LAS} = 10m)

MOST ??

$\overline{u_*}$ = 0.3 m s^{-1}

$\overline{H_{LAS}}$ = 130 W m^{-2}

H$_1$ = 50 W m^{-2} $\quad$ H$_2$ = 100 W m^{-2} $\quad$ H$_3$ = 150 W m^{-2} $\quad$ H$_4$ = 200 W m^{-2} $\quad \longrightarrow \quad$ $\overline{H} = \sum f_i H_i$ = 125 W m^{-2}

1 $\qquad$ 2 $\qquad$ 3 $\qquad$ 4

Heterogeneous surface

Figure 2.12: Schematic example showing the non-linearity between C_T^{2} and H.
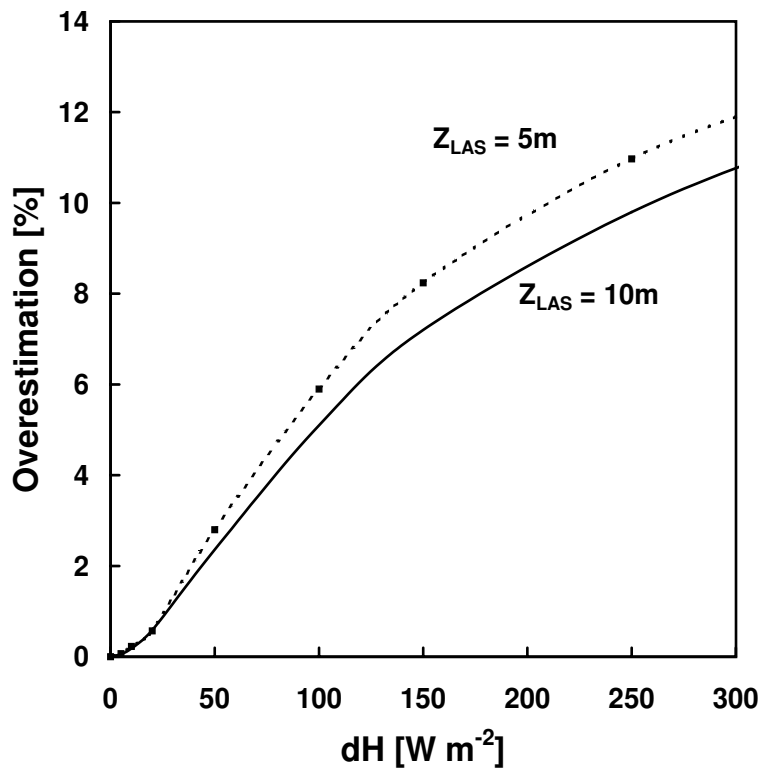

Figure 2.13: Non-linearity as function of measurement (LAS) height.

Chapter 3

Determination of area-averaged water vapour fluxes with large aperture and radio wave scintillometers over a heterogeneous surface

Meijninger, W.M.L., Green, A.E., Hartogensis, O.K., Kohsiek, W., Hoedjes, J.C.B., Zuurbier, R.M. and De Bruin, H.A.R.

3.1 Introduction

The demand for reliable information of the components of the energy and water balance of land surfaces on a spatial scale of watersheds, river basins, and up to the scale size of countries is increasing. One example is the need for reliable estimates of area-averaged evaporation, which is crucial for water management and distribution of sparse fresh water recourses. The development of catchment models can contribute to a greater understanding of the physical hydrological process at these scales. An important aspect is that the performance of most hydrological models relies on robust input data such as area-averaged rainfall and surface fluxes.

Existing measuring techniques e.g., a network of eddy covariance stations or remote sensing techniques (Bastiaanssen et al., 1998), can provide surface fluxes at the required spatial scales. In this paper we will focus on another alternative, the scintillation method. This method has the potential to provide surface fluxes of sensible heat (H) and water vapour (E) at a scale of several kilometres. De Bruin et al. (1996) have demonstrated that this method can be applied over distances of 5 km. Kohsiek et al. (2002a,b) extended the distance to almost 10 km. The scintillation method, using laser and large aperture scintillometers (LAS), has been

extensively tested over homogeneous areas (e.g., Hill et al., 1992; Thiermann, 1992; De Bruin et al., 1995; Green et al., 1997). Recently, the applicability of the LAS in providing area-averaged sensible heat fluxes over heterogeneous terrain has been investigated by Lagouarde et al. (1996), Chehbouni et al. (2000) and Meijninger et al. (2002a).

Laser and large aperture scintillometers operate in the visible and near-infrared wavelength region. In this wavelength region scintillometers are primarily sensitive to temperature fluctuations (Wesely, 1976; Hill et al., 1980; Andreas, 1989), i.e. from these measurements fluxes of sensible heat can be derived. Due to their relatively cheap design and simple use they are used nowadays regularly in micrometeorological experiments (e.g., Poulos et al., 2000 (CASES-99); Beyrich et al., 2002a (LITFASS-98)). A scintillometer that operates at radio wavelengths (radio wave scintillometer or RWS) is most sensitive to humidity fluctuations (Andreas, 1989). Therefore this scintillometer type is more suitable for obtaining water vapour fluxes. Because the system components are expensive, and the set-up and maintenance are demanding, this scintillometer type has not been used often.

In principle, fluxes of sensible heat and water vapour can be obtained using two scintillometers, one operating in the visible to near-infrared region and the other in the radio wavelength region (this is called the two-wavelength method, see Andreas, 1989). Kohsiek and Herben (1983) were the first to estimate E using a radio wave scintillometer ($\lambda = 10$ mm) over a distance of 8.2 km. They obtained water vapour fluxes, which agreed fairly well with Priestley-Taylor estimates. McMillen et al. (1983) tested a LAS and a radio wave scintillometer ($\lambda = 1.7$ mm) over flat farmland over a distance of 1.37 km at a height of 3.7 m. The results of this experiment were discussed by Hill et al. (1988). It must be noted that the measurement height used in this experiment may have been too low (see Section 4.2). Recently, Green et al. (2000, 2001) did experiments with a radio wave scintillometer ($\lambda = 11$ mm) and a LAS over flat pastoral land and over a vineyard valley, respectively. One of the findings of Green et al. (2000) was that at low frequencies, absorption scintillations caused by humidity fluctuations resulted in an overestimation of E. Furthermore, Green et al. (2001) experienced problems possibly caused by dry air advection from the surrounding area.

The main objective of this paper is to investigate the applicability of a combined large aperture scintillometer and radio wave scintillometer (further denoted as LAS-RWS) to obtain

fluxes of sensible heat and water vapour over a flat heterogeneous terrain. Because it is possible to estimate the water vapour flux indirectly also from a stand-alone LAS, using estimates of the area averaged net radiation (R_n) and soil heat flux (G_s), we will also consider L_vE obtained in this way (L_v is the latent heat of vaporisation). In order to achieve these goals a field experiment has been conducted in Flevoland (The Netherlands) where the selected flat patchy area consisted of rectangular plots (500 m × 250 m) compromising crops of sugar beet, potatoes, wheat and onions. The Flevoland area can be classified as a type A area (Shuttleworth, 1988; De Bruin, 1989). Eddy covariance (EC) devices were installed in four plots, each covered with a different crop, to provide independent observations of the surface fluxes. Meijninger et al. (2002a) showed that reasonable area-averaged sensible heat fluxes could be derived from a LAS installed over this area for unstable atmospheric conditions. In this study we will again confine ourselves to unstable conditions and will consider only the water vapour flux.

3.2 Theory

Both the LAS and the RWS used in this study measure the variance of the logarithm of intensity fluctuations ($\sigma_{\ln I}^2$), obtained as follows. The transmitter part of the scintillometer emits a beam of electromagnetic radiation with a certain wavelength (λ) along the surface at height z_s and path length L to the receiver part of the system. At the receiver side the intensity fluctuations of the electromagnetic signal (called scintillations) are measured ($\sigma_{\ln I}^2$), which are caused by atmospheric turbulence in the path of propagation. For the LAS the connection between the propagation statistics of the electromagnetic radiation ($\sigma_{\ln I}^2$) and the atmospheric turbulence (the path-averaged structure parameter of the refractive index of air $\langle C_n^2 \rangle$) is as follows (Wang et al., 1978),

$$\sigma_{\ln I}^2 = 0.892 \langle C_n^2 \rangle D^{-7/3} L^3, \qquad l_o << F << D << L_o \qquad (3.1)$$

where D is the aperture diameter of LAS, L the path length and F is the first Fresnel zone ($F = \sqrt{\lambda L}$). F must lie within the inertial subrange of eddy sizes, which is bordered by the inner length scale ($l_o \approx 1$ mm) and the outer length scale of turbulence ($L_o \approx$ measurement

height). Since D (= 0.15 m) is larger than F (≈ 0.04 m) this scintillometer can be regarded as a large aperture scintillometer. The RWS is a small aperture scintillometer (or point source/detector) since F (≈ 5 m) is larger than D (= 0.6 m). In this case the relationship is as follows (Wang et al., 1978),

$$\sigma_{\ln I}^2 = 0.496 \langle C_n^2 \rangle k^{7/6} L^{11/6}, \qquad l_o << D << F << L_o \qquad (3.2)$$

where k ($= 2\pi / \lambda$) is the optical wavenumber. Again F must lie within the inertial subrange, although the height of the RWS in this experiment (i.e. L_o) is rather close to F (see Section 3.3).

The structure parameter of the refractive index of air C_n^2 is primarily related to temperature and humidity fluctuations in the atmosphere (Hill et al., 1980)

$$C_n^2 = \frac{A_T^2}{\overline{T}^2} C_T^2 + \frac{2 A_T A_Q}{\overline{T Q}} C_{TQ} + \frac{A_Q^2}{\overline{Q}^2} C_Q^2. \qquad (3.3)$$

The variables A_T and A_Q are dependent on the wavelength of the electromagnetic radiation, the absolute temperature (T) and the absolute humidity (Q). Note that in this study Q is expressed in kg m^{-3}. This means that if C_n^2 is measured at two different wavelengths, which are most sensitive to temperature or humidity fluctuations, respectively, both the structure parameters of temperature (C_T^2) and humidity (C_Q^2) can be determined and assuming T and Q are perfectly correlated ($C_{TQ} = (C_T^2 C_Q^2)^{0.5}$). This method is called the two-wavelength method. A sensitivity analysis done by Andreas (1989) revealed that using a combination of near-infrared and radio wave scintillometers is best for deriving the structure parameters of both temperature and humidity. At visible and near infrared wavelengths C_n^2 is primarily determined by temperature fluctuations, whereas in the radio wave region humidity fluctuations are dominant. In this study we will adopt the method of Hill et al. (1988) to determine C_T^2 and C_Q^2 from the C_n^2 values obtained from the LAS and the RWS.

Once C_T^2 and C_Q^2 are known the fluxes of heat and water vapour can be derived by applying the Monin-Obukhov Similarity Theory (MOST) (Wyngaard et al., 1971),

$$\frac{C_T^2(z_s - d)^{2/3}}{T_*^2} = \frac{C_Q^2(z_s - d)^{2/3}}{Q_*^2} = f_{TT}\left(\frac{z_s - d}{L_{Ob}}\right),$$ (3.4)

where f_{TT} is a universal function of $(z_s\text{-}d)/L_{Ob}$, with the Obukhov length $L_{Ob} = \dfrac{u_*^2 T}{g k_v T_*}$, the

temperature scale $T_* = \dfrac{-H}{\rho c_p u_*}$, the humidity scale $Q_* = \dfrac{-E}{u_*}$ and the friction velocity u_*. Here ρ

is the density of air, k_v the von Kármán constant, c_p the specific heat of air at constant pressure, g the gravitational acceleration and d the zero-displacement height. In this study we will confine ourselves to unstable conditions and we will use the MOST relationship f_{TT} in Equation (3.4) given by De Bruin et al. (1993). Furthermore we will focus on the applicability of Equation (3.4). For that reason we will use an aggregated momentum flux derived from the eddy covariance measurements, notably

$$-\left\langle \overline{u'w'} \right\rangle = \sum_i - f_i \left(\overline{u'w'}\right)_i ,$$ (3.5)

where f_i is the fractional area of each crop.

Note that for the derivation of the structure parameters C_T^2 and C_Q^2 the correlation coefficient between T and Q (R_{TQ}) within the inertial subrange is required. Hill et al. (1988) found values of R_{TQ} between -0.99 to $+0.98$, while Kohsiek (1984) found an average value of $+0.75$. In the Flevoland experiment R_{TQ} values were found that varied between $+0.7$ and $+0.95$ for unstable conditions, although these values were derived from eddy covariance data (i.e. integrated over the entire spectrum instead of within the inertial subrange). This justifies also the use of the same MOST function for the derivation of the sensible heat and water vapour flux from path averaged structure parameters (Hill, 1989). It should be noted that R_{TQ} values are observed that differ significantly from ± 1 (De Bruin et al., 1999), but this applies to other conditions.

3.3 Aspects of surface heterogeneity and scintillometry

As shown in the previous section one has to rely on MOST in order to derive the fluxes from path-averaged structure parameters (C_T^2 and C_Q^2) measured with scintillometers. Since MOST requires horizontal homogeneity the question arises whether the scintillation method can be applied over heterogeneous areas. To deal with surface heterogeneity Wieringa (1976) introduced the concept of a blending height. The blending height is thought to be the level where the signatures of individual patches tend to merge due to turbulent mixing (i.e. blending). Figure 3.1 shows schematically the various layers above a heterogeneous surface. In this case the blending height can be regarded as the upper limit of the internal boundary layers (IBL) that develop as the flow encounters different surface types.
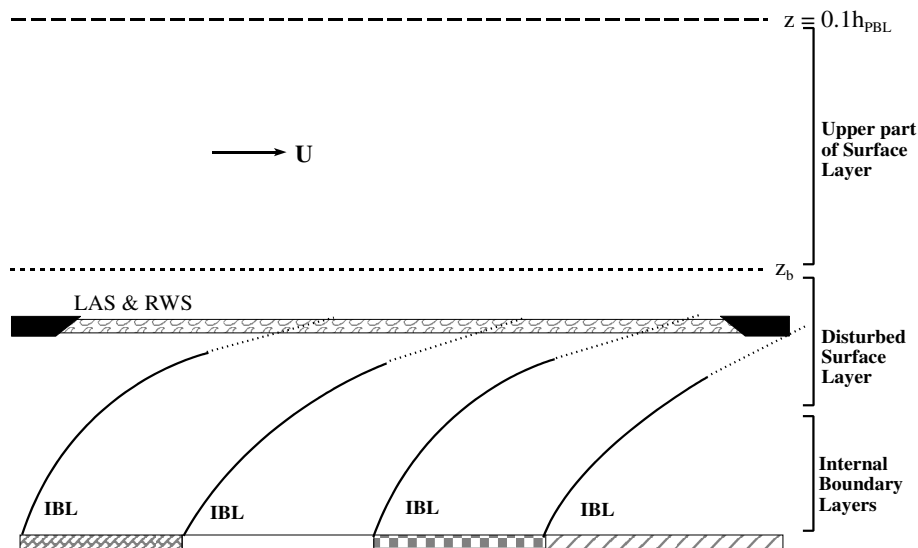

Figure 3.1: Schematic diagram of the various layers over a heterogeneous flat landscape, showing the heights of the top of the internal boundary layers, the top of the surface layer (z), which is assumed to be a tenth of the boundary layer and the blending height (z_b).

The blending height primarily depends on the horizontal scale of the inhomogeneities (Mason, 1988; Mahrt, 1996); to a lesser degree the stability also plays a role (Wood and Mason, 1991). Furthermore, there are indications that there are different blending heights for different quantities. Wood and Mason (1991), as well as Ma and Daggupaty (1998), found different blending heights for momentum and heat transfer. In this study we will use as a working

hypothesis the blending height proposed by Mason (1988) as the level where the path-averaged C_T^2 and C_Q^2 are in equilibrium with the area-averaged surface fluxes H and E.

For type A landscapes (Shuttleworth, 1988; De Bruin, 1989), such as the Flevoland area, the horizontal scales of inhomogeneities are much smaller than 10 km. In this case it is expected that primarily the lower part of the surface layer (SL) is affected by the inhomogeneities (see Figure 3.1). In contrast the uniform well-developed planetary boundary layer (PBL), which is not affected, 'feels' one area-averaged surface flux of heat, water vapour and momentum. Meijninger et al. (2002a) demonstrated that reliable area-averaged surface fluxes of sensible heat could be derived from scintillometer measurements, which were conducted above the blending height.

When the scintillometer is located below the blending height, inside the disturbed SL (see Figure 3.1), the situation is more complicated. The scintillometer will 'see' the fluxes from the individual patches. Because turbulence is not in equilibrium with the local vertical gradients or structure parameters, MOST might be violated. However, Lagouarde et al. (1996) and Chehbouni et al. (1999) showed that reasonable fluxes could be derived from path-averaged structure parameters measured with a LAS, installed well below the blending height, over two adjacent surfaces with contrasting vegetation. Their findings revealed that the violation of MOST was small. Also Meijninger et al. (2002a) found that the scintillation technique performed reasonably well below the blending height. The derived fluxes of sensible heat agreed fairly well with the averaged surface fluxes of the source area.

Below the blending height a portion of the upstream surface, called the source area (SA), influences the sensors. This area can be interpreted as the 'field of view' of the instrument. Footprint models can estimate the SA (Schuepp et al., 1990; Horst and Weil, 1992, 1994; Horst, 1999). Meijninger et al. (2002a) applied the analytical flux footprint model proposed by Horst and Weil (1992) to estimate the source area of a LAS. In this case the footprint function has to be combined with the spatial weighting function of the scintillometer. In Figure 3.2 and Figure 3.3 two examples are presented for a LAS installed at a height of 11.6 m and a path length of 2.2 km. In Figure 3.2 the wind direction is perpendicular and in Figure 3.3 parallel to the path of the scintillometer. In both examples the atmospheric conditions are similar (z_o = 0.1 m, L_{Ob} = -50 m and σ_v = 0.5 m s^{-1}). The black diamonds stand for the transmitter and receiver part of the scintillometer and the bars line represents the beam. It can

be seen in both Figure 3.2 and Figure 3.3 that the area, which contributes most to the scintillometer, lies approximately in the centre of the path shifted a little in the upwind direction. The size of the area and the peak of the source area primarily depend on the measurement height and the stability of the atmosphere. In this study we will apply the same blending height and footprint approaches following Meijninger et al. (2002a).
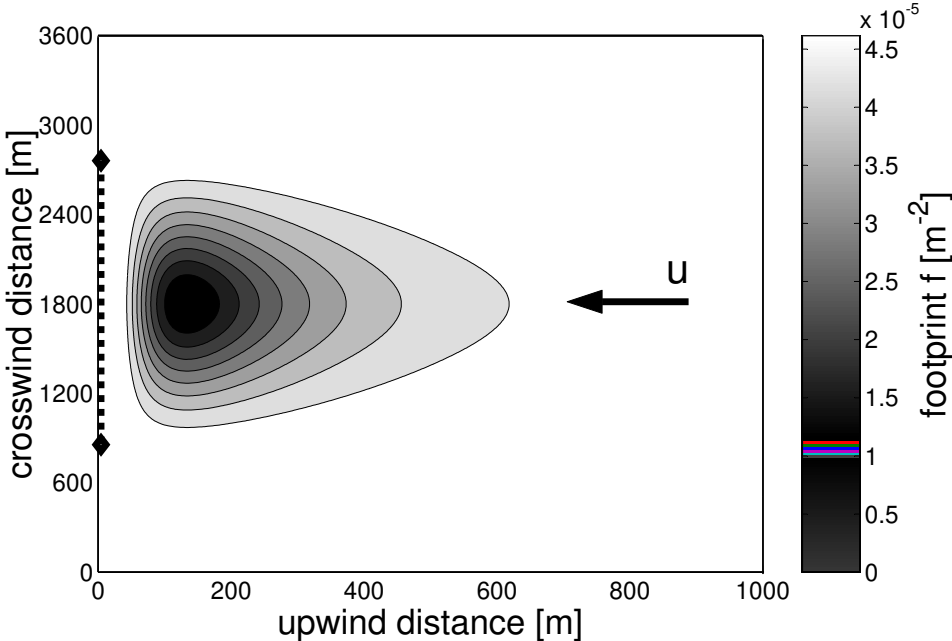

Figure 3.2: The footprint of a LAS when the wind direction is perpendicular to its path. The bars line represents the beam of the scintillometer and the diamonds stand for the transmitter and receiver part.
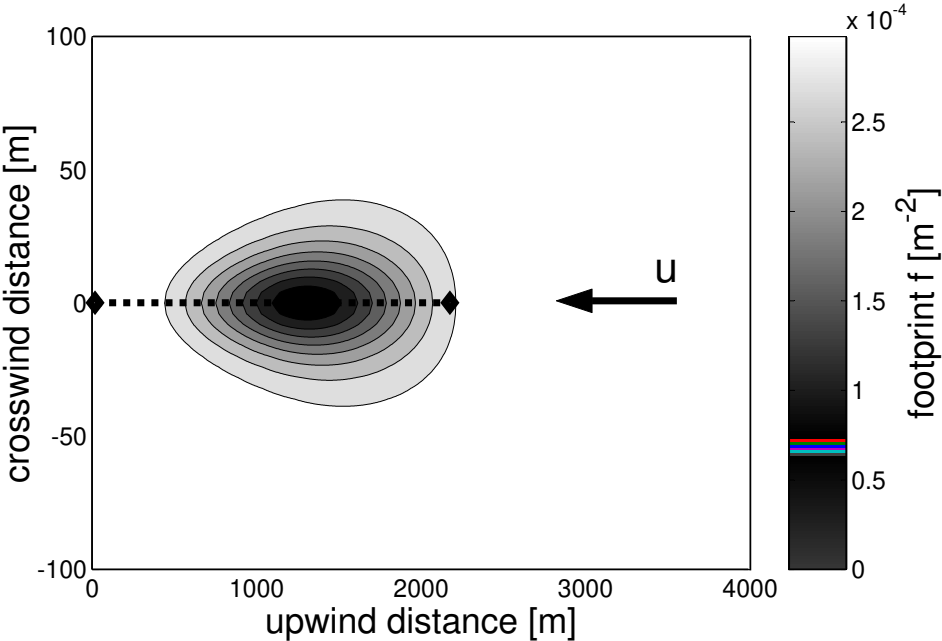

Figure 3.3: As Figure 3.2, except the wind direction is parallel to the optical path.

3.4 Experimental site and measurements

Flevoland (The Netherlands, $52^o22'51"$ N, $05^o23'42"$ E) is mainly used for agricultural purposes; the area is completely flat and consists of rectangular plots where different crops are grown. The experiment, which was part of a larger experiment to study the behaviour of the scintillation method (Meijninger et al., 2002a), took place in the summer of 1998 between the 18th July and the 20th August. The main reason that this heterogeneous area was selected is that in general only four crops were grown namely sugar beet, potatoes, wheat and onions. Each crop type covered approximately 25% of the total area, which is shown in Figure 3.4, independent of the wind direction (i.e., isotropic conditions). By measuring the surface fluxes over the four crops using eddy covariance systems and assuming that all fields with the same crop behave similarly, independent measurements of the area-averaged surface fluxes were obtained.
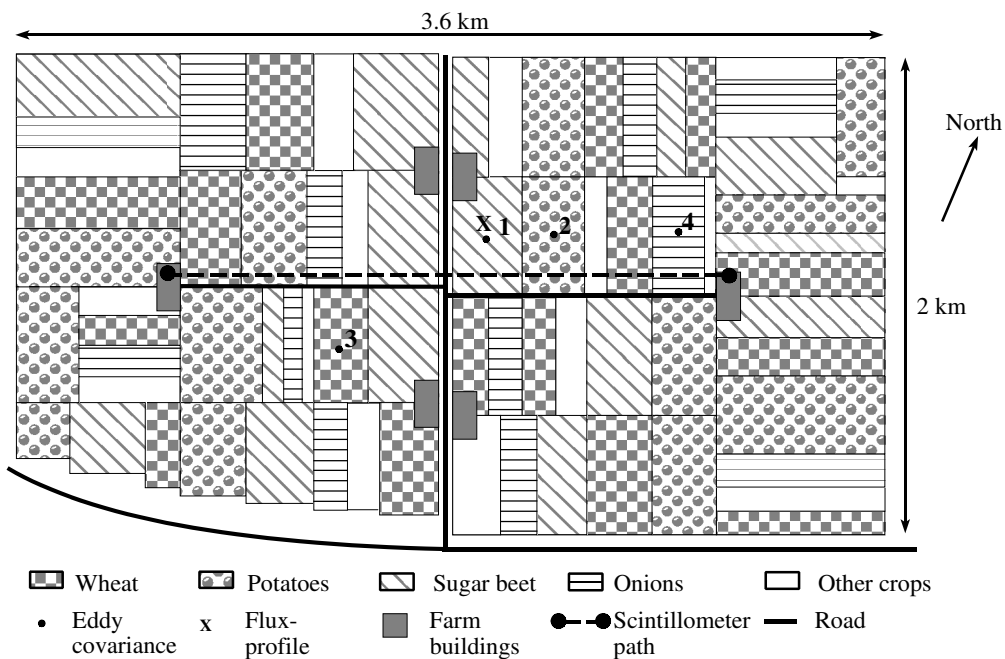

Figure 3.4: A plan of the experimental area (area A) showing the vegetable plots. The dashed line represents the beam of both scintillometers (LAS and RWS) installed on two windmills. The numbered circles and x indicate the locations of the eddy covariance and profile systems.

The scintillometers were mounted in two suitable windmills at a height of 11.6 m (LAS) and 10.9 m (RWS). The path length was 2.2 km. Half-hourly averaged spectra were measured in order to check whether windmill vibrations affected the scintillometer signal. Scintillometer

data whose spectra showed spikes, induced by windmill vibrations, were eliminated; this occurred primarily on days with strong winds. Especially for the RWS, which was mounted on small platforms welded on the sides of the tubular towers of the windmill, a large percentage of data had to be removed. It was found that the platforms also produced vibrations induced by the windmill. As a result a small data set, primarily collected at the beginning of the experiment, remained. The LAS experienced less vibration since it was fixed on a small handle that was welded on to the tubular towers.

The LAS designed and built by the Meteorology and Air Quality Group at Wageningen University and Research Centre (METAIR) has an aperture size (D) of 0.15 m and the wavelength of the light beam, emitted by the transmitter, is 930 nm. The instrument is similar to the design of Ochs and Wilson (1993). The output signal, C_n^2 expressed as a voltage, was recorded by a data logger at 1 Hz (21X, Campbell Scientific Ltd, Shepshed, UK) after it had been band-pass filtered between 0.2 and 400 Hz. The lower cut-off frequency of the LAS was set at 0.2 Hz, to avoid absorption fluctuations that could corrupt the signal and lead to increased C_n^2 values (Nieveen et al., 1998).

The RWS, developed by the Eindhoven University of Technology (The Netherlands), is the same as used by Green et al. (2000, 2001). The instrument operates at a wavelength of 11 mm (27 GHz) and the diameter (D) of the antenna is 0.6 m. The signal was band-pass filtered between 0.03 and 20 Hz and was sampled at a rate of 10 Hz by a datalogger (21X, Campbell Scientific Ltd, Shepshed, UK). In this study the lower cut-off frequency was set at 0.03 Hz, as suggested by Green et al. (2000), since they observed enhanced C_n^2 values caused by humidity absorption scintillations.

In four plots eddy covariance instruments were installed (see Figure 3.4). The systems consisted of a three-dimensional ultrasonic anemometer (Solent Research R2, Gill instruments Ltd., Lymington, UK), a thermocouple (manufactured at METAIR, Van Asselt et al., 1991) and a krypton hygrometer (KH20, Campbell Scientific Ltd., Shepshed, UK). Except for the system in the onion field whose EC system had no krypton hygrometer. The krypton hygrometers were calibrated before and after the experiment by METAIR. Raw data were collected at a rate of 20.8 Hz. Means, (co-)variances and fluxes (30-minute) together with their uncertainties, were calculated, taking into account corrections for tilt and additive trends, frequency response corrections to account for limited sensor response, separation and path

averaging. The sonic temperature was corrected for humidity effects and the krypton hygrometer was corrected for oxygen effects. Furthermore, the Webb-correction was applied. Finally, footprint analyses were conducted to investigate the representativeness of the measurements (Horst and Weil, 1992).

Net radiation (R_n) and soil heat flux (G_s) were measured at the same four locations, using ventilated Schulze-Däke (BDA065, Firma Walter Finck, Industrielle Fertigung mechanischer Kleinteile, Crinitz, Germany) and Funk (CN1, McVan Instruments Pty Ltd, Victoria, Australia) net radiometers. The soil heat flux was measured with heat flux sensor plates (WS31soil, TNO TPD, Delft, The Netherlands) and corrected afterwards for differences in thermal properties between the plate and the soil (Philip, 1961). Vertical profiles of dry-bulb and wet-bulb temperatures, using ventilated psychrometers (manufactured by METAIR), and wind speed (cup anemometers, manufactured by METAIR) were measured at the sugar beet site. An overview of the instruments and the sensor heights is given in Table 3.1. For more detailed information the reader is referred to Meijninger et al. (2002a).

Table 3.1: Overview of instrumentation and sensor heights for each site.

Site	1: sugar beet	2: potatoes	3: wheat	4: onions
u,v,w and T_s	Solent R2 (4.8 m)	Solent R2 (3.5 m)	Solent R2 (3.5 m)	Solent R2 (2.8 m)
Temperature (T)	Thermocouple (4.8 m)	Thermocouple (3.5 m)	Thermocouple (3.5 m)	Thermocouple (2.8 m)
Humidity (Q)	KH20 (4.8 m)	KH20 (3.5 m)	KH20 (3.5 m)	-
Net radiation (R_n)	Schulze-Däke (2.8 m)	Schulze-Däke (1.9 m)	Schulze-Däke (1.9 m)	Funk (1.6 m)
Soil heat flux (G_s)	WS31soil (0 cm)	WS31soil (0 cm)	WS31soil (0 cm)	Ws31soil (0 cm)
Wind speed (u)	Cup anemometers (3.9, 2.6 and 1.8 m)	-	-	-
Dry and wet bulb (T, T_w)	Psychrometers (3.1 and 1.8 m)	-	-	-

3.5 The eddy covariance results

Shortly after the start of the experiment sugar beet, potatoes and onions reached their reproductive stage. Together with the very wet conditions this resulted in a high evaporation rate for most crops. In contrast to the other crops, wheat was already at the end of its reproductive stage, resulting in a lower evaporation rate. The measured Bowen-ratio values varied between 0.2 and 0.3, except for wheat where values of about 1.2 were observed. These features can be seen in Figure 3.5 and Figure 3.6. In Figure 3.5 the measured sensible heat fluxes of the four crops are compared. In Figure 3.6 the latent heat fluxes L_vE are compared, where L_v is the latent heat of vaporisation of water. Figure 3.5a, c and Figure 3.6a, c show the similarity between the sugar beet, potatoes and onions. The contrasting fluxes for wheat are
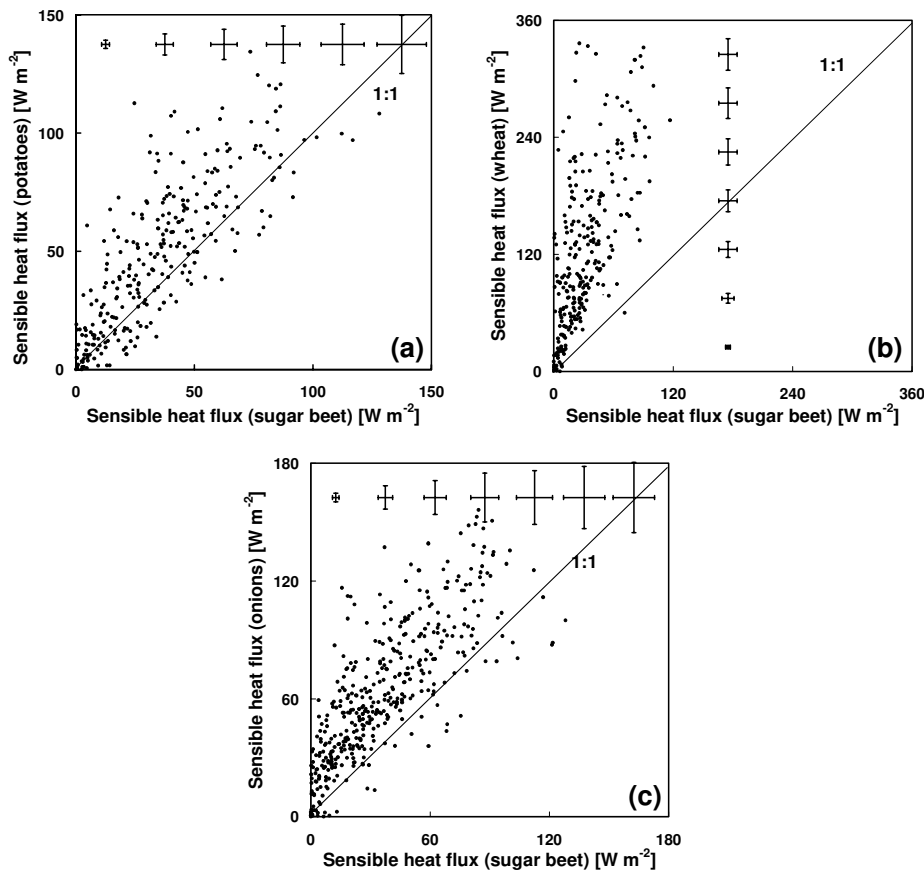

Figure 3.5: Comparison of the 30-minute average eddy covariance measurements of sensible heat (*H*) over the four plots. (a): *H*potatoes versus *H*sugar beet. (b): *H*wheat versus *H*sugar beet. (c): *H*onions versus *H*sugar beet. The error bars in all three sub-figures represent the average uncertainty of the measured fluxes for each 25 W m-2 interval (for (b): 50 W m-2).
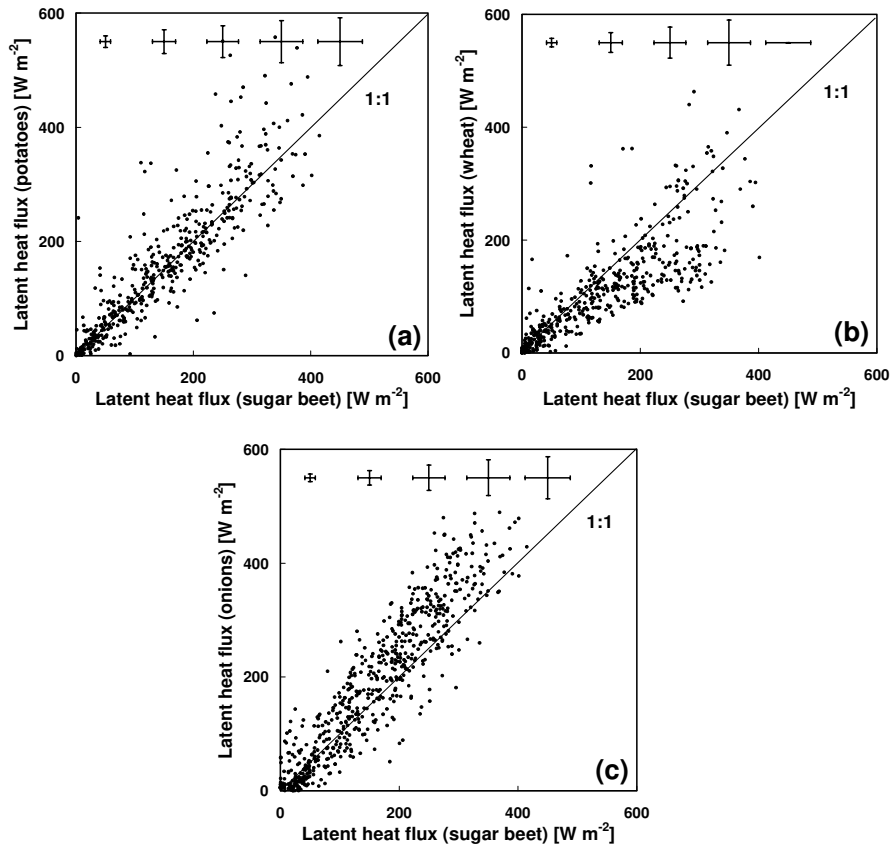
62

Figure 3.6: As Figure 3.5 except for the measured fluxes of latent heat (L_vE). (a): $L_vE_{potatoes}$ versus $L_vE_{sugar beet}$. (b): L_vE_{wheat} versus $L_vE_{sugar beet}$. (c): L_vE_{onions} versus $L_vE_{sugar beet}$. The error bars in all three sub-figures represent the average uncertainty of the measured fluxes for each 100 W m^{-2} interval.

clearly noticeable in Figure 3.5b where the fluxes of sensible heat are compared with the observations above the sugar beet. Also Figure 3.6b, although less noticeable, shows the different behaviour of wheat. Note that all fluxes here are derived from turbulence measurements, except for the onion data set, where the latent heat flux was derived as the energy budget residual term, since no turbulent water vapour fluctuations were available.

Comparison of the momentum fluxes between all four crops revealed that no variations in the aerodynamic roughness length (for momentum) were observed, implying that the inhomogeneities in the Flevoland area are mainly caused by differences in thermal properties, i.e. the contrasting fluxes of sensible and latent heat between the crops. In the context of MOST, and thus also the scintillation method, the Flevoland area must be regarded as a heterogeneous area due to the considerable contrast in sensible heat fluxes and likewise the buoyant production term of MOST.

A footprint analysis conducted by Meijninger et al. (2002a) revealed that the source area of the scintillometers, during unstable conditions, lies within the area shown in Figure 3.4. This area will be further denoted as area A. Several authors reported energy balance closure problems when analysing their eddy covariance data (Oncley et al., 2000); non-closure gaps of 10% to 30% are quite common. An analysis of the closure of the energy budgets of the eddy covariance measurements in the Flevoland area revealed that the fluxes of heat, latent heat and soil heat close about 75% to 80% of the net radiation for the sugar beet and potatoes data set. For the wheat data set a closure of about 90% was found. These results are also shown in Table 3.2. Finally the closure of the energy budget of area A is presented in Figure 3.7. A closure of 88% was found.

Table 3.2: Energy balance closure of eddy covariance measurements ($y = H + L_vE + G_s$, $x = R_n$) over the four crops.

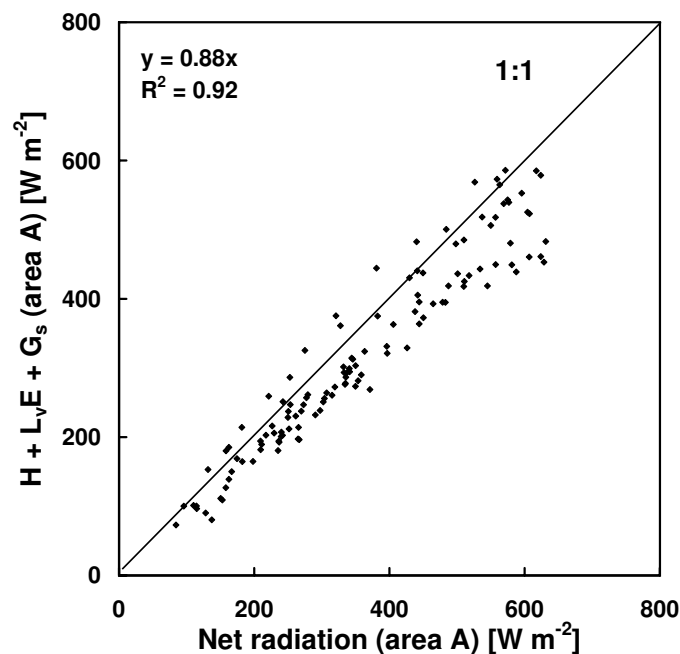| Site	1: sugar beet	2: potatoes	3: wheat	4: onions
Energy b. closure	$y = 0.75x$	$y = 0.78x$	$y = 0.91x$	
	$R^2 = 0.84$	$R^2 = 0.86$	$R^2 = 0.88$	-
RMSD [W m^{-2}]	106	89	56	

Figure 3.7: The energy balance closure for area A, based on the aggregated in-situ eddy covariance, net radiation and soil heat flux measurements (30-minute averages). Regression analysis ($H + L_vE + G_s$) = $0.88R_n$ ($R^2 = 0.92$, RMSD = 45 W m^{-2}).

The results in Table 3.2 clearly show that for the low evaporating crops (i.e. wheat) the closure is almost 100%. For the high evaporating crops (i.e. sugar beet and potatoes) a gap of about 20% was found. Important to note is that all three-eddy covariance systems were identical as well as the processing of the data. During the experiment eddy covariance measurements were made over bare soil conducted by the University of Lleida (Spain) using slightly different instruments. They found a closure of about 95%. These results suggest that the EC sensors miss a small part of the turbulent exchange over the high evaporating crops. Whether this is caused by methodological and/or instrumental problems is not known (see also first workshop of the Energy Balance EXperiment (EBEX) 2000, http://www.geo.uni-bayreuth.de/mikrometeorologie/EBEX2000/EBEX.html).

3.6 The scintillometer results

3.6.1 The LAS-RWS configuration

The sensible heat fluxes derived from the combined LAS-RWS system are identical to the sensible heat fluxes derived from the stand-alone LAS, which were evaluated by Meijninger et al. (2002a). Before evaluating the LAS-RWS derived latent heat fluxes ($L_vE_{LAS-RWS}$) with the area-averaged latent heat fluxes derived from eddy covariance systems, first the energy balance closure of the LAS-RWS system was analysed. The results are shown in Figure 3.8. A regression analysis yields: $(H + L_vE + G_s) = 0.95R_n$, $R^2 = 0.82$. Although the energy budget closes fairly well, the scatter is quite large compared with the results shown in Figure 3.7. At near-neutral conditions the fluxes derived from the LAS-RWS tend to be too high (within the circle shown in Figure 3.8). A plausible explanation is that low frequency humidity absorption fluctuations, which do not contribute to the flux, corrupted primarily the C_n^2 values of the RWS (and thus L_vE) as was noted by Nieveen et al. (1998) and Green et al. (2000).

Due to the rectangular shape of most plots of crops in the Flevoland area the blending height in the area depends primarily on the wind direction. Meijninger et al. (2002a) found a blending height of about 5 m for conditions when the wind direction was parallel to the path of the scintillometers. For non-parallel wind directions the horizontal scale of the plots was larger (see Figure 3.4) and the blending height varied between 9 and 14 m, depending on the

65

stability of the atmosphere. The findings indicate that for parallel wind directions the signatures of the different plots start to blend well below the measurement height of the scintillometers. For all other wind directions this blending process starts at a higher level, which is situated above the measurement height. Based on these findings Meijninger et al. (2002a) could explain the systematic lower fluxes of sensible heat derived from the LAS measurements by accounting for the spatial flux distribution in the source area of the scintillometers.
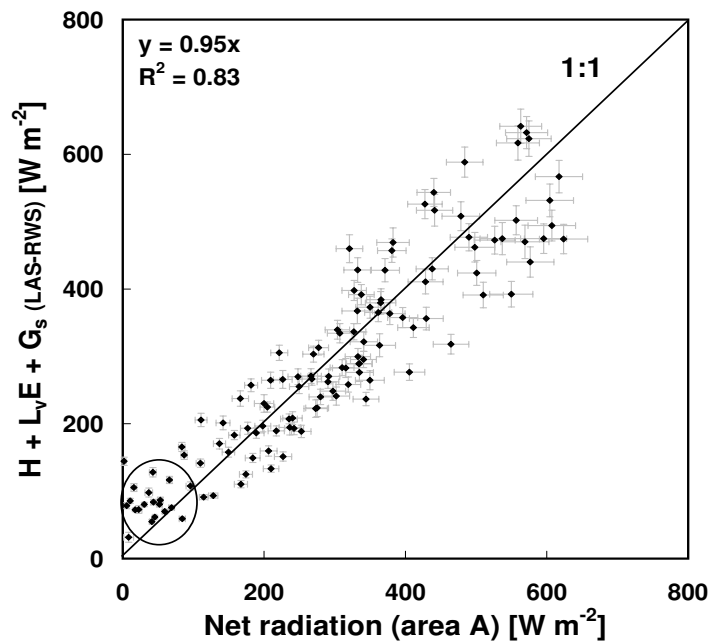

Figure 3.8: The energy balance closure of area A, based on the fluxes derived from the combined LAS-RWS system and aggregated net radiation and soil heat flux measurements. Regression analysis ($H + L_vE + G_s$) = $0.95R_n$ (R^2 = 0.83, RMSD = 66 W m^{-2}). The error bars represent the uncertainties (δ) of the measured fluxes.

Following the same approach as Meijninger et al. (2002a) we arranged the area-averaged latent heat flux for area A and the source areas based on the observed wind direction. This means that for parallel wind conditions the area-averaged latent heat fluxes for area A were selected (L_vE_A); for all other wind directions the area-averaged latent heat fluxes for the source areas (L_vE_{SA}) were taken. In Figure 3.9 the 30-minute fluxes of latent heat derived from the combined LAS-RWS scintillometer are plotted against the arranged area-averaged surface latent heat fluxes. A regression analysis yields: $L_vE_{LAS-RWS}$ = 1.08(L_vE_A & L_vE_{SA}) and R^2 = 0.78. It can be seen that the scintillometer-derived latent heat fluxes are slightly higher than

66

the area-averaged latent heat fluxes. It must be noted that the overall effect of the blending height and footprint approach was small. Similar results were found when only the area-averaged fluxes for area A were selected. The small amount of scintillometer data and the relatively wet conditions at the start of the experiment (i.e. moderate heterogeneous conditions) may have diminished the effectiveness of the approach.
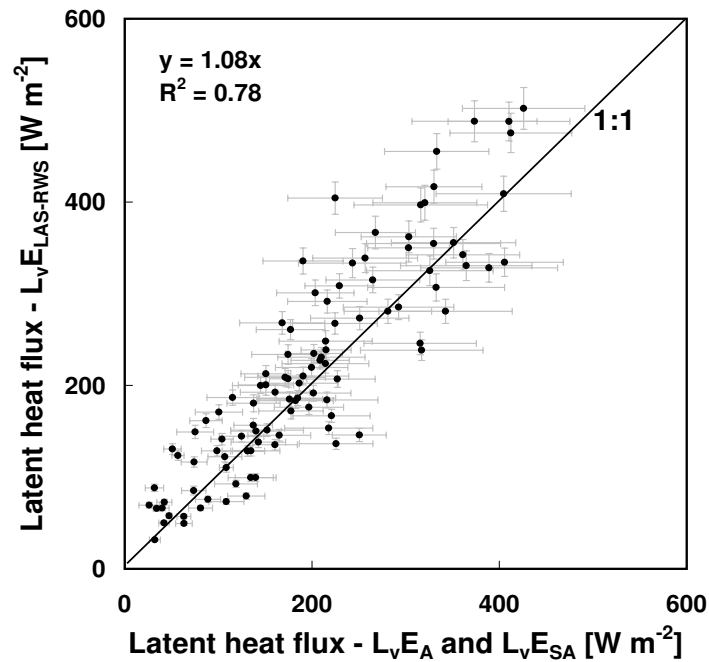

Figure 3.9: Comparison of 30-minute latent heat fluxes derived from the LAS-RWS configuration and the area-averaged latent heat fluxes for area A (L_vE_A) and the estimated source area (L_vE_{SA}). Regression analysis $L_vE_{LAS-RWS}$ = 1.08(L_vE_A & L_vE_{SA}) (R^2 = 0.78, RMSD = 56 W m^{-2}). The error bars represent the uncertainties (δ) of the measured fluxes.

There are several possible reasons for the slight difference and scatter in Figure 3.9. First, the closure failure of the energy budget of the EC technique; second there is a non-linear relationship between structure parameters and fluxes (Meijninger et al., 2002a). It was found that for the Flevoland area this might result in typically 8% higher fluxes of latent heat derived from the RWS. Finally, it is possible that some external vibrations passed the already strict filter criteria and corrupted the C_n^2 values from the RWS.

3.6.2 The 'stand – alone' LAS

Meijninger et al. (2002a) have demonstrated that a LAS can provide representative fluxes of sensible heat for this particular Flevoland area. Therefore it is worthwhile to investigate whether a stand - alone LAS, as an alternative to the RWS, can also provide accurate fluxes of water vapour. By using the method proposed by Green and Hayashi (1998), i.e., including the energy balance equation, to correct for humidity fluctuations of the LAS signal, H, the Bowen-ratio (β) and also L_vE are solved. In Figure 3.10a the latent heat fluxes derived from the LAS are plotted against the area-averaged fluxes, thereby following the same procedures as was done for the LAS-RWS system. A regression analysis gives: $L_vE_{LAS} = 1.16(L_vE_A$ & $L_vE_{SA})$, $R^2 = 0.88$. It is obvious from the EC results in Section 3.5 that the closure failure of the energy budget is the reason for the 16% offset in Figure 3.10a. It is interesting to note that when the latent heat flux is evaluated as the residual term of the energy balance (i.e., assuming H is correct) for the in-situ EC measurements, a perfect 1:1 was found between these aggregated latent heat fluxes and the fluxes from the LAS.
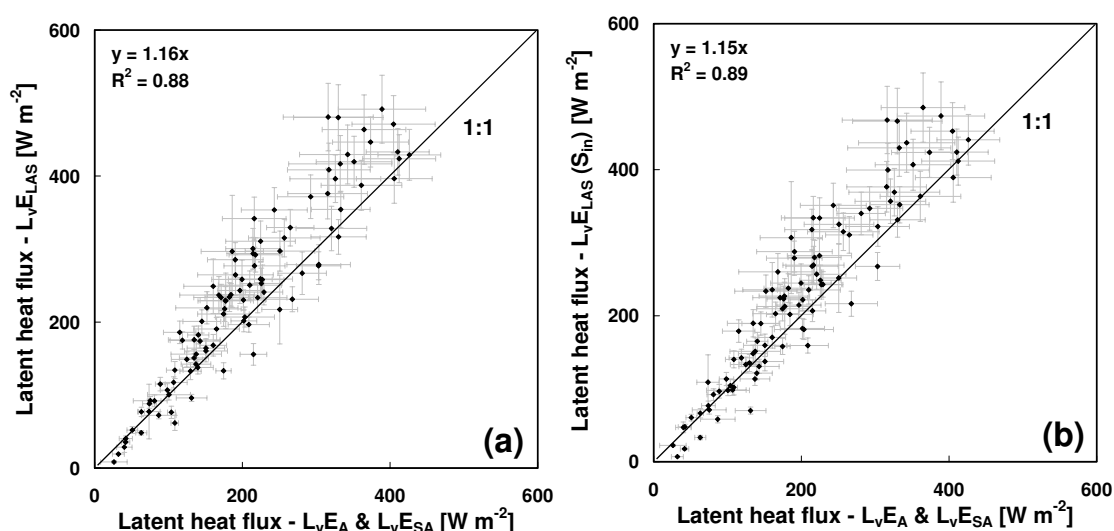

Figure 3.10: (a): Comparison of 30-minute latent heat fluxes derived from the stand-alone LAS and the area-averaged latent heat fluxes for area A (L_vE_A) and the estimated source area (L_vE_{SA}). Regression analysis $L_vE_{LAS} = 1.16(L_vE_A$ & $L_vE_{SA})$ ($R^2 = 0.88$, RMSD = 55 W m^{-2}). The error bars represent the uncertainties (δ) of the measured fluxes. (b): As (a) except the net radiation and soil heat flux are estimated from incoming solar radiation. Regression analysis L_vE_{LAS} (S_{in}) = 1.15(L_vE_A & L_vE_{SA}) ($R^2 = 0.89$, RMSD = 54 W m^{-2}).

In many practical applications area average observations of net radiation and soil heat flux are not available. The net radiation can be estimated from global radiation (S_{in}) and the soil heat flux can be assumed to be 10% of the net radiation. For conditions in the Netherlands and when the soil is fully covered with vegetation this is a good approximation for G_s (see e.g., Stull, 1988). The results are presented in Figure 3.10b. It can be seen that the results are almost identical with the results shown in Figure 3.10a. A regression analysis gives: $L_vE_{LAS} = 1.15(L_vE_A \& L_vE_{SA})$, $R^2 = 0.89$.

3.7 Conclusions

An experiment was conducted in Flevoland (The Netherlands) to test the applicability of the scintillation method over more non-uniform areas. A large aperture scintillometer (LAS) and a radio wave scintillometer (RWS) were installed over a heterogeneous terrain, which consisted of many plots and where the heterogeneity was primarily caused by variations in thermal properties in the presence of a uniform surface roughness. The fluxes of water vapour derived from the LAS-RWS configuration (also called the two-wavelength method) agreed reasonably well with the area-averaged fluxes of water vapour derived from aggregated in-situ eddy covariance systems. As far as we know these are the first published results of a relatively large time series of combined LAS and RWS data over a well-defined area compared with independent flux measurements.

This study also has demonstrated that a stand - alone LAS can provide good estimates of area-averaged fluxes of water vapour. These results from a single LAS and some additional data such as wind speed, air temperature and global radiation emphasise the potential of the scintillation technique for future meteorological, hydrological and other related studies.

Further study of the scintillation method over heterogeneous areas having significant variations in both thermal properties and surface roughness are required, and also the applicability of the technique during stable conditions. Evidence obtained from the Flevoland experiment supports the notion that so long as the scintillometers are located above the blending height the scintillation method can be expected to work well.

Chapter 4

Sensible heat fluxes over irrigated areas in western Turkey determined with a large aperture scintillometer

Meijninger, W.M.L. and De Bruin, H.A.R.

4.1 Introduction

The loss of water by evaporation from the soil (E) and transpiration from the vegetation (T) (together ET) is an important factor in water resource and hydrological and meteorological studies especially in arid and semi-arid areas. In the past decades several methods have been developed for estimating evaporation, transpiration and the sensible heat flux (H). Direct measurements (lysimeters, eddy covariance), hydrological models like SWAP (Droogers, 2000) or SLURP (Kite, 2000) or more recent applied remote sensing methods like SEBAL (Bastiaanssen, 2000) are examples of methods to estimate E, T and H.

The objective of this special issue of the Journal of Hydrology is to compare the actual evapotranspiration (ET) determined with various remote sensing methods as well as with existing operational hydrological models with ground-truth observations (Kite and Droogers, 2000). This paper deals with these ground-truth data. Since the spatial scale of these models is of several kilometres or more we decided to use the large aperture scintillometer. Note that the eddy-covariance method (nowadays considered the most reliable method to estimate H and ET) cannot be applied on this scale. The scintillation method, which is based on the Monin-Obukhov Similarity Theory (MOST), has been applied and tested by several authors

(Wesely 1976b; Hill et al., 1992; Green et al., 1997; De Bruin et al., 1995). De Bruin et al. (1996) were one of the first who applied the method over a path as long as 5 km. Their results show that the scintillation method is a good alternative for estimating the sensible heat flux. Readers are referred to the collection of papers about micrometeorology and scintillation compiled by Andreas (1990).

Two large aperture scintillometers (LAS) were manufactured and installed near Menemen in western Turkey by the Meteorology and Air Quality Group of the Wageningen Agricultural University (METAIR). In addition, METAIR installed a small micrometeorological station over an irrigated cotton field next to the second LAS. The results from June 26 and August 29 (the LANDSAT overpass dates) will be presented. Furthermore, to illustrate the operational applicability of the long-path LAS, the 24-hour averages of the sensible heat flux derived from the LAS installed over the valley, will be shown for the entire growing season.

4.2 Theory

The large aperture scintillometer is a device that measures the turbulent intensity of the refraction index of air. The instrument consists of a transmitter and a receiver. The transmitter emits electromagnetic radiation at a wavelength λ (0.94 µm) over a known path length (L) to the receiver, where the fluctuations of the light intensity are analysed. These fluctuations in intensity, known as scintillations, are caused by inhomogeneities in the refraction index of air (n) along the path of propagation.

The turbulent intensity of the refraction index of air can be expressed in the refractive index structure parameter (C_n^2), defined as

$$C_n^2 = \frac{\overline{\left[n(r_1)^2 - n(r_2)^2\right]}}{r_{12}^{2/3}},$$

(4.1)

where $n(r)$ is the refraction index at location r and the distance r_{12} lies in between the so-called inner scale of turbulence (marks the transition between the inertial and viscous dissipation range of eddy sizes and is of the order of 0.5 - 1 cm) and the outer scale (dominant inhomogeneities which are of the order of the height of the beam above the surface). Other

72

structure parameters such as those of temperature, humidity or a velocity component are defined similarly.

Primarily, temperature and humidity fluctuations cause fluctuations in the refractive index of air. C_n^2 is therefore related to the structure parameter of temperature C_T^2, humidity C_Q^2 and the covariance term C_{TQ}. This is expressed in the following relationship (Kohsiek, 1982b; Hill et al., 1992)

$$C_n^2 = \frac{A_T^2}{\overline{T}^2}C_T^2 + \frac{2A_T A_Q}{\overline{TQ}}C_{TQ} + \frac{A_Q^2}{\overline{Q}^2}C_Q^2 .$$

(4.2)

The constants A_T and A_Q are a function of wavelength (λ), temperature (T), absolute humidity (Q in kg m^{-3}) and air pressure (P). Generally, the first term, containing C_T^2, is much greater than the other two terms, except for the case when the Bowen-ratio β (= $H/L_v E$, where L_v is the latent heat of vaporisation) is much smaller than 1. Assuming that temperature and humidity are perfectly correlated Equation 4.2 can be written as (Wesely, 1976a)

$$C_T^2 \approx C_n^2 \left(\frac{T^2}{A_T^2}\right)^2 \left(1 + \frac{0.03}{\beta}\right)^{-2} .$$

(4.3)

It is seen that ignoring the last term will lead to an underestimation of the C_T^2 of 10% or more if $\beta \approx 0.5$ resulting in an underestimation of the sensible heat flux (see e.g. Green and Hayashi, 1998). In this study we will use Equation 4.3 with different values for β.

According to Monin-Obukhov Similarity Theory (MOST) the normalised temperature structure parameter C_T^2 is a universal function (f_T) of $(z-d)/L_{Ob}$. Wyngaard et al. (1971) found for unstable conditions ($L < 0$) that

$$\frac{C_T^2 (z-d)^{2/3}}{T_*^2} = f\left(\frac{z-d}{L_{Ob}}\right) = c_{T1}\left(1 - c_{T2}\frac{z-d}{L}\right)^{-2/3} ,$$

(4.4)

in which the temperature scale $T_* = -H/(\rho c_p u_*)$, H the sensible heat flux, L_{Ob} the Obukhov length, z the height, d the displacement height, ρ the air density, c_p the specific heat of air at

constant pressure, u_* the friction velocity and c_{T1} and c_{T2} are empirical constants. In this study we used the values of $c_{T1} = 4.9$ and $c_{T2} = 9$ found by De Bruin et al. (1993). The Obukhov length L_{Ob} is defined as

$$L_{Ob} = \frac{u_*^2 T}{g k_v T_*},$$

(4.5)

where k_v is the von Kármán constant. If z becomes large (> 30 m) the conditions of local free convection are approached. In that case Equation 4.4 transforms into

$$H = \rho c_p b (z - d) \left(\frac{g}{T} \right)^{1/2} \left(C_T^2 \right)^{3/4},$$

(4.6)

where b is an empirical constant (De Bruin et al., 1995). It is seen that the sensible heat flux becomes independent of u_* in the free convection limit. In general, a second equation for u_* is required. In this study we will use the standard flux-profile relationship (Panofsky and Dutton, 1984)

$$u_* = \frac{k_v u}{\ln \left(\frac{z_u - d}{z_0} \right) - \Psi_m \left(\frac{z - d}{L_{Ob}} \right) + \Psi_m \left(\frac{z_0}{L_{Ob}} \right)},$$

(4.7)

where Ψ_m is a known universal stability function of $(z-d)/L_{Ob}$, u the wind speed and z_0 the roughness length. By solving the Equations 4.4, 4.5 and 4.7 iteratively, T_* and u_* (and thus H) can be obtained.

4.3 Experimental

The Gediz river basin is situated in the western part of Turkey. Its coastal plain is bordered on the Gulf of Izmir and its origin in the east lies close to Usak. About 10% of the total area is irrigated and fed by two reservoirs. The main crops are grapes, cotton and fruit trees. Further details about the field sites can be found in Kite and Droogers (2000). METAIR installed two

large aperture scintillometers (0.15 m aperture) near Menemen. These were manufactured by METAIR using the design of Ochs et al. (1980). METAIR improved the electronics and added a low cost programmable data logger (BL1500, Z-World, Davis, CA, US) that reboots after a power failure. The first LAS was set-up over a transect across the valley east of Menemen between Belen and Suluklu. Both transmitter (north side) and receiver (south side) were installed on the roof of a house using local main voltage for the power supply. Since short power failures are rather common in the area a backup battery system was installed at the receiver site. The orientation of the path of the LAS' beam was almost north-south and had a length of 2700 m. The effective height of the LAS, derived from the weighting function and a topographical map, was estimated to be 18 m (Figure 4.1). Ten minute averages and standard deviations from both C_n^2 and the signal strength were stored on a built in small data logger. The effective roughness length (z_0) was derived from the Davenport classification (Davenport, 1960) and photographs of the area. We found z_0 = 0.25 m. The displacement height (d) was set at zero because it fell within the uncertainty of the effective height of the LAS.
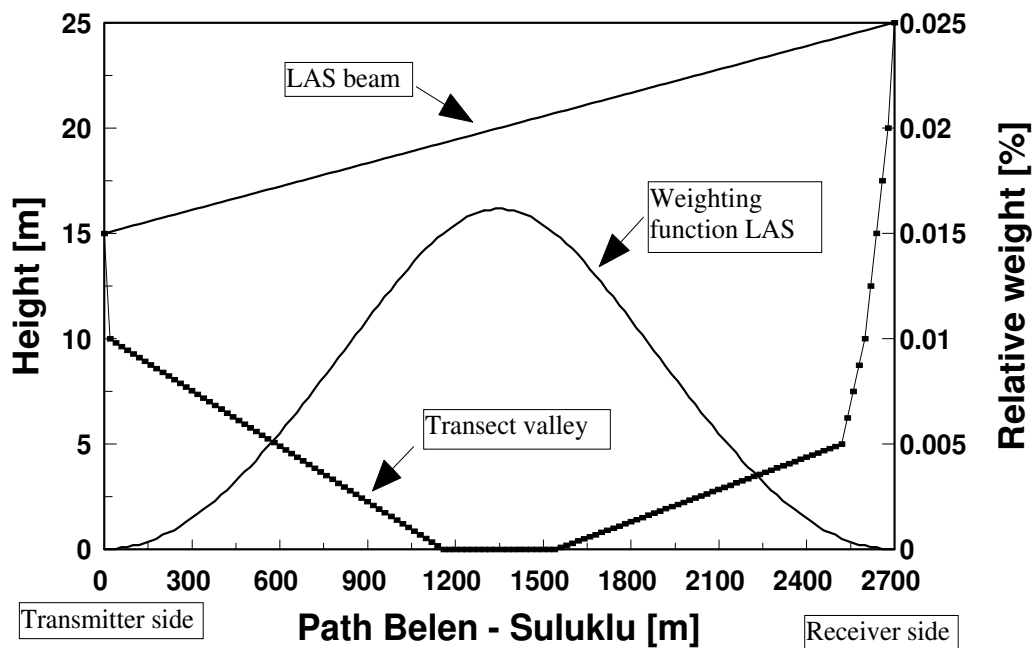

Figure 4.1: The weighting function of the LAS and a cross-section of the valley between Belen and Suluklu.

The second LAS was located at an irrigated cotton field (surrounded by other cotton fields) west of the first location within the Menemen west bank irrigation area. The height and the

path length were 3.2 m and 670 m, respectively. Both parts of the scintillometer were placed on tripods at two opposite corners of the field. Solar panels and batteries were used as power supply. Again ten minute averages and standard deviations were stored on a built in data logger (BL1500, Z-World, Davis, CA, US). A mast was placed in the field to provide continuous measurements of air temperature at 3 m (fine wire thermocouple, manufactured at METAIR), horizontal wind speed at 3 m (cup anemometer, manufactured at METAIR), net radiation at 2.5 m (ventilated Schulze-Däke net radiometer, BDA065, Firma Walter Finck, Industrielle Fertigung mechanischer Kleinteile, Crinitz, Germany) and soil heat flux (WS31soil, TNO TPD, Delft, The Netherlands). Ten minute averages and standard deviations from temperature and wind speed were stored on a data logger (21X, Campbell Scientific Ltd., Shepshed, UK). The height of the crop (h) was measured every week allowing the estimation of the roughness length and zero-plane displacement using the rules of thumb $0.1h$ and $0.67h$, respectively.

4.4 Results

4.4.1 Valley

To calculate the sensible heat flux (H) for the valley using the scintillation method, C_T^2 derived from the scintillometer and additional wind speed measurements are required. It can be seen from the results presented in Table 4.1 that the free convection method underestimates the daytime average (i.e. unstable period) H by 30%. This indicates that the mechanically produced turbulence (contribution by u_*) cannot be neglected. Because no meteorological measurements were collected in the direct vicinity of the first LAS site, wind speed and temperature data of the Menemen Climate Station 6 km from the LAS site, were used in the calculations. We estimate that the non-representativeness of the wind speed data (estimated to be approximately 20%) introduces an error in the daytime average sensible heat flux of the order of 5%. We solved Equations 4.3, 4.5, 4.6 and 4.7 using a Bowen-ratio value of 0.3, 0.5 and 1, respectively. In Figure 4.2 and Figure 4.3, the results are shown for June 26 (DOY 177, before the irrigation season) and August 29 (DOY 241, during the irrigation season). We expect that the Bowen-ratio is close to 1 on June 26 and about 0.3 on August 29. Both figures show a daily course of the sensible heat flux but on August 29 the sensible heat flux is about

150 W m^{-2} smaller around noon. This effect is due to irrigation. It can be seen that the sensible heat flux depends on the Bowen-ratio. A variation of the Bowen-ratio from 0.3 to 1 causes a variation in the sensible heat flux of about 15%.
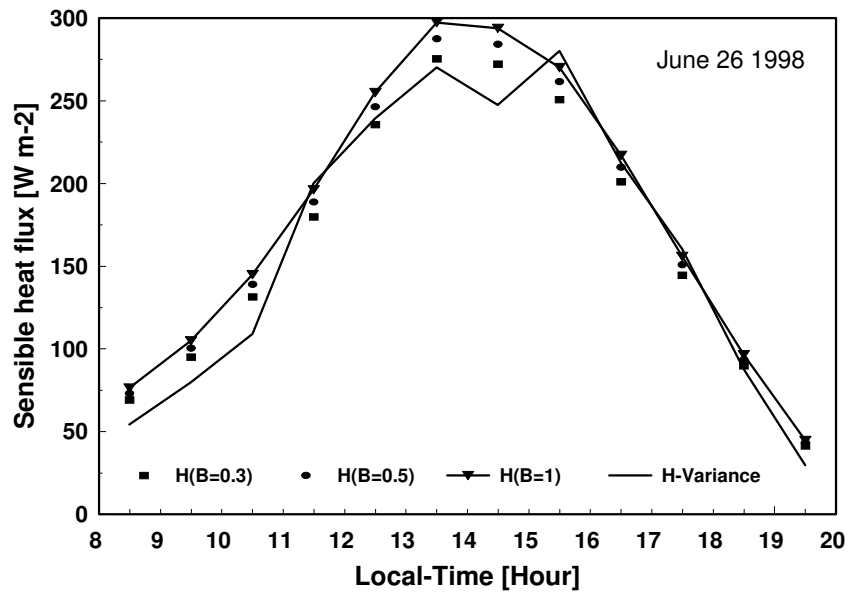

Figure 4.2: The daily course of the sensible heat flux using the scintillation method with a Bowen ratio of 0.3 (■ -markers), 0.5 (∇ -markers) and 1 (+ -markers) over the valley and the temperature variance method (×-markers) over the cotton field for June 26.
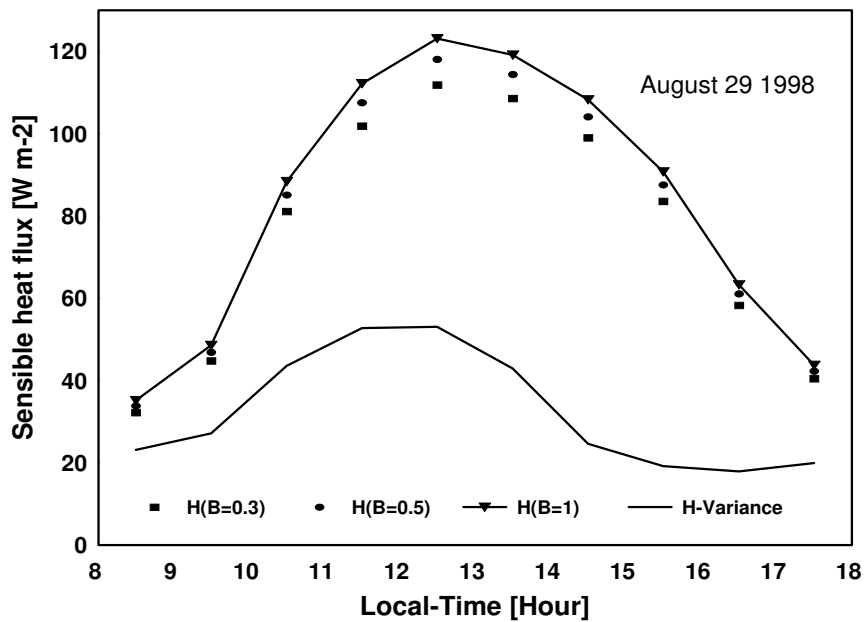

Figure 4.3: As Figure 4.2, except for August 29.

Since during nighttime H is expected to be small, we ignored the night-time fluxes (i.e. $H = 0$ W m^{-2}) in the determination of the 24-hour average H. To demonstrate the operational skill of the scintillometer the 24-hour average values of H for the entire growing season, using a simple "common-sense" estimate for β, are depicted in Figure 4.4 together with the global radiation. Due to missing additional data from the Menemen Climate Station the 24-hour average H could not calculated for the days 121 to 151 (the month of May). Figure 4 shows a relationship between H and the global radiation. Small values in the global radiation, i.e. cloudy days with possibly rain, occurring at the start and at the end of the growing season corresponds with small H's. The LAS' derived sensible heat flux shows a sudden drop around day 193 (July 12). Around this day the irrigation season started. Following irrigation events cannot be noticed in the sensible heat flux records of the valley. This can be explained by the fact that the agricultural fields in the valley are relatively small and have different irrigation schemes. The number of irrigated and non-irrigated fields seen by the LAS is apparently fairly constant. At the end of the growing season global radiation is decreasing, whereas H is fairly constant. Apparently, this is due to irrigation. Note that the LAS is able to detect this phenomenon. The 24-hour average H and the day-time average H for June 26 and August 29, the LANDSAT overpass dates, and the hourly H at 9:30, LANDSAT overpass time, are presented in Table 4.1.
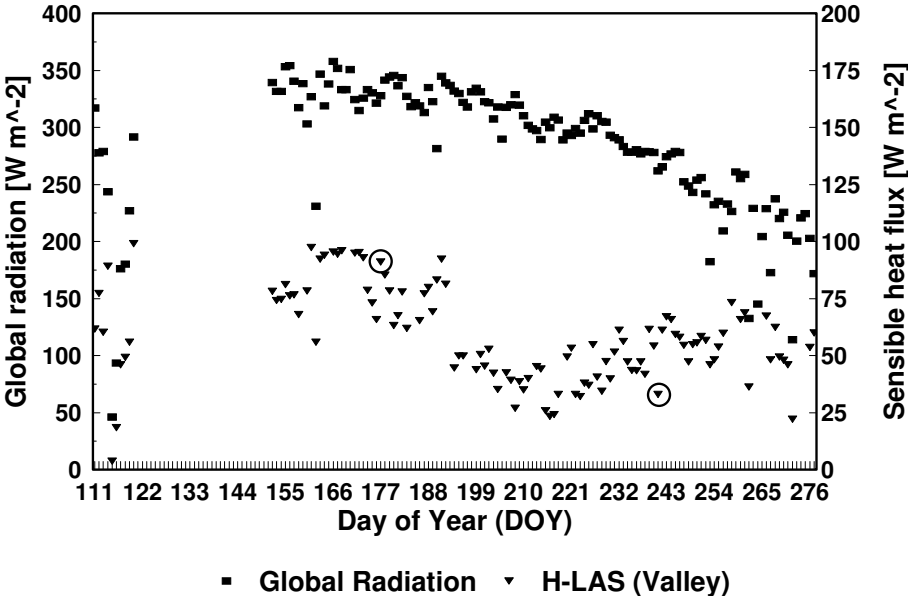

Figure 4.4: The daily average sensible heat flux derived from the LAS over the valley as function of day number together with corresponding values of global radiation measured at the standard weather station. June 26 (DOY 177) and August 29 (DOY 241) are the LANDSAT overpass dates.

Table 4.1: The 24h and day-time averages of the sensible heat flux results for the valley and cotton field derived from the scintillation and variance method for the LANDSAT overpass dates (June 26 and August 29).

Location	Valley	Valley	Cotton	Cotton
Date	June 26	August 29	June 26	August 29
Method	Scintillation	Scintillation	Variance	Variance
H (24h average) [W m^{-2}]	90	35	83	14
H (day-time average) [W m^{-2}]	180	83	164	32
H_{free} (day-time average) [W m^{-2}]	125	61	-	-
H (9:30 local time) [W m^{-2}]	100	42	75	25

4.4.2 Cotton

The LAS data from the second location, over the cotton field, were processed in a similar way. However, due to unforeseen experimental problems the scintillometer data could not be processed. Fortunately the data gathered with the micrometeorological station allowed the application of the temperature variance method (Tillman, 1972; De Bruin et al., 1993; De Bruin et al., 1994). That implies that instead of Equation 4.4 we used (for $L < 0$)

$$\frac{\sigma_T}{T_*} = -c_1\left(1 - c_2\frac{z-d}{L}\right)^{-1/3}$$
(4.8)

where σ_T is the standard deviation of the temperature and c_1 (= 2.9) and c_2 (= 28.4) are empirical constants. Equations 4.7 and 4.8 using 4.5 have to be solved by iteration to derive H. In this paper we used the analytical solution presented by De Bruin et al. (1994) to determine the hourly day-time values of H for June 26 and August 29. The results are also depicted in Figures 4.2 and 4.3. On June 26 the field was not irrigated yet and H reached a maximum of about 270 W m^{-2}, which is approximately the same as for the valley. On August 29, when the cotton was well watered with a fully developed canopy, H around noon was about 55 W m^{-2}. On this day the 24-hour average evapotranspiration is expected to be close to the 24-hour average of net radiation. A more detailed inspection of Figure 4.3 reveals that H reaches a minimum value around 16.00h. This might indicate local advection. However this could not be confirmed due to lack of temperature profile data. The 24-hour, day-time average

and the instantaneous *H* from the cotton field for June 26 and August 29 are also presented in Table 4.1.

4.5 Discussion

In general the results show that the LAS proves to be a robust and reliable instrument to produce "ground-truth" area averaged sensible heat fluxes. Provided the scintillometer is mounted on a stable platform, the equipment requires little maintenance. The scintillometer, installed over the valley has been operated as a 'stand-alone system' during the full growing season without major problems. In order to calculate the sensible heat flux additional data (wind speed and Bowen-ratio) are required also. In this study wind speed was available from the Menemen Climate station only, 6 km from the LAS site. A sensitivity study reveals that an error in the wind speed of 20% leads to an error in the daytime *H* of about 5%. So H is fairly insensitive to wind speed. During the non-irrigated season the Bowen-ratio term in equation 3 can be ignored because β is about 1. During irrigation β has to be known. In this study we used a "common-sense" value for β. Some authors determined β iteratively using the measured net radiation (R_n), soil heat flux (G_s) and the energy balance equation (Green and Hayashi, 1998). This approach could not be applied in this study because net radiation and soil heat flux data were not available for the valley. We expect that both uncertainties (20% in *u* and 0.2 in β) result in an uncertainty of the daytime sensible heat flux of approximately 10% (June 26) and 13% (August 29). Because during nighttime *H* is unknown, it is more difficult to give an error estimate for the 24-hour *H* values. We assumed that *H* is zero during nighttime. In order to get an impression in the systematic error made in this way we assume that in the period between transition hours (sunset and sunrise) *H* is about –20 W m^{-2}. In this way we estimate the underestimation of the 24-hour average *H* is about 10%. More research is needed to improve the 24-hour average *H* derived from the scintillometer. The Monin-Obukhov Similarity Theory, on which the scintillation method is based, refers to surface layers over a flat and horizontally homogeneous area. The question arises whether the scintillation method can be applied over the non-homogeneous valley. METAIR studied this issue extensively during a field experiment in the summer of 1998 performed in Flevoland (The Netherlands). In this study a LAS was installed over a heterogeneous terrain consisting of agricultural fields with different crops. The surface type was similar to that in the Gediz river basin. The first results show that the scintillation method can be applied over such a

surface type. Unfortunately, the LAS over the cotton field did not perform well due to (yet unknown) technical problems. The variance method was applied to provide "ground-truth" data instead. We expect that the variance method is reliable over this homogeneous field. See for instance De Bruin et al. (1993). We found that for June 26 the H derived for the cotton field is very close to that found with the LAS for the valley. Apparently, most fields in the area were still bare on that day (see Figure 4.2). We estimated the uncertainty in the 24-hour average sensible heat flux derived from the variance method by calculating again the relative difference between 24-hour ($H = 0$ W m^{-2} between sunset and sunrise) and 24-hour (assuming $H = -20$ W m^{-2} between sunset and sunrise). We found an error of approximately 10% for June 26. For August 29 the situation is more complicated because advection might have taken place. We estimate an uncertainty in the 24-hour average sensible heat flux of approximately 60 - 80% for this day. Note this error will have little effect on ET since H is very small on this day.

Chapter 5

Satellite, scintillometer and variance based sensible heat fluxes over an irrigated area - an inter comparison study

Meijninger, W.M.L., Gieske, A. and De Bruin, H.A.R.
(submitted to *Int. J. Remote Sensing*)

5.1 Introduction

Nowadays remote sensing algorithms for estimating the regional surface fluxes (e.g. evaporation) are widely used. Most of these algorithms have been developed in the last decade (see e.g. Bastiaanssen et al., 1998; Bastiaanssen and Bos, 1999; Li and Lyons, 1999) and can be applied to imagery of different satellites, such as Landsat, AVHRR and others. The main advantage of a remote sensing technique is that it can provide regional estimates of the surface energy balance terms, while most conventional techniques are point measurements that are representatives of small areas (i.e. source area). Most of these algorithms have been validated against ground point observation data collected during intensive field campaigns (e.g. HAPEX-Sahel and EFEDA). A frequently occurring problem in most of these validation studies are the differences in both spatial and temporal scale as noted by Carlson et al. (1995) and Watts et al. (2000). Although satellites with more advanced imagers have been launched that have a greater spatial resolution (e.g. Landsat and ASTER) coarse resolution imagers are still widely used. For example the successful NOAA-AVHRR (National Oceanic and Administration - Advanced Very High Resolution Radiometer with a pixel resolution of approximately 1 km at nadir) is well suited for agroclimatological monitoring. The NOAA-AVHRR data record spans until now 20 years and it is expected to continue until 2018 with

the launch of the European Meteorological Observational satellite (METOP). Also the Moderate Resolution Imaging Spectroradiometer (MODIS), as replacement of the NOAA-AVHRR has a relative medium resolution (a global resolution of 1 km and in a few channels a resolution of 250 m and 500 m).

Recently, validation studies of remote sensing algorithms have been conducted using ground based scintillometer data (Bastiaanssen, 2000; Hemakumara et al., 2002; Lagouarde et al., 2003; Roerink et al., 2000; Watts et al., 2000). The scintillation method can estimate the sensible heat flux from the propagation statistics of an electromagnetic wave emitted over a certain distance along the surface (see e.g. De Bruin et al., 1995). The advantage of the method is that it can provide surface fluxes of sensible heat at scales comparable to remote sensing methods, e.g. Kohsiek et al. (2002a,b) have demonstrated that the scintillation method can be applied over distances up to 10 kilometres. As a result the difference in observational scale between the remote sensing method and the ground observations decreases. An additional advantage of the scintillation method is that statistically reliable fluxes can be obtained over relative short intervals because the instrument averages in both space and time (Hartogensis et al., 2002). It is known that the eddy covariance method requires averaging intervals of approximately 30-minutes in order to derive reliable estimates (Mahrt, 1998). A delicate aspect of the scintillation method is whether it can be applied over heterogeneous areas. Recently, Meijninger et al. (2002a, 2002b) and Beyrich et al. (2002a) explored this aspect and found good agreement between scintillometer and eddy covariance based area-averaged sensible heat fluxes.

In this study a remote sensing algorithm known as SEBAL (Surface Energy BALance) (Bastiaanssen et al., 1998) is applied to NOAA-14 AVHRR imager data, which have been downloaded from the Satellite Active Archive (SAA). SEBAL consists of a number of steps to solve the energy balance for each satellite pixel. The algorithm computes most essential hydro-meteorological parameters empirically and requires only little field information (incoming solar radiation, air temperature and wind speed data). The sensible heat flux is solved iteratively using Monin-Obukhov Similarity Theory (MOST) and selected wet and dry pixels, which bracket the sensible heat flux between minimum and maximum values. Finally, the latent heat flux is derived as the closure term of the surface energy balance equation.

The primary purpose of this study is to compare the SEBAL derived sensible heat fluxes with ground based scintillometer and in-situ (variance method) surface fluxes from two different sites for a period spanning a growing season (118 days). We have used data from an experiment that took place in the Gediz river basin (Turkey) in 1998 (Kite and Droogers, 2000). In Section 5.2 all three methods are explained and the experimental set-up is described in Section 5.3. In Section 5.4 the results are presented and discussed. Finally, in Section 5.5 the conclusions are given.

5.2 Materials and methods

5.2.1 The scintillation method

The scintillation method is based on the analysis of intensity fluctuations (known as scintillations), of a near-infrared light beam (λ = 0.94 µm) that has propagated over a horizontal distance (L) between the transmitter and the receiver. In this case a large aperture scintillometer (LAS) is used with an aperture diameter (D) of 0.15 m, which makes it possible to measure over distances up to 5 km. The observed intensity fluctuations ($\sigma_{\ln I}^2$) can be related to the structure parameter of the refractive index of air (C_n^2) as follows (Wang et al., 1978)

$$\left\langle C_n^2 \right\rangle = 1.12 \sigma_{\ln I}^2 D^{7/3} L^{-3},$$
(5.1)

where $\left\langle C_n^2 \right\rangle$ is the path averaged structure parameter of the refractive index of air.

At near-infrared wavelengths primarily temperature (T) fluctuations cause the fluctuations in the refractive index of air, i.e. C_n^2 is related to C_T^2 (Wesely, 1976b),

$$C_T^2 = C_n^2 \left(\frac{T^2}{-0.78 \times 10^{-6} P} \right)^2 \left(1 + \frac{0.03}{\beta} \right)^{-2}.$$
(5.2)

The latter term between the brackets accounts for humidity fluctuations, which is expressed by the Bowen-ratio (β). Here, the Bowen-ratio is solved iteratively as proposed by Green and Hayashi (1998) using estimates of the net radiation (R_n) and soil heat flux (G_s), which are derived from global radiation data.

Next, the sensible heat flux (H) can be derived iteratively by applying the Monin-Obukhov Similarity Theory (MOST) (Wyngaard et al., 1971)

$$\frac{C_T^2 (z_{LAS} - d)^{2/3}}{T_*^2} = f_{TT}\left(\frac{z_{LAS} - d}{L_{Ob}}\right) = c_{T1}\left(1 - c_{T2}\frac{z_{LAS} - d}{L_{Ob}}\right)^{-2/3}, \tag{5.3}$$

where c_{T1} (=4.9) and c_{T2} (=9) are empirical constants (De Bruin et al., 1993), the height of the LAS z_{LAS}, the zero-displacement height d, the Obukhov length $L_{Ob} = \dfrac{u_*^2 T}{g \kappa T_*}$, the temperature scale $T_* = \dfrac{-H}{\rho c_p u_*}$ and the friction velocity u_*. In this study the friction velocity is derived from wind speed measurements, taken from a near-by meteorological station, and an estimate of the aerodynamic roughness length ($z_0 = 0.25$ m) representative for the source area of the LAS. For stable conditions the validity of the scintillation method is uncertain. Because the fluxes are usually small the nighttime flux is set at 0 W m^{-2} for estimating the daily average sensible heat flux (H_{24}).

5.2.2 The variance method

The variance method, a conventional 'point' method, is also based on MOST and can estimate the sensible heat flux from temperature fluctuation measurements (σ_T) collected by a fast response thermocouple (Tillman, 1972). Instead of Equation 5.3 the following relationship is used

$$\frac{\sigma_T}{T_*} = -c_1\left(1 - c_2\frac{z_T - d}{L}\right)^{-1/3}, \tag{5.4}$$

where c_1 (= 2.9) and c_2 (= 28.4) are empirical constants (De Bruin et al., 1993) and z_T the height of the fast temperature measurements. In this case on site wind speed data is used to estimate the friction velocity. The aerodynamic roughness length and displacement height are derived from crop height (h), measured over the growing period ($z_o = 0.1h$ and $d = 0.67h$). As the scintillation method the validity of the variance method during stable conditions is uncertain. Therefore we followed the same procedure to derive the daily average sensible heat flux.

5.2.3 SEBAL

In this study a remote sensing method known as SHEBA (SHort Energy Balance Algorithm) is used, which can solve the surface energy balance from visible, near infrared and thermal infrared images. The SHEBA algorithm follows the physics of SEBAL (Surface Energy BALance, see Bastiaanssen et al, 1998; Bastiaanssen, 2000) but is specifically designed to be more efficient and faster ($\approx$ 5×) in calculating the sensible heat fluxes (Gieske, 2003). Throughout this paper we will therefore use SEBAL to denote the remote sensing method. The algorithm consists of a number of steps to solve the energy balance for each pixel. Here it is applied to surface albedo, brightness temperature and NDVI (Normalised Difference Vegetation Index) maps based on NOAA-14 AVHRR data. The surface temperature is derived from band 4 and 5 using a split window algorithm. The required broadband surface emissivity of a vegetated surface is approximated by the relationship proposed by Van de Griend and Owe (1993) using the NDVI maps. Furthermore, NDVI and SAVI (Soil Adjusted Vegetation Index) indices are used to derive the vegetation characteristics z_o (Bastiaanssen et al., 1998) and d (Verhoef et al., 1997). Here, the roughness length for heat (z_{oh}) is set constant at 0.01 m. The instantaneous net radiation (R_n) is computed from incoming and reflected solar and thermal radiation, where the incoming short wave radiation is taken from the Menemen climate station. The outgoing long wave radiation is computed from the radiometric surface temperature. The incoming long wave radiation is derived from the air temperature taken from the Menemen climate station and the effective atmospheric emissivity, which in turn is derived from the atmospheric transmittance (Bastiaanssen et al., 1998). The instantaneous soil heat flux (G_s) is determined according to the empirical relationship proposed by Bastiaanssen et al. (1998). The sensible heat flux for each pixel (H_x) was derived from flux inversion at a

selected dry pixel (where $H_{dry} = (R_n - G_s)_{dry}$) and a wet pixel (where $H_{wet} = 0\,\text{W m}^{-2}$) inside the image. The sensible heat flux for each pixel x is then expressed as

$$H_x = \left(\frac{\rho_x c_{p\_x} (R_n - G_s)_{dry} r_{ah\_dry}}{r_{ah\_x} \rho_{dry} c_{p\_dry}} \right) \cdot \left(\frac{T_x - T_{wet}}{T_{dry} - T_{wet}} \right),$$

(5.5)

where T is the surface temperature, ρ the density of air, c_p the specific heat of air at constant pressure and r_{ah} the aerodynamic resistance to heat transport for the pixels, i.e. wet, dry and x. The extreme pixels within the image were carefully selected in the Aegean Sea (wet pixel) and north of the city Izmir (dry pixel). The sensible heat flux is solved iteratively applying MOST and using wind speed data that was extrapolated to the blending height and assumed to be constant for the entire image. Finally, the latent heat flux (L_vE) is computed as the residual of the surface energy balance equation. Assuming that the evaporative fraction (Λ) is constant over the day the daily average sensible heat (H_{24}) can be derived from the daily average net radiation (R_{n24})

$$H_{24} = (1 - \Lambda)R_{n24}.$$

(5.6)

5.3 Experimental design

The LAS was deployed over a transect of the valley located in the Gediz river basin east of Menemen (western part of Turkey). The path length of the LAS was 2.7 km and the effective height of instrument over the valley was 18 m. The land use in the valley consisted of raison grape (60%), cotton (15%), fruit trees (15%), pasture (5%) and other trees (5%) (Kite and Droogers, 2000). Other measurements were conducted over an irrigated cotton field located west of Menemen (the distance between both locations is approximately 11 km). In turn other cotton fields surrounded this cotton field. A small mast with a cup anemometer (manufactured by METAIR) and a fast thermocouple (manufactured by METAIR) provided statistics of wind speed and temperature at a height of 3 m (mean and standard deviation (σ_T) for each 10-minute interval). Also a ventilated net radiometer (Schulze-Däke, BDA065, Firma Walter Finck, Industrielle Fertigung mechanischer Kleinteile, Crinitz, Germany) and a soil heat flux plate (WS31soil, TNO TPD, Delft, The Netherlands) were installed to measure net radiation

and soil heat flux. Additional meteorological data (hourly values of temperature, wind speed and global radiation) were taken from the Meteorological station in Menemen. In Figure 1 the locations (cotton field, Menemen climate station, LAS) are shown. More detailed information on the experiment can be found in Meijninger and De Bruin (2000).
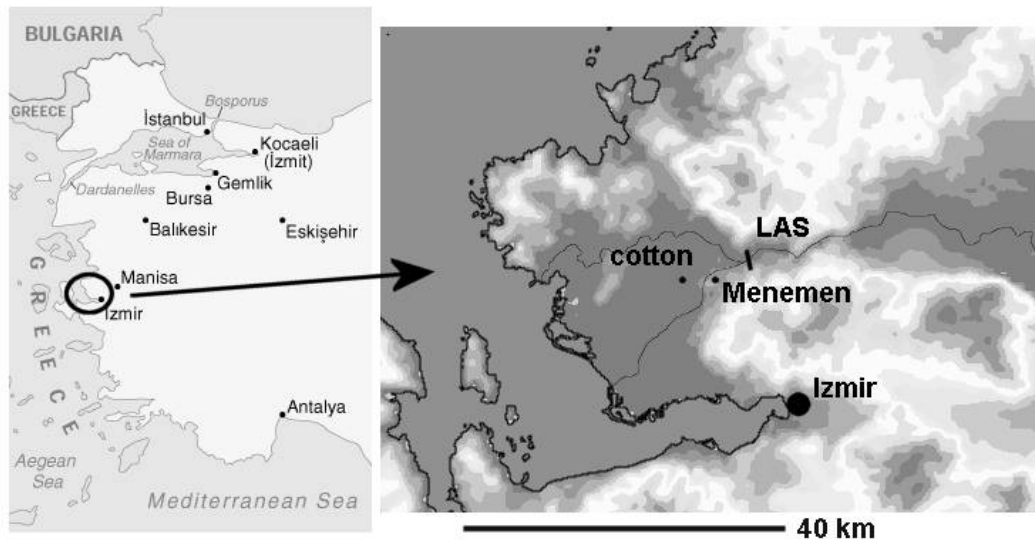

Figure 5.1: Map of western part of Turkey (left) showing the locations of the cotton field, the LAS set-up in the valley and the Menemen climate station (right).

The level 1b NOAA-14 AVHRR data were downloaded from the Satellite Active Archive (SAA, www.saa.noaa.gov). Images that were distorted (extreme viewing angles) or too cloudy were discarded, resulting in 56 images between day number (DOY) 152 and 277. Pre-processing of AVHRR channels 1 and 2 consisted of the conversion of raw counts to % reflectance values with post-launch NOAA-14 calibration (Rao and Chen, 1996) using NPR1b (Gieske, 2001). The thermal channels 4 and 5 were calibrated into radiances and then into brightness temperatures by inverting the Planck function. The images were geometrically corrected and rescaled to a pixel size of 0.01×0.01 degree. The atmospheric correction algorithm used for channel 1 and 2 was the 6S code (Vermote et al., 1997). The following atmospheric parameters have been used: a mid-latitude summer atmosphere, a maritime aerosol type, an aerosol optical depth of 0.3 at 550 nm and a homogeneous land surface type. For the narrow-band to broad conversion using channel 1 and 2 the empirical constants proposed by Valiente et al. (1995) were applied. Finally, to correct for the fluctuations in the surface reflectance due to angular variability of the AVHRR sensor and bi-directional effects the method of Gutman (1988) was used to derive monthly mean surface albedo values.

5.4 Results and discussion

The instantaneous and daily average net radiation from SEBAL are compared with the ground observations in Figure 5.2 and 5.3. The plotted SEBAL net radiation is the average of 4 neighbouring pixels. For the instantaneous and daily average SEBAL results the spatial variation was less than 15 W m^{-2} and 10 W m^{-2}, respectively. A regression analysis for the instantaneous results yields $R_{n\_cotton} = 0.91 R_{n\_SEBAL}$ and a RMSD of 62 W m^{-2}, which is equal to 13%. In Figure 5.3 the regression analysis yields $R_{n24\_cotton} = 0.95 R_{n24\_SEBAL}$ and a RMSD of 20 W m^{-2}, equal to 12%. Most of the scatter in both Figures (see encircled points) is caused by flood-irrigation. On days of irrigation and following days (~ 4) the ground measurements show a distinctive increase in the net radiation, which is a combined effect of a decrease in the surface albedo and the surface temperature. Although monthly mean surface albedo values have been used (see Table 5.1) to derive the net radiation, the raw AVHRR data did not clearly reveal the effects of irrigation because most variation is caused by changes in sun and satellite viewing angles.
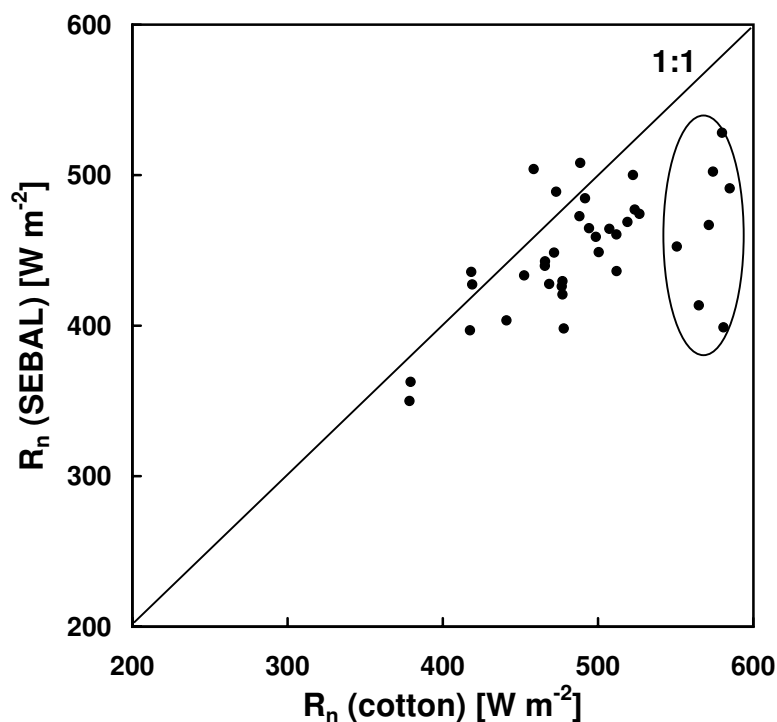

Figure 5.2: Comparison of the instantaneous net radiation obtained from SEBAL and the ground measurements for the cotton site. The satellite overpass time varied between 15:00 and 16:00 local time. The data points within the circle are days when the field was flood irrigated.
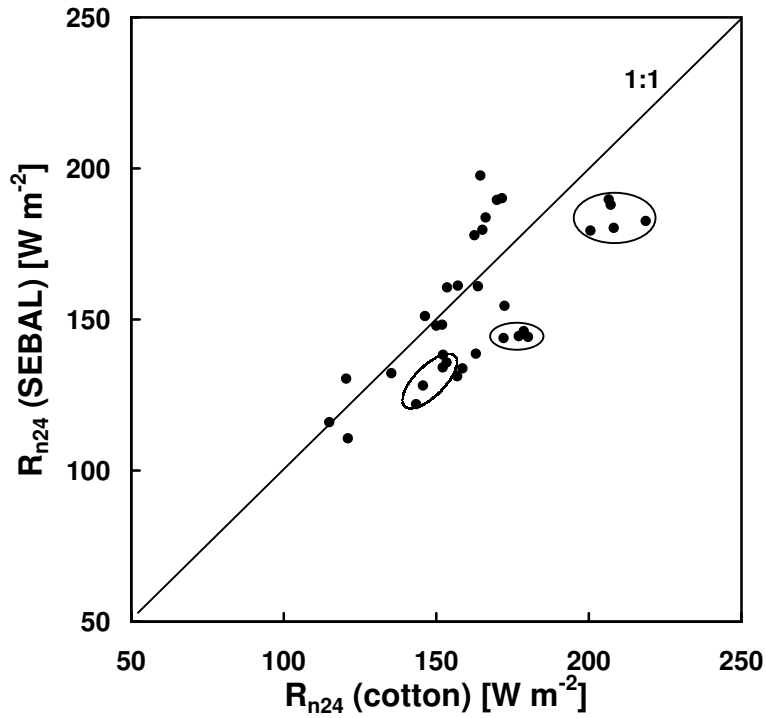
Figure 5.3: As Figure 5.2 except for daily average values. The data points within the circle are days when the field was flood irrigated.

Table 5.1: Monthly mean surface albedo for the cotton field and the valley.

Month	Cotton field	Valley
albedo (June)	18%	18%
albedo (July)	18%	18%
albedo (August)	19%	18%
albedo (September)	16%	15%

In Figure 5.4(a,b) and Figure 5.5 the SEBAL estimates of the instantaneous sensible heat flux are compared with the fluxes derived from the variance and the scintillation (LAS) method at the cotton site and the valley, respectively. Note that the LAS method applied here is slightly different from the LAS method used by Meijninger and De Bruin (2000). Instead of a 'common sense' estimate of the Bowen-ratio the iterative Bowen-ratio approach is used. Comparison of the results reveals a close agreement ($H_{\text{Bowen-iter}} = 1.05H_{\text{Bowen-const}}$, RMSD = 9 W m^{-2}). The SEBAL results depicted in Figure 5.4(a,b) are averages of 4 neighbouring pixels and in Figure 5.5 of 6 neighbouring pixels. The spatial variation of the surface flux was less than 15 W m^{-2} and 30 W m^{-2} for the cotton site and the valley, respectively. For the cotton site the results are in good agreement ($H_{\text{variance}} = 1.06H_{\text{SEBAL}}$ with RMSD = 38 W m^{-2} = 38%),

except for some outliers that occurred in the beginning before the irrigation season. Note that in Figure 5.4(b) also the results are plotted for days when one of the two methods was not functioning or could not provide a reliable flux (see open squares and open circles). As mentioned before the cotton field is surrounded by a number of other cotton fields, creating ideal homogeneous conditions, which mean that both methods clearly reflect the same crop. Furthermore, any shift in geo-location of the AVHRR images does not affect the validation. For the valley site (Figure 5.5) the SEBAL results show a discrepancy compared with the LAS observations ($H_{LAS} = 0.99H_{SEBAL}$ with RMSD = 62 W m^{-2} = 55%). The dynamic range of the SEBAL fluxes is small as SEBAL has the tendency to overestimate the small fluxes. Two possible reasons that might have caused this mismatch are offered. In Figure 5.6 the cumulative contribution to the LAS flux is shown as a function of the upwind distance, which is based on the footprint function following Horst and Weil (1992). The thick black line, which is representative for most atmospheric conditions at the time of the satellite overpass, shows that 90% of the measured LAS' flux originated from the first km upwind area. The grey lines represent the extreme cases, i.e. the most unstable case (upper grey line, e.g. smallest source area) and less unstable cases (lower grey line, e.g. largest source area). Following Meijninger et al. (2002a,b) and combining the footprint function with the spatial weighting function of the LAS it is found that the total source area of the LAS is approximately 2 × 1 km^2. Note that the size of the source area solely depends on the measurement height, the surface roughness, the path length and the atmospheric stability. The latter variable is the only variable that changes here. Compared to the resolution of the raw AVHRR images, which range between 1.1 km^2 and 4 km^2, the source area of the LAS is relatively small. This scaling mismatch together with the heterogeneous surface conditions in the valley might have caused the observed discrepancy. A second reason is that the width of the valley, where the LAS is located, is too narrow for the NOAA imager. As a result the satellite pixels can be partly affected by the dry slopes.
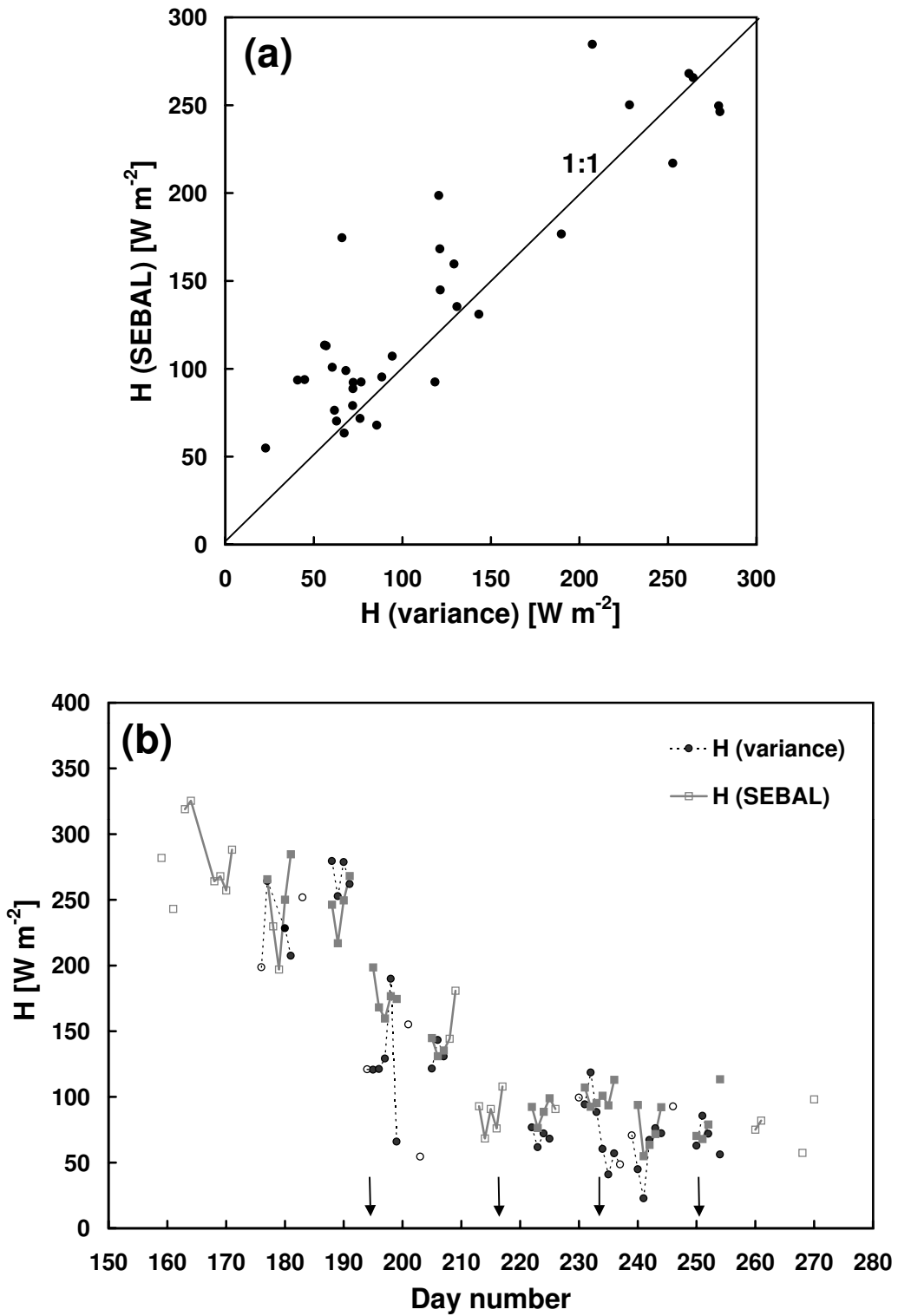
Figure 5.4: Comparison of the variance and SEBAL estimates of instantaneous sensible heat fluxes for the cotton site (a) and plotted against day number (b). The arrows show the days when the field was flood-irrigated. The open symbols represent the results of either SEBAL or the variance method for days were one of the methods (i.e. SEBAL or variance method) did not work or no data was available.
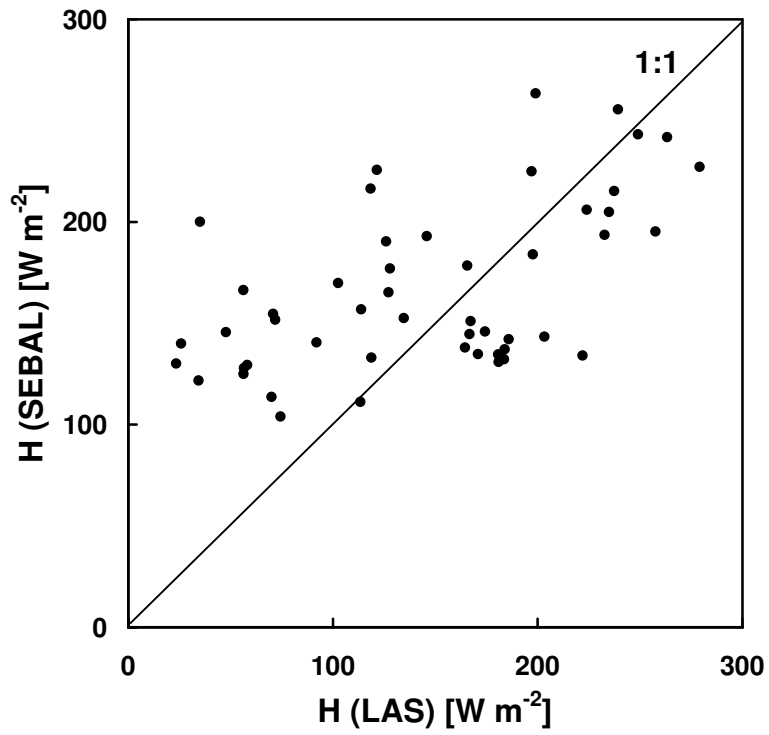
Figure 5.5: As Figure 5.4(a) except for the valley (i.e. LAS versus SEBAL).
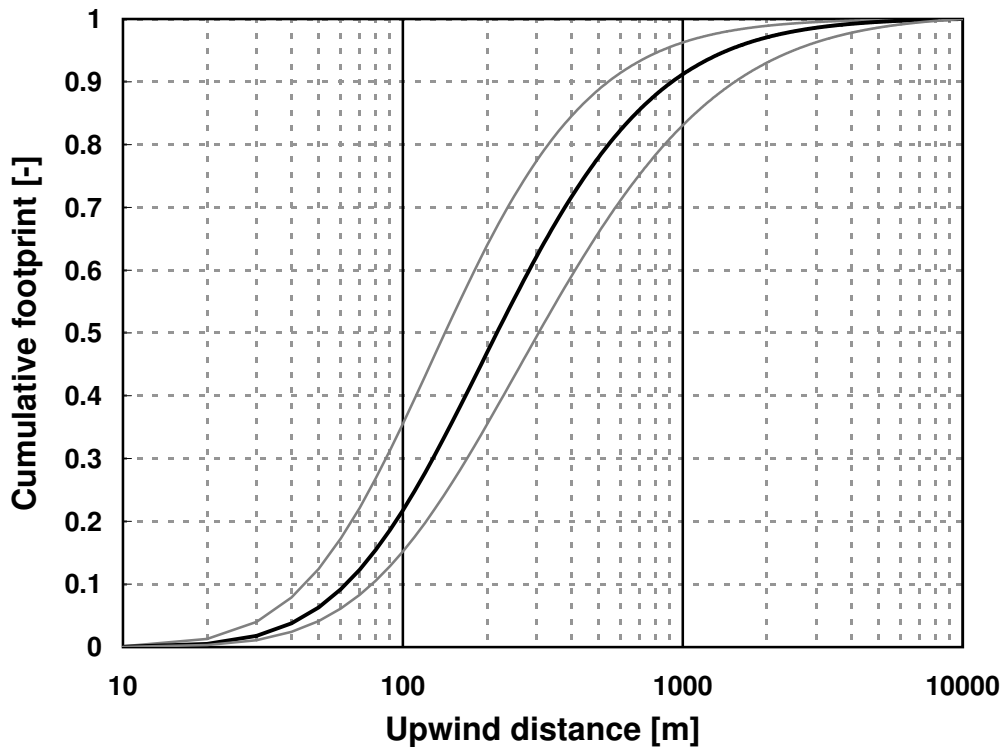

Figure 5.6: The cumulative footprint of the LAS in the upwind direction plotted for three cases, namely the average (black line), most unstable (upper grey line) and least unstable case (lower grey line).

94

In Figure 5.7 the daily average sensible heat flux estimates for SEBAL and the variance method (e.g. the cotton site) are plotted against day number (regression analysis: $H_{24\text{-variance}} = 1.6 H_{24\text{-SEBAL}}$, RMSD = 40 W m^{-2} = 54%). The plotted open circles and squares are days when the fluxes of only one of the two methods were available. The arrows in the Figure point the days when the cotton field was flood-irrigated. It can be seen that in the beginning SEBAL systematically overestimates the daily average sensible heat flux. After the first irrigation period the discrepancy between the two methods decreases. The main reason for this discrepancy is illustrated in Figure 5.8. In this Figure the mean diurnal cycle of the surface fluxes, based on the variance method, is plotted. The left Figure (a) shows the mean diurnal cycle for the non-irrigated period and the right Figure (b) for the irrigated period. Similar diurnal cycles were found for the LAS fluxes (not shown here). The evaporative fraction is also plotted (instantaneous and daily) together with the evaporative fraction provided by SEBAL. By comparing the evaporative fraction systematic errors related to differences in the energy budget are overcome. It can be seen that SEBAL underestimates the evaporative fraction, especially in the non-irrigated period, which is in fact the main reason for the observed difference shown in Figure 5.7. In turn the underestimation of the evaporative fraction is caused by the selected 'dry' pixels, which might not be completely dry. Especially in the beginning when the overall surface conditions are still humid and the presence of dry pixels are rare. As a result the sensible heat flux for the selected pixels and also the predicted fluxes will be overestimated leading to an underestimation of the evaporative fraction. Note that the assumption of a constant evaporative fraction of SEBAL is not the reason for the discrepancy in Figure 5.7, although in the irrigated period this assumption holds (see Figure 5.8(b)). In fact the intersection between the diurnal cycle of Λ and daily mean Λ in Figure 5.8(a) indicates that the overpass window of the NOAA satellite, which lies between 15:00 and 16:00 local time, is the ideal moment.
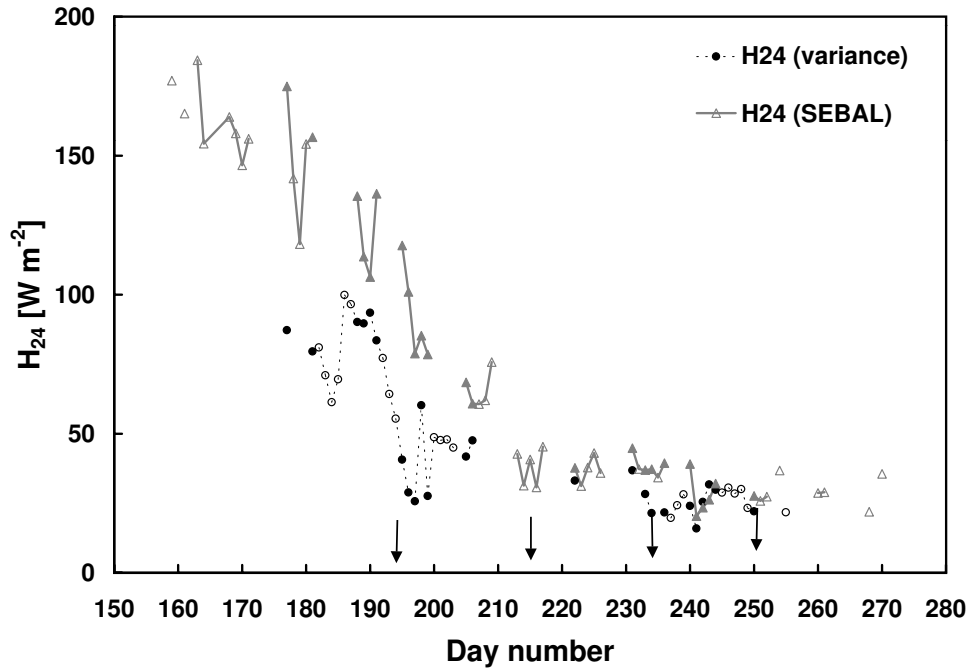
Figure 5.7: The daily average sensible heat flux derived from the SEBAL and variance method for the cotton site plotted against day number (DOY). The arrows show the days when the field was flood-irrigated. The open symbols represent the results of either SEBAL or the variance method for days were one of the methods (i.e. SEBAL or variance method) did not work or no data was available.
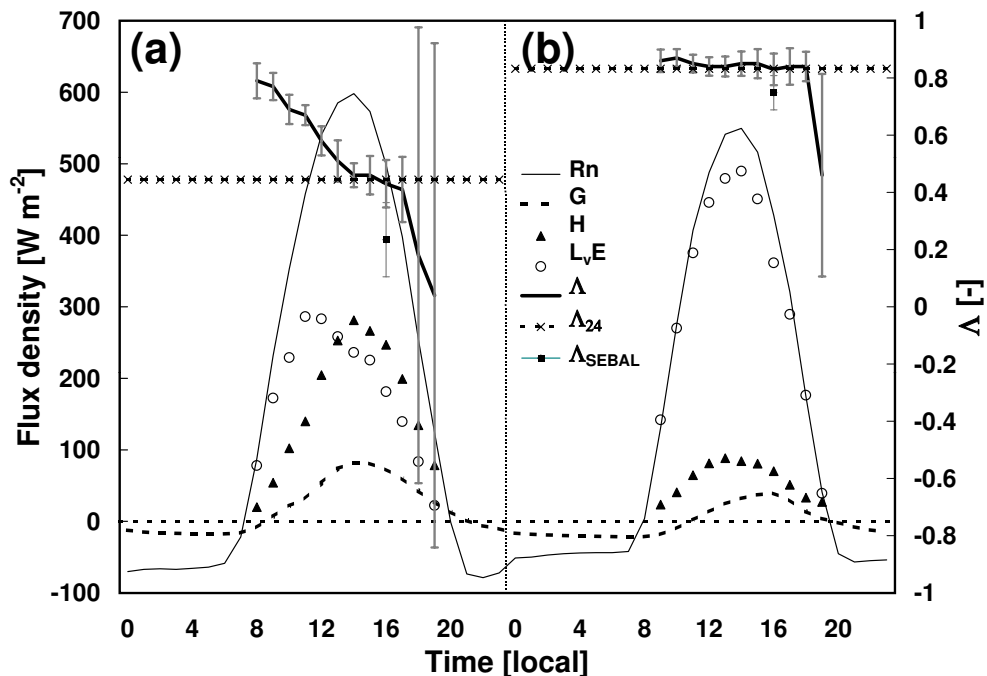

Figure 5.8: The mean diurnal cycle of net radiation, soil heat flux, sensible heat flux, latent heat flux and evaporative fraction for the non-irrigated period (a: day number 150-190) and irrigated period (b: day number 210-277) plotted together with the mean evaporative fraction of SEBAL. The error bars show the variation of the evaporative fraction over the days.

5.5 Conclusions

In this study surface flux maps of sensible heat generated by a satellite remote sensing technique (SEBAL) have been compared with ground observations. The ground measurements were conducted at two different locations using the variance method and the scintillation method. The instantaneous fluxes provided by SEBAL showed a good agreement with the ground measurements for the cotton site over the entire growing season. For the valley site, where the LAS was installed, the results show a discrepancy. It was found that the spatial coverage of the LAS (i.e. source area) in the heterogeneous valley is too small compared to the spatial resolution of the AVHRR imager. Furthermore, we suspect that the valley is too narrow for the AVHRR imager and that the satellite results have been affected by the dry slopes. Therefore a convincing validation of SEBAL for this location could not be performed. Also, the daily average sensible heat fluxes for the cotton site have been compared. It was found that in the first period SEBAL systematically overestimates the daily average sensible heat flux, which is caused by an underestimation of the evaporative fraction. We suspect that in the beginning of the period the selected dry pixels were not actually dry, which resulted in a systematic underestimation of the evaporative fraction. In our continuing work we hope to validate satellite remote sensing techniques using longer scintillometer path lengths up to 5 km (the maximum distance of the LAS) and 10 km using the XLAS (Kohsiek et al., 2002a,b), which allows a better comparison even with the new METEOSAT second generation. Furthermore, a satellite-scintillation combination will be investigated where relative extreme 'scintillometer' pixels will be used to apply SEBAL to areas where wet and dry pixels are not present.

Chapter 6

Summary

Motivated by the demand for reliable area-averaged fluxes associated with natural landscapes this thesis investigates a relative new measurement technique known as the scintillation method. For homogeneous areas the surface fluxes can be derived with reasonable accuracy. However, fluxes representative for large natural landscapes (comparable to the horizontal grid box size of numerical models or the pixel size of satellite imagers) are more difficult to obtain because at these scales the surface is mostly heterogeneous. At this moment only a few techniques are available that can provide flux information at spatial scales of several kilometres, such as the scintillation method.

Based on the propagation statistics of EM radiation that has propagated through the atmosphere over a horizontal path of several kilometres it is possible to derive the surface fluxes of sensible heat, water vapour and momentum. In this study a Large Aperture Scintillometer (LAS) has been developed that can be used over distances up to 5 km. Since the LAS operates at a near-infrared wavelength hence it is primarily sensitive to temperature related scintillations, from which the sensible heat flux can inferred. In this thesis the following aspects regarding the LAS are investigated:

- The performance of the LAS over heterogeneous land surfaces (**Chapter 2**)
- The reliability of area-averaged water vapour fluxes provided by the LAS and in combination with a radio wave scintillometer over heterogeneous land surfaces (**Chapter 3**)
- Its practical applicability and usefulness in other scientific areas (**Chapter 4** and **5**)

For the derivation of the sensible heat flux from the LAS signal one must rely on the Monin-Obukhov Similarity Theory (MOST). However, MOST requires homogeneous surface conditions. The question arises whether the LAS can be used over distances of several kilometres, since at these scales the surface is mostly heterogeneous. In order to test

experimentally the applicability of the LAS over heterogeneous areas and the reliability of the derived fluxes of sensible heat a field campaign was carried out in Flevoland (The Netherlands). The results of this experiment are presented and discussed in **Chapter 2**. The general characteristics of the Flevoland area are as follows: a vast and completely flat area covered by four crops in a chessboard configuration of patches of 500 m × 250 m. Based on the horizontal length scale of the patches this landscape is classified as a Type A landscape, meaning that only the lower part of the surface layer is affected by the irregularities. Eddy covariance (EC) measurements were performed over the main types of farmland to provide to aggregation independent area-averaged fluxes. The EC observations reveal that the heterogeneity in the Flevoland area is primarily the result of spatial variations in the thermal properties. The fluxes of two large aperture scintillometers, installed at a height of 11.6 m and 20.4 m, respectively, show a close resemblance with the area-averaged EC fluxes, especially for the upper LAS. The lower LAS shows a slight underestimation of the sensible heat flux of approximately 7%. This underestimation is assessed using a blending height approach and an analytical footprint model for estimating the source areas and the associated fluxes. The blending height is considered as the level above the surface where the influences of the patches gradually decay. It is found, using a heuristic model that the blending height for the Flevoland area varies between 9 m and 14 m. Based on the found blending heights it is concluded that the upper LAS always measured above the blending height, which is consistent with the depicted LAS results. For the lower LAS the situation is more complicated as the individual fields influence the measurements, suggesting that the MOST may be violated. After dividing the Flevoland area into 8 wind-sectors and re-arranging the area-averaged fluxes for the entire area and for the 8 source areas, a closer agreement is found. These results indicate that from a LAS, which measures just below the blending height, still reliable area-averaged fluxes can be derived and that the violation of MOST is small.

In **Chapter 3** the performance of a combined LAS and radio wave scintillometer (LAS-RWS) over a heterogeneous land surface is studied. Although this scintillation technique, known as the two-wavelength method, provides both the sensible heat flux and the water vapour flux, most attention is focussed at the water vapour flux. The water vapour flux provided by a 'stand-alone' LAS is evaluated also. In the latter case the water vapour flux is estimated as the residual of the surface energy balance equation using a simple parameterisation scheme (based on global radiation data) for estimating the area-averaged available energy (i.e. R_n - G_s). The results shown in Chapter 3 are based also on data of the Flevoland experiment. As

shown in Chapter 2 the EC observations reveal that the heterogeneity in the area is primarily the result of spatial variations in the thermal properties and likewise in the buoyant production term of MOST. The same blending height and footprint approach is used for the analysis of the fluxes as in Chapter 2. First, the water vapour fluxes from the combined LAS-RWS system are investigated. It was found that these fluxes agree well with the area-averaged water vapour flux aggregated from the in-situ observations. The found scatter is explained to be caused by: closure failure of the energy balance for the EC measurements, the non-linearity between the structure parameters and the inferred fluxes, and low frequency water vapour absorption fluctuations that affect the RWS. Finally, the water vapour fluxes derived from the stand-alone LAS are discussed. These results show that the 'stand-alone' LAS can provide also reliable estimates of the area-averaged water vapour flux over heterogeneous areas (type A).

In Chapter 4 and Chapter 5 operational aspects of the LAS are studied. For that purpose two LAS devices and a small micrometeorological station were installed in the Gediz Basin near Menemen (Turkey) in 1998 as part of an international experiment. The main objective of this experiment was to compare actual evapotranspiration estimates based on satellite remote sensing methods, hydrological models and field methods. **Chapter 4** deals only with the field methods, i.e. the variance method and in particular the LAS. One LAS was set-up over a transect of the valley of the Gediz river basin. For the derivation of the sensible heat flux additional wind speed and temperature data are taken from a nearby meteorological station. In addition a small micro-meteorological station was placed at an irrigated cotton field. The fluxes for this site are inferred from collected temperature fluctuation data using the variance method. Due to experimental problems with a second LAS installed at the same site these data are excluded from this study. The presented time series of 24-hour average fluxes for the valley clearly shows the seasonal trend of the sensible heat flux, including the irrigation events. This time series demonstrates from an operational perspective that the LAS, which was operational during the entire growing season, is a robust and reliable instrument that requires only occasional servicing.

Based on the LAS results shown in Chapter 4 it is investigated in **Chapter 5** whether these fluxes can be used as 'ground-truth' data in other scientific studies such as remote sensing. For that purpose a large number of surface flux maps are generated using the SEBAL remote sensing algorithm, and are compared with the LAS results. In this validation study the in-situ

fluxes and radiation measurements of the irrigated cotton field are included also. The SEBAL fluxes are derived from moderate resolution AVHRR visible and thermal-infrared images taken from the NOAA-14 satellite. Both instantaneous and daily average sensible heat fluxes are determined for the entire growing season. It is found that the SEBAL based instantaneous fluxes agree closely with the in-situ fluxes for the cotton site. However, the results for the valley site, i.e. SEBAL versus LAS, reveal a discrepancy. The following reasons are offered: the scaling mismatch between the source area of the LAS and the pixel size of the raw AVHRR images; a possible distortion by the dry slopes in the relative narrow valley compared to the resolution of the AVHRR imager. Therefore a convincing validation of SEBAL for the valley cannot be done. Finally, the daily average sensible heat fluxes for the cotton field are compared. It is found that only during the irrigation period the daily average results agree. Not actually dry reference pixels, which lead to underestimated evaporative fractions, are suggested to be the reason for the observed difference.

Chapter 7

Perspectives

The results shown in this thesis together with the results of some parallel scintillometer studies (see Chapter 1) clearly demonstrate the potential of the scintillation method. Various research studies can benefit from the wide range of applications of the scintillation method:

- agriculture (crop yield production; irrigation schemes)
- hydrology (water balance studies; water management; irrigation; model validation; parameterisation)
- meteorology (energy balance studies; validation studies of operational weather forecast models; parameterisation studies)
- environmental (air pollution monitoring; gas exchange processes)
- climatology (climate monitoring; climate impact; desertification monitoring; validation of operational weather forecast models)
- remote sensing (validation; 'reference' pixels for online calibration)

Some examples:

A very obvious application of the scintillation method is in validation studies. As discussed in Chapter 1 most numerical models (meteorological or hydrological) have a grid box size of several kilometres. This also accounts for operational satellite based sensors, such as the NOAA-AVHRR (~ 1.1 km at nadir) series, its successor MODIS (~ 250 m at nadir) and the METEOSAT Second Generation (MSG) (~ 4 km at equator). Note that despite the increase in number of the more advanced satellite imagers, which have a higher resolution (e.g. Landsat-TM, ASTER, IRSUTE, ESA-PRISM), moderate resolution satellite imagers are still widely used and will be also in the future. The scintillation method with its path-integrating capabilities is an ideal instrument for providing reliable 'ground-truth' observations at various scales required in validation studies of models (ranging from weather-prediction models to LES models) and satellite remotes sensing techniques (see e.g. Figure 7.1).
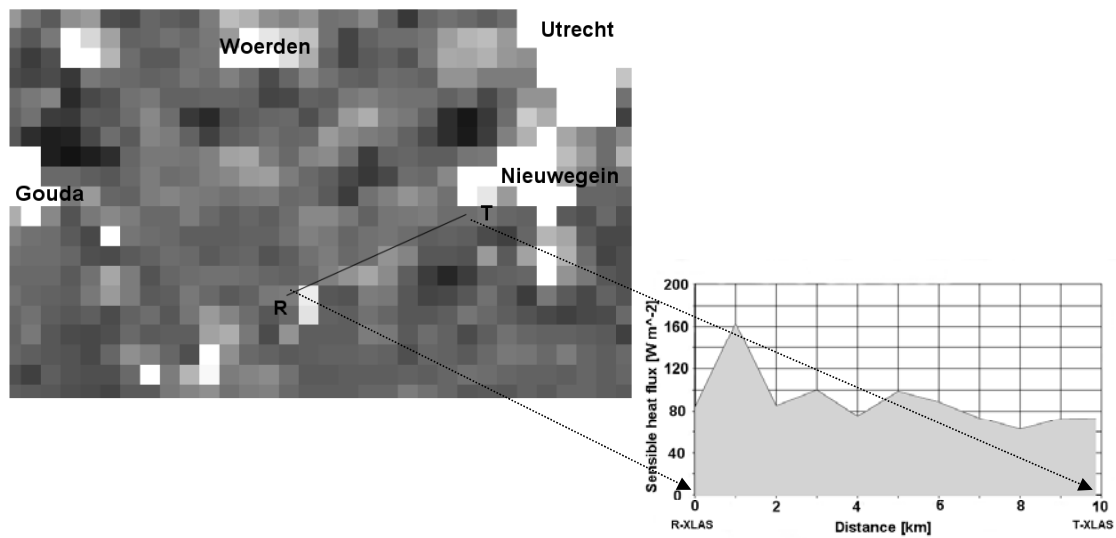
Figure 7.1: An instantaneous surface flux map (of sensible heat) for the Cabauw-area (The Netherlands) for Doy 225 (2000). The white pixels represent built-up areas (high sensible heat fluxes ~ 180 W m^{-2}), the dark black pixels are open water areas (low sensible heat fluxes ~ 0 W m^{-2}). The left figure shows the sensible heat flux for each pixel along the path of the XLAS scintillometer between the Cabauw tower (R) and the TV tower at Lopik (T).

Another approach is to integrate (routine) scintillometer observations in e.g. remote sensing techniques such as the remote sensing algorithm SEBAL (discussed in Chapter 5). This algorithm requires carefully selected wet and dry pixels within the image in order to determine the sensible heat flux for each individual pixel. It is assumed that the selected wet and dry pixels are completely wet (i.e. $H = 0$) and dry ($H = R_n - G_s$), respectively. When this assumption does not hold, e.g. during relative wet conditions or the extreme pixels are simply not present in the image (due to clouds), this has consequences for the derivation of the fluxes. By installing scintillometers at relative 'dry' and 'wet' areas and using these as wet and dry pixels this dilemma can be circumvented. The recently launched geo-stationary satellite MSG in combination with several (X)LAS sites can provide surface flux maps for large areas (catchment scale to continental scale) at a temporal scale of 15 minutes.

An interesting aspect is stable boundary layers. Recently, De Bruin et al. (2002) and Hartogensis et al. (2002) performed scintillometer experiments focussed on its performance during stable conditions. Although one must recognise its limitations, since the derivation of fluxes relies on MOST, the scintillation method can provide valuable information (i.e. the

structure parameter and/or inner scale length) especially over short time intervals (< 1 minute) due to its path-integrating capabilities.

The scintillation technique can also be used for monitoring gas exchange processes such as CO_2 fluxes or other atmospheric gasses. First of all it is important to note that the scintillation method cannot measure scintillations produced by atmospheric gasses. Scintillations are primarily the result of turbulent temperature and humidity fluctuations. However, the path-averaged turbulent exchange coefficient of heat (K_H) provided by a scintillometer and additional temperature profiles can be used to determine the flux of CO_2 from CO_2-concentration profiles (see Figure 7.2), thereby assuming that temperature and CO_2 are perfectly correlated ($R_{T-CO_2} = \pm 1$). The use of a DOAS (Differential Optical Absorption Spectrometer) system that can provide path-averaged concentration profiles of various gasses and a scintillometer is an interesting combination (see e.g. Poggio et al., 2000).
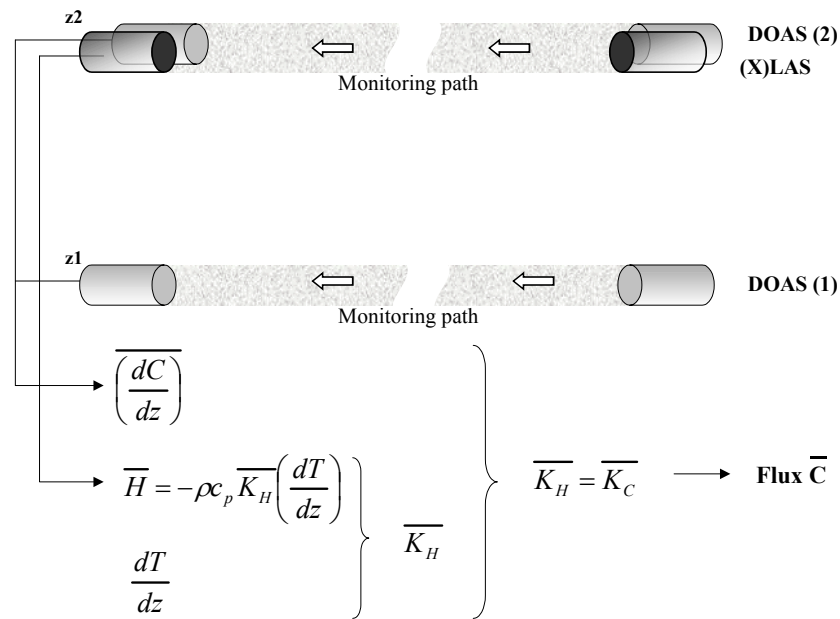

Figure 7.2: Schematic overview of a (X)LAS in combination with two DOAS systems.

This thesis mainly dealt with heterogeneity, evaporation and application aspects of the scintillation method. In Chapter 1 also some other aspects were discussed, such as the long-range scintillometry, saturation and advection. Some aspects that require further research are the ULAS (see Appendix C), the 'Hill-bump' (i.e. the turbulent spectrum at micro scales), TQ-similarity, saturation and stable conditions (i.e. the stability functions). As explained in

Appendix C, the placing of vertical stripes for the transmitting and receiving apertures of the LAS (preferable the XLAS) provide information about the path-averaged mean crosswind and variance and in turn the friction velocity (i.e. the ULAS). The latter is required for deriving the sensible heat flux from the scintillometer signal. An alternative option is to place the stripes vertically, by which the mean vertical wind speed (and variance) might be determined.

Appendix A

The scintillation method

A.1 Introduction

When electromagnetic (EM) radiation propagates through the atmosphere it is distorted by a number of processes that can influence its characteristics, e.g., its intensity (or amplitude), polarization and phase. Two of these processes are scattering and absorption by constituent gases and atmospheric particles of the atmosphere, which remove energy from the beam and thus lead to attenuation. Note that by far the most important characteristic of scattered radiation is its intensity. The most serious mechanism that influences the propagation of EM radiation is small fluctuations in the refractive index of air (n). These turbulent refractive index fluctuations in the atmosphere lead e.g., to intensity fluctuations and are also known as scintillations. Some examples that clearly show the distortion of wave propagation by the turbulent atmosphere, which can be seen regularly, are the twinkling of stars, image dancing and image blurring above a hot surface.

In most cases the atmosphere behaves turbulent. Turbulence is described as three-dimensional air motions or eddies, which have sizes ranging between millimetres to tens of metres. Turbulence in the atmosphere is the most effective transport mechanism for many scalar quantities, such as heat and water vapour. The refractive index of air is a function of the temperature (T) and to a lesser degree the humidity (Q) of the air, i.e., the density of the air (ρ). As eddies transport both heat and water vapour their refractive indices are different from their surroundings, resulting in refractive index fluctuations and thus scintillations.

Since the 1950s many scientists have conducted theoretical studies trying to explain scintillation phenomena. Several different theoretical approaches have been proposed to describe the propagation of EM radiation in a turbulent medium. In some approaches the turbulent eddies are visualized as a collection of positive and negative lenses, which focus or

defocus the beam resulting in scintillations. In others diffractional effects are taken into account. In the 1960s with the invention of the laser, experimental studies were conducted to validate the proposed propagation models. It was found that some of these models were very successful in describing certain phenomena for certain regimes.

Due to the success of the models that were able to relate the propagations statistics of EM radiation with the turbulent properties of the atmosphere, it is now possible to measure and quantify the turbulent characteristics of the atmosphere using a remote sensing method, also known as the scintillation method. A scintillometer is an instrument that consists of a light source (transmitter part) and a detector (receiver part) that measures intensity fluctuations. Because the measured variance of intensity fluctuations is a measure of the turbulent behaviour of the atmosphere it can indirectly be related to the transport of certain quantities. Depending on the configuration of the scintillometer, e.g. the aperture size, wavelength and the number of receivers the fluxes of heat, water vapour and momentum can be derived.
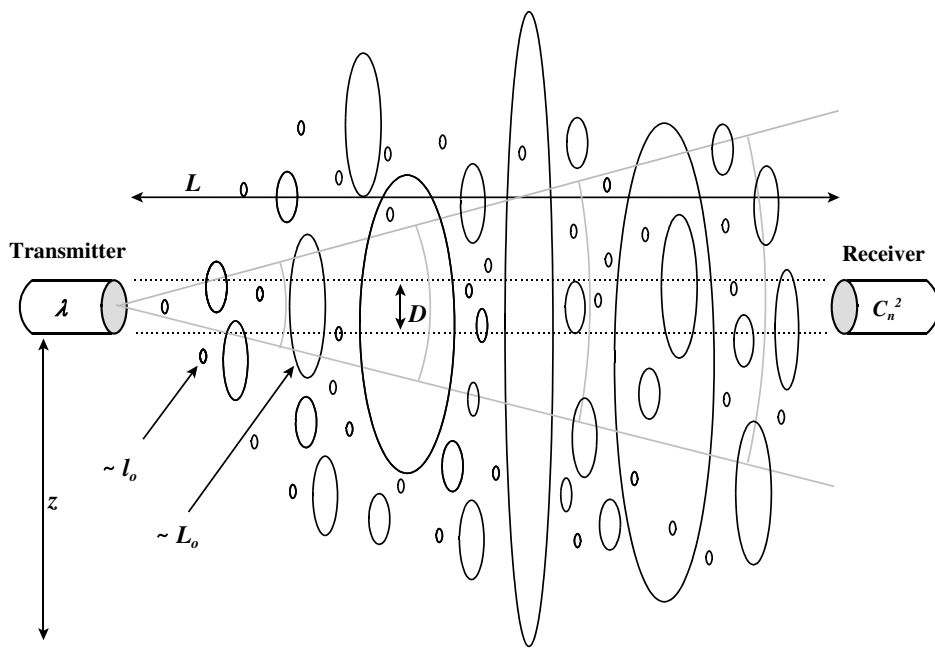

Figure A.1: Schematic drawing of a scintillometer set-up where the EM beam emitted by the transmitter is scattered by turbulent eddies in the atmosphere. Also some important length scales are shown.

A schematic of a scintillometer set-up is shown in Figure A.1. The transmitter emits a beam of light with a certain wavelength (λ). At a known distance L from the light source the receiver analyses the intensity fluctuations (expressed as C_n^2) that are caused by the turbulent

eddies. Also a number of length scales are shown that play a role in scintillometry; the diameter of the beam (D), the different eddy sizes bounded by l_o and L_o and the height of the scintillometer above the surface (z).

In the next sections the basics of the scintillation method will be explained. As reference the papers selected by Andreas (1990) and the comprehensive review paper by Moene (2000a) were used. The turbulent spectrum of refractive index fluctuations will be discussed in Section A.2. Structure functions, which are used to describe the behaviour of EM waves in random media, are explained in Section A.3. Several different wave propagation models have been proposed to describe the propagation of EM radiation in a turbulent medium. In Section A.4 the approaches and limitations of some of them are discussed briefly. The most successful approach that links the propagation statistics of EM radiation with the turbulent characteristics of the atmosphere is given in Section A.5. An important limitation of the scintillation method, known as saturation, is discussed in Section A.6. By increasing the aperture size of the scintillometer the path length can be extended without saturation effects. The basics of aperture averaging and the large aperture scintillometer (LAS) are explained in Section A.7. Both temperature and humidity fluctuations are responsible for fluctuations in the refractive index of air. This means that the measured C_n^2 can be related to C_T^2 and C_Q^2. Section A.8 will show that the contribution of temperature and humidity fluctuations is wavelength dependant. In Section A.9 is explained how the fluxes of heat (H) and latent heat (L_vE) can be derived from C_T^2 and C_Q^2 using the Monin-Obukhov similarity theory. Finally, Section A.10 gives a short summary of the scintillation method and the scintillometers used in the subsequent Chapters.

A.2 The turbulent spectrum

In the atmospheric boundary layer (ABL) the flow behaves generally very chaotic, i.e., turbulent. Turbulence consists of a wide range of three-dimensional whorls, usually called eddies. In general the largest eddies are generated by both wind shear and convection (dependant on local climatology) and have a size in the order of the boundary layer depth. The large scale eddies are unstable and brake down into smaller and smaller eddies, known as the

cascade process. Finally, the turbulent kinetic energy is dissipated into heat at the smallest molecular length scales, called the Kolmogorov micro scale

$$\eta = \left(\frac{\nu^3}{\varepsilon}\right)^{\frac{1}{4}}.$$

(A.1)

With typical values for the viscosity of air (ν) and the molecular dissipation rate of turbulent kinetic energy (ε), η is in the order of 1 mm.

In Figure A.2 a representation of the energy spectrum is depicted, which shows the distribution of the turbulent kinetic energy with wave number (κ). The wave number is defined as $\kappa = 2\pi/l$, where l is the size of the eddy. At eddy scales larger than the outer scale L_o ($K_o = 2\pi/L_o$) energy is introduced in the turbulent spectrum. In this part of the spectrum turbulence is not isotropic and inhomogeneous. In general the size of the outer scale is in the order of half the height above the surface (z). At wave number higher than K_m, which is related to the inner scale l_o ($K_m = 2\pi/l_o$), the turbulent kinetic energy is dissipated into heat. Typical size of the inner scale is 1 mm to 10 mm. Hill and Clifford (1978) defined the inner sale as the intersection point of the asymptotic forms of the structure functions (see Section A.3) in the inertial and dissipation ranges. They showed that the inner scale is related to the Kolmogorov micro scale as follows

$$l_o = 7.4 \left(\frac{\nu^3}{\varepsilon}\right)^{\frac{1}{4}}.$$
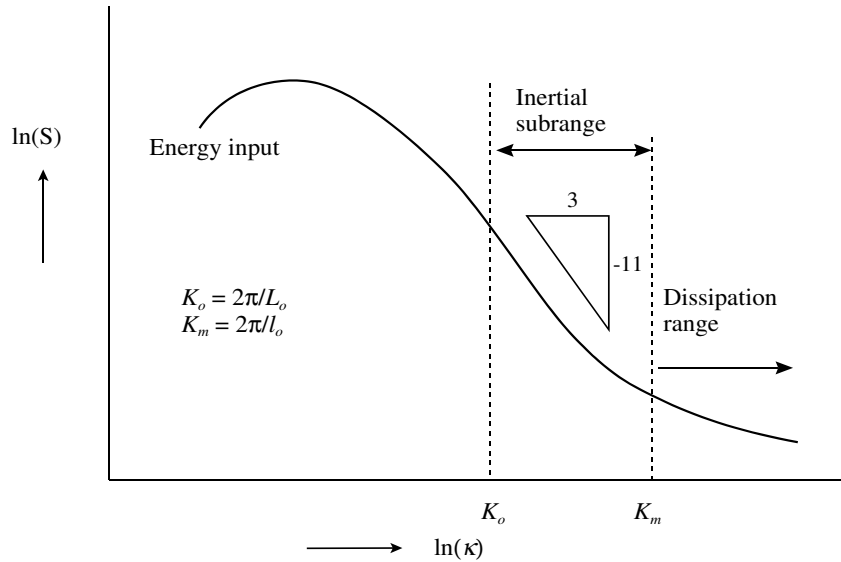
(A.2)

110

Figure A.2: Schematic representation of the energy spectrum of turbulence.

Part of the spectrum, which lies between the inner scale and outer scale of turbulence, is called the inertial sub range. This part of the spectrum is independent of the energy input and the viscous dissipation and only the inertial transfer of energy is important. In the cascade process from large to intermediate and small size eddies Kolmogorov hypothesized that these small eddies have no memory of the large-scale processes and turbulence becomes isotropic at the high wave numbers (Garratt, 1992).

Based on the concept of the cascade process Kolmogorov proposed the following form for the three-dimensional spectrum of refractive index fluctuations ($\Phi_K(\kappa)$) in the atmosphere (Tatarskii, 1961)

$$\Phi_K(\kappa) = 0.033 C_n^2 \kappa^{\frac{-11}{3}} , \qquad (A.3)$$

where κ is the wave number and C_n^2 is the structure parameter of the refractive index of air (see Section A.3). This model is only valid for the inertial sub range, although it is often extended over all wave numbers by assuming the inner scale is zero and the outer scale is infinite. However, it was found that the model overestimates $\Phi_K(\kappa)$ in the dissipation range (i.e. it falls off more rapidly than $-11/3$). Therefore, Tatarskii (1961) proposed the following model

$$\Phi_T(\kappa) = 0.033 C_n^2 \kappa^{\frac{-11}{3}} \exp\left(\frac{-\kappa^2}{\kappa_m^2}\right), \tag{A.4}$$

where $\kappa_m = 5.92/l_o$. This model uses a Gaussian cut-off at high spatial wave numbers, which results in a steeper falloff than $\kappa^{-11/3}$. This can be seen in Figure A.3 where both the Kolmogorov ($\Phi_K(\kappa)$) and Tatarskii ($\Phi_T(\kappa)$) spectral model are shown.
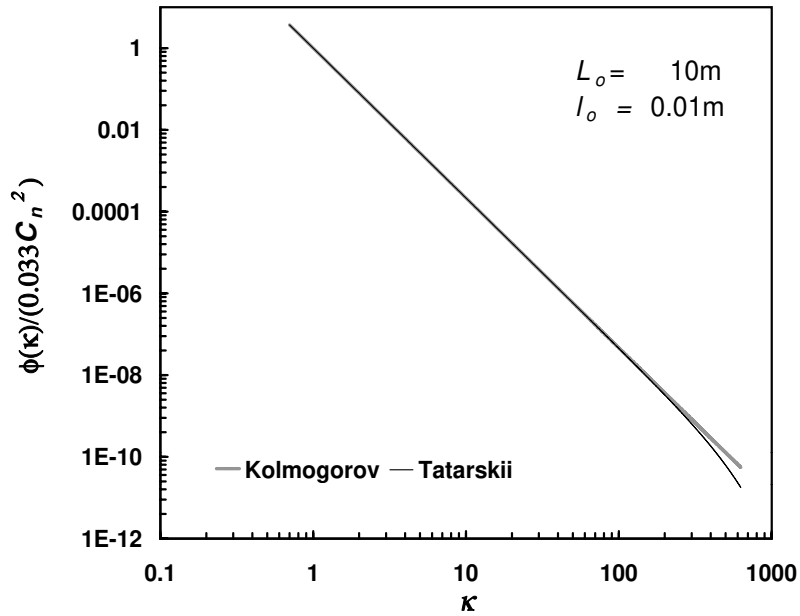

Figure A.3: Spectral models by Kolmogorov ($\Phi_K(\kappa)$) and Tatarskii ($\Phi_T(\kappa)$) of refractive index fluctuations.

Fast temperature and velocity measurements by Champagne et al. (1977) and Williams and Paulson (1977) revealed a 'bump' in the spectrum at high wave numbers near l_o^{-1}. Neither the model of Kolomogorov nor that of Tatarskii exhibits this bump. Based on the data of Champagne et al. (1977), Hill (1978) developed a theoretical model ($\Phi_H(\kappa)$) that describes this bump and agrees well with the observations. Churnside (1990) derived an analytical approximation to the Hill model

$$\Phi_C(\kappa) = 0.033 C_n^2 \kappa^{\frac{-11}{3}} \left[\exp\left(-70.5 \kappa^2 \left(\frac{l_0}{7.5}\right)^2\right) + 1.45 \exp\left(-0.97\left(\ln\left(\kappa \frac{l_0}{7.5}\right)+1.55\right)^2\right) \right]. \tag{A.5}$$

Frehlich (1992) determined $\Phi_F(\kappa)$ directly from laser scintillation measurements. In Figure A.4 the Hill-spectrum (1978) is shown together with the models of Churnside (1990) and Frehlich (1992). It can be seen that the model of Tatarskii shows no bump and the models of Churnside and Frehlich slightly differ from the Hill spectrum. In Section A.5 it will be shown that the exact form of the spectrum $\Phi(\kappa)$ at high wave numbers is important to know, especially when a near infrared point source/detector scintillometer is used (see e.g., Hartogensis et al, 2002; De Bruin et al., 2002). The reason is that these scintillometer types are most sensitive to eddy sizes in the order of the inner scale l_o, i.e. close to the bump in the spectrum. On the other hand a large aperture scintillometer is most sensitive to eddy sizes in the order of the aperture diameter (D) and is therefore less sensitive to the bump and thus the exact form of $\Phi(\kappa)$.
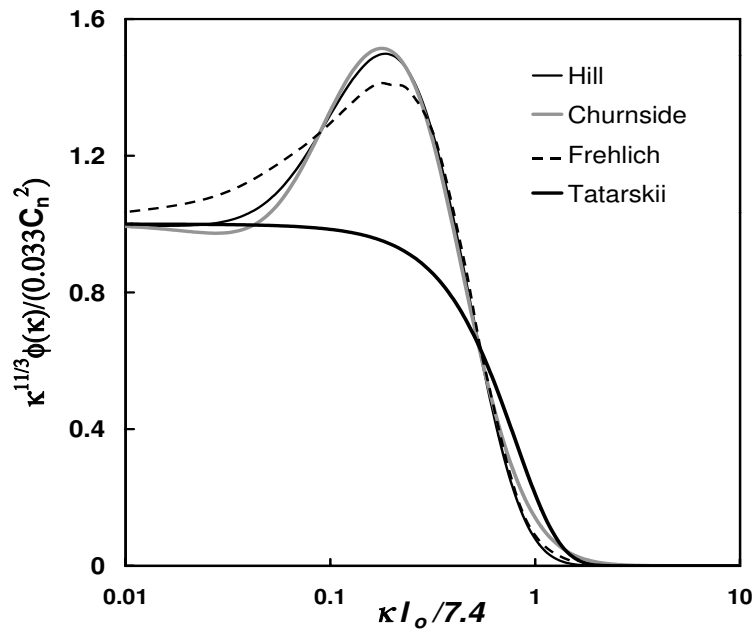

Figure A.4: Scaled spectral models of refractive index fluctuations of Hill (1978), Churnside (1990) and Frehlich (1992) showing the 'Hill' bump plotted together with the Tatarskii spectrum as a function of the wave number scaled by the inner scale (l_o/7.4).

A.3 The structure parameter of the refractive index of air $C_n{}^2$

Wind speed (u), air temperature (T), the refractive index (n) and other quantities undergo irregular random fluctuations in a turbulent atmosphere. Random processes in space and time can be described by random functions, e.g., $n(t)$, which is a random function describing the refractive index of air. However random functions are difficult to determine. In practice one uses statistical characteristics of the random functions. An important characteristic of a random function is the correlation function $B(\mathbf{r}_1,\mathbf{r}_2)$, which describes the spatial structure of turbulence. The correlation function describing the refractive index fluctuations in a random field $n(\mathbf{r})$ is as follows (Tatarskii, 1961)

$$B_n(\mathbf{r}_1,\mathbf{r}_2) = \left\langle \left[n(\mathbf{r}_1) - \langle n(\mathbf{r}_1) \rangle \right]\left[n'(\mathbf{r}_2) - \langle n'(\mathbf{r}_2) \rangle \right] \right\rangle, \qquad (A.6)$$

where a random field can be considered as a random function of three variables (e.g. the three velocity components in a velocity field) and the angle brackets denote an ensemble average. B_n describes the mutual relation between the fluctuations of a scalar n at different locations in space ($\mathbf{r}_1$ and $\mathbf{r}_2$). A random field is statistically homogeneous if it has a constant mean and B_n is unaffected by a simultaneous translation of $\mathbf{r}_1$ and $\mathbf{r}_2$ in the same direction by the same amount, i.e.

$$\langle n(\mathbf{r}) \rangle = \text{const}, \qquad B_n(\mathbf{r}_1,\mathbf{r}_2) = B_n(\mathbf{r}_1 + \mathbf{r}_0, \mathbf{r}_2 + \mathbf{r}_0). \qquad (A.7)$$

Choosing $\mathbf{r}_0 = -\mathbf{r}_2$, the correlation function in a homogeneous field depends only on the difference $\mathbf{r}_1 - \mathbf{r}_2$

$$B_n(\mathbf{r}_1,\mathbf{r}_2) = B_n(\mathbf{r}_1 - \mathbf{r}_2, 0) = B_n(\mathbf{r}_1 - \mathbf{r}_2). \qquad (A.8)$$

A homogeneous random field is isotropic if B_n only depends on $r = |\mathbf{r}|$, i.e. only on the distance between the points and not the direction

$$B_n(\mathbf{r}_1,\mathbf{r}_2) = B_n(r). \qquad (A.9)$$

However homogeneous and isotropic random fields are only crude approximations to real meteorological fields. For example, most statistical characteristics of atmospheric turbulence are a function of altitude. Therefore, as with non-stationary random processes, it is better to use structure functions instead of correlation functions.

The difference of the field values $n(\mathbf{r})$ between $\mathbf{r}_1$ and $\mathbf{r}_2$ is mainly influenced by those inhomogeneities of the field n, which are smaller than $|\mathbf{r}_1 - \mathbf{r}_2|$. If this distance is not too large, the largest inhomogeneities have no effect on $n(\mathbf{r}_1) - n(\mathbf{r}_2)$ and therefore the (second order) structure function

$$D_n(\mathbf{r}_1, \mathbf{r}_2) = \left\langle \left[(n(\mathbf{r}_1) - \langle n(\mathbf{r}_1) \rangle) - (n(\mathbf{r}_2) - \langle n(\mathbf{r}_2) \rangle) \right]^2 \right\rangle,$$
(A.10)

depends on $\mathbf{r}_1$ - $\mathbf{r}_2$ only. This hypothesis, proposed by Kolmogorov, is known as local homogeneity. Thus the value of D_n characterizes the intensity of those fluctuations of n with scales smaller than or equal to $\mathbf{r}_1$ - $\mathbf{r}_2$. On the other hand $B_n(\mathbf{r}_1, \mathbf{r}_2)$ depends not only on the distance $\mathbf{r}_1$ - $\mathbf{r}_2$ but also on $\mathbf{r}_1$ and $\mathbf{r}_2$ separately and therefore depends on inhomgeneities of all scales.

In case of a locally homogeneous random field ($\langle n(\mathbf{r}) \rangle = \text{const}$), the structure function only depends on $\mathbf{r}_1$ - $\mathbf{r}_2$

$$D_n(\mathbf{r}_1, \mathbf{r}_2) = D_n(\mathbf{r}_1 - \mathbf{r}_2).$$
(A.11)

Finally, a locally homogenous random field is locally isotropic if D_n only depends on $|\mathbf{r}_1 - \mathbf{r}_2|$, i.e. only on the distance and not the direction, which leads to the following simplified form of the structure function

$$D_n(\mathbf{r}) = D_n(r) = \left\langle \left[n(\mathbf{r'}+\mathbf{r}) - n(\mathbf{r'}) \right]^2 \right\rangle.$$
(A.12)

The structure function is related to the three-dimensional spectrum as follows (Tatarskii, 1961)

$$D_n(r) = 8\pi \int_0^\infty \left(1 - \frac{\sin \kappa r}{\kappa r}\right) \Phi(\kappa) \kappa^2 d\kappa . \qquad\qquad\qquad \text{(A.13)}$$

By inserting only the inertial sub range part of the spectrum the following well-known relationship for a locally isotropic field can be derived

$$D_n(r) = C_n^2 r^{2/3} , \qquad\qquad l_o << r << L_o \qquad\qquad\qquad \text{(A.14)}$$

where C_n^2 is the structure parameter of the refractive index of air. When turbulence is homogeneous and isotropic within the inertial sub range C_n^2 is independent of r and is a measure of the amount of turbulent refractive index fluctuations. A larger value corresponds to more turbulent mixing of air.

A.4 Wave propagation theory in random media

When an EM wave propagates through a turbulent medium (e.g., the atmosphere) it suffers from scattering mechanisms and absorption. The most important mechanism that causes scattering in the atmosphere is random fluctuations in the refractive index of air. Both Obukhov and Tatarskii were one of the first who did theoretical studies on scintillation phenomena based on wave equations. Later on followed by experimental studies using lasers. So far the theory of optical propagation of EM waves through random media is not fully understood, except for certain regimes.

Several theoretical models have been developed that describe certain phenomena of line-of-sight wave propagation in a random medium (Lawrence and Strohbehn, 1970; Strohbehn, 1968; Tatarskii, 1961). One of these is the geometrical optics approach (Tatarskii, 1961; 1971). In this approach amplitude fluctuations are attributed to the focusing and defocusing of the EM rays by the curvature of the turbulent eddies along the path, i.e. the eddies are considered as a collection of positive and negative lenses. This approach has been successfully applied to the line-of-sight propagation of short wavelengths, i.e. wavelengths that are small compared to the inner scale of turbulence ($\lambda << l_o$). This is mainly needed to

ensure that small-angle scattering can be assumed (Strohbehn, 1968). Tatarskii (1961; 1971) showed that in the geometrical optics method the smallest inhomogeneities of the order of l_o are the most essential for intensity fluctuations (small eddies are more curved than large ones). The main restriction of the geometrical optics method is that it ignores diffractional spreading. Diffractional spreading, which has a scale size of $F = \sqrt{\lambda L}$ also known as the first Fresnel zone, can be seen around the shadow of a certain object at a screen. In case the object is much larger than the scale of diffractional spreading, diffraction effects can be ignored ($F \ll l_o$). Because F depends on the propagation distance L a certain point will be reached where F will become larger. When this happens the focusing and defocusing process by lenses of the order of l_o no longer contribute to the observed intensity fluctuations, instead diffractional effects become dominant. Because F depends on L the geometrical optics method is restricted to short path lengths (see Section A.6).

An alternative approach is the method of smooth perturbations, which takes diffraction effects into account (Tatarskii, 1961; 1971). As a result this approach is valid over longer distances. However, the method assumes that the wave is only perturbed slightly from its original state (i.e. weak scattering), which in practise again limits the distance.

The best method so far is the so-called Rytov method, which is also a perturbation method and accounts for diffractional effects. Originally it was claimed that it would overcome the latter limitation of the smooth perturbation method. Later, experimental studies proved otherwise. The main difference between the two perturbation methods is that the Rytov method is applied to a transformation of the wave equation used in the original perturbation approach. Nevertheless, a perturbation method is only valid when the perturbations are small (i.e. weak turbulence conditions) and thus restricts the propagation distance.

The starting point of all methods is the wave equation, which represents the propagation of a monochromatic wave through a random medium thereby neglecting polarisation effects (Lawrence and Strohbehn, 1970; Andrews et al., 2001)

$$\nabla^2 E(r) + k^2 n^2(r) E(r) = 0 \ . \tag{A.15}$$

∇^2 is the three-dimensional Laplacian operator of an electromagnetic wave E, k the optical wave number (= $2\pi/\lambda$) and n the refractive index of the medium. The first term includes diffraction effects, which are ignored in the geometrical optics method.

In the atmosphere it is known that the refractive index fluctuations around its mean value are very small. Based on this fact a perturbation expansion is used in order to solve Equation A.15. I.e. a perturbation expansion of E and n; $E = E_0 + E_1$ where E_o is the incident electric field and E_1 the scattered field and $n = 1 + n_1$ where $n_1 \ll 1$. It must be noted that in the perturbation expansion only the first scattering term is considered (i.e. E_2, E_3 …= 0) in order to derive an analytical solution. In Section A.6 experimental evidence will reveal that ignoring these higher-order terms restricts the validity of derived solutions of Equation A.15. In the Rytov method the wave equation is transformed by substituting $\Psi = \ln(E)$. Considering a plane wave $E = Ae^{iS}$, where A is the amplitude and S the phase, Ψ becomes

$$\Psi = \chi + iS .$$
(A.16)

If the perturbations are small, i.e. $E_1 \ll E_0$, a solution of Equation A.15 can be derived in the form of an unperturbed and perturbed part, where the amplitude (χ) and phase (S') fluctuations can be expressed as

$$\chi = \ln\left(\frac{A}{A_0}\right)$$
(A.17)

and

$$S' = S - S_0 ,$$
(A.18)

where A_0 and S_0 are the amplitude and phase of the unperturbed wave E_0. A similar perturbation approach is applied to Equation A.15 for spherical waves (i.e., a point source/detector). In the next Section the solution of the Rytov method for spherical waves will be discussed, which is applicable for small aperture scintillometers.

A.5 Statistical solution of the wave equation

The solution of the wave equation following the Rytov approach for spherical waves (i.e. point source/detector) propagating through a random medium, which is statistically homogeneous and locally isotropic, is as follows (Lawrence and Strohbehn, 1970)

$$\sigma_\chi^2 = 4\pi^2 k^2 \int\limits_0^L dx \int\limits_0^\infty d\kappa \kappa \Phi(\kappa) \sin^2\left(\frac{\kappa^2 x(L-x)}{2kL}\right).$$
(A.19)

σ_χ^2 is the variance of the logarithm of amplitude fluctuations (χ) measured by a small aperture scintillometer (SAS), k the optical wave number, L the path length, κ the (spatial) wave number and $\Phi(\kappa)$ the three-dimensional spectrum of refractive index fluctuations. Inserting the Kolmogorov spectrum thereby ignoring small-scale effects and carrying out the integration gives the following relation between σ_χ^2 and the path averaged C_n^2 (Tatarskii, 1961)

$$\sigma_\chi^2 = 0.124 k^{\frac{7}{6}} L^{\frac{11}{6}} \overline{C_n^2}, \qquad\qquad l_o << F << L_o, \ \sigma_\chi^2 < 0.3.$$
(A.20)

This equation, which is based on the first-order scattering theory, is only valid in the weak scattering regime and is therefore only applicable when $\sigma_\chi^2 < 0.3$ (Clifford et al., 1974, Section A.6). Small scale effects can be ignored when $F >> l_o$. For example a scintillometer that operates at a radio wavelength of 11 mm has a Fresnel size of several meters, thus $F >> l_o$. When the wavelength lies in the visible to near-infrared wavelength region F approximately equals l_o. In that case small effects cannot be ignored and an accurate three-dimensional spectrum (i.e. the Hill spectrum) must be substituted instead, which leads to the following expression

$$\sigma_\chi^2 = 0.124 k^{\frac{7}{6}} L^{\frac{11}{6}} \overline{C_n^2} \Phi\left(\frac{l_o}{F}\right), \qquad\qquad l_o \approx F << L_o, \ \sigma_\chi^2 < 0.3,$$
(A.21)

where the function $\Phi(l_o/F)$ accounts for the small scale effects. Important to note is that due to the large Fresnel zone of a scintillometer that operates at a wavelength of 11 mm the

scintillometer becomes more sensitive to outer scale effects because F approaches L_o. Note that Equations A.20 and A.21 are often expressed as a function of intensity fluctuations ($\sigma_{\ln I}^2 = 4\sigma_{\ln A}^2 = 4\sigma_\chi^2$) because most scintillometers measure intensity fluctuations.

When Equation A.19 is written in a more convenient form, showing the averaging of C_n^2 along the path L

$$\sigma_\chi^2 = \int_0^L C_n^2(x)W(x)dx \qquad (A.22)$$

the path weighting function $W(x)$ can be derived

$$W(x) = 4\pi^2 k^2 \int_0^\infty d\kappa\,\kappa\,\Phi(\kappa)\sin^2\left(\frac{\kappa^2 x(L-x)}{2kL}\right) \quad \approx \left(\frac{x}{L}\left(1-\frac{x}{L}\right)\right)^{5/6}. \qquad (A.23)$$

An example of the path weighting function is depicted in Figure A.5 (assuming the detector approximates a point detector), which shows that the path weighting function has its maximum in the centre of the path and gradually drops to zero at the ends. This means that the scintillometer is most sensitive to 'scintillating' eddies in the middle of its path.
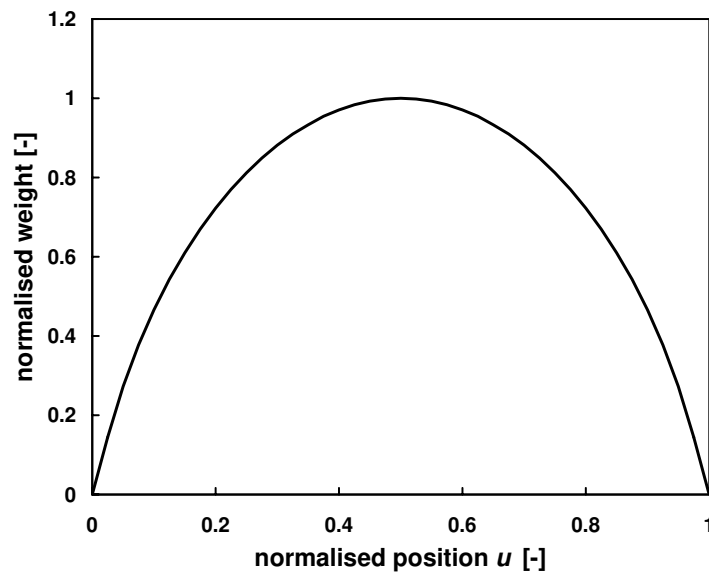

Figure A.5: The path weighting function (W) of a point source transmitter/detector (i.e. a spherical wave) as a function of the relative position u ($= x/L$).

In order to analyse the size of the eddies that produce the most powerful scintillations the integrand of Equation A.23, rewritten as

$$\kappa\Phi(\kappa)\sin^2\left(\frac{\kappa^2\dfrac{x}{L}\left(1-\dfrac{x}{L}\right)F^2}{4\pi}\right), \tag{A.24}$$

has to be analysed. For $x/L = 0.5$ and 0.05 this integrand is plotted in Figure A.6 as a function of F/l ($= F\kappa/2\pi$). The Figure reveals that the optically most effective eddies are of the order of the diameter of the first Fresnel zone F in the centre of the path ($x/L = 0.5$) and decreases in size towards the transmitter and receiver ends ($x/L = 0.05$). As mentioned before, depending on the configuration of the scintillometer (i.e. λ) and its set-up (i.e. L) F varies between several millimetres to a few meters.
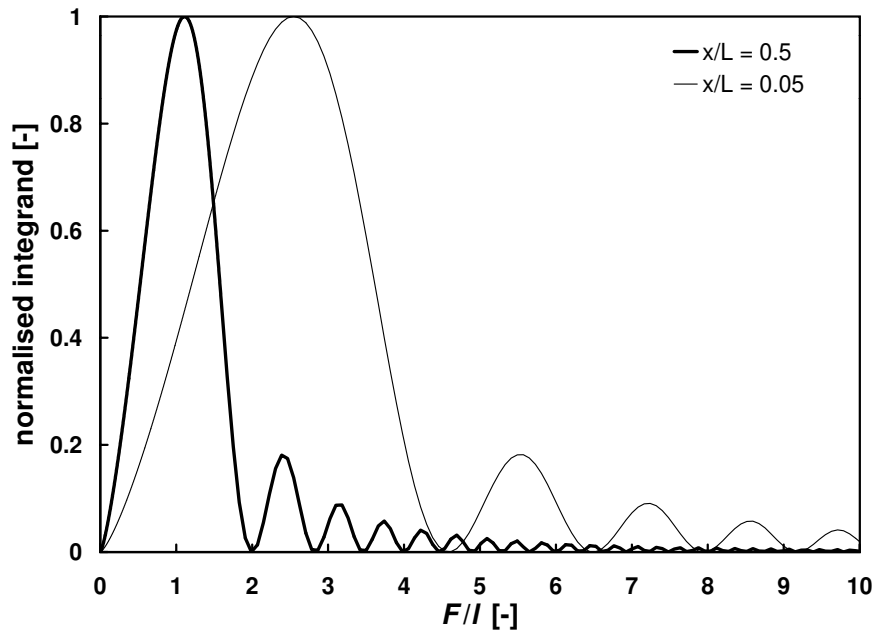

Figure A.6: Values of the integrand (normalized to 1) as a function of the size of the inhomogeneity l, which is normalized by the first Fresnel zone F (for $x/L = 0.5$ and 0.05).

A more simple physical model to derive the size of the optically most effective eddies is shown in Figure A.7 (Clifford et al., 1974). This Figure shows an irregularity (e.g., an eddy) of diameter $2l$ at an arbitrary point X between the transmitter (S) and the receiver (at distance

L). The eddy will be most effective in producing a 'scintillation' at point L when the difference between path SAL and SL equals $\lambda/2$, i.e. in this way the two rays interfere destructively. Note that it is assumed that the spherical wave is scattered only once. Working out the geometry gives

$$l \approx \sqrt{\pi\left(\frac{x}{L}\right)\left(1-\frac{x}{L}\right)}\sqrt{\lambda L} \ . \tag{A.25}$$

Again the most optically effective eddy has a size of approximately F in the centre ($x/L = 0.5$) and decreases in size towards the ends ($x/L \rightarrow 0$ and 1). If there are smaller eddies than F at point X scintillations will be produced at places, which lie between point X and the receiver (L). Although these scintillations eventually will reach point L their contribution to the total variance at the receiver is small. On the other hand eddy sizes larger than F will not produce intensity fluctuations because of their long focal lengths and will only tilt the wave.
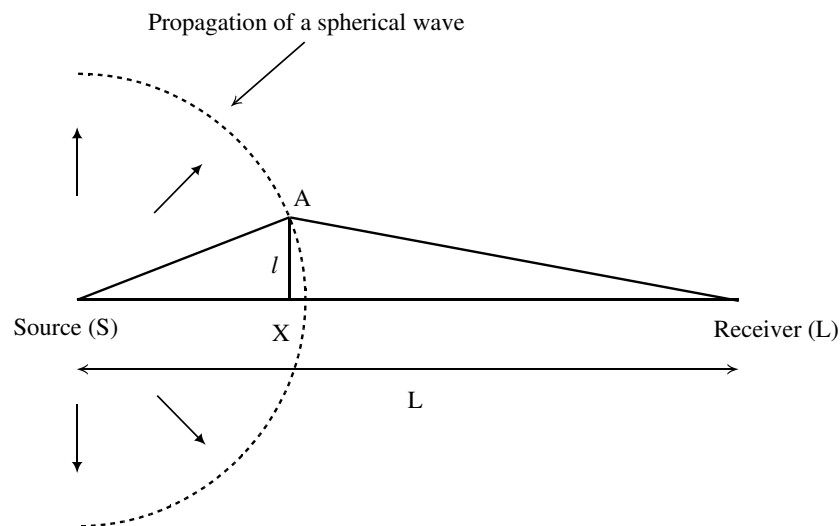

Figure A.7: The geometry of a simple eddy model. The receiver (L) observes scintillations of a spherical wave emitted by the transmitter (S), which are produced by an eddy/irregularity at point X.

A.6 Saturation

Equation A.19 is based on first-order scattering theory (i.e., the wave is scattered only once, see Section A.4). Therefore, this Equation is only valid in a weak scattering medium. If the turbulence becomes too intense (i.e. a strong scattering medium where scattering occurs more than once) the proportionality between σ_χ^2 and C_n^2 will fail. This phenomenon is known as saturation of the signal. Clifford et al. (1974) found that saturation occurs when $\sigma_\chi^2 > 0.3$. When this happens a further increase of C_n^2 no longer results in an increase of σ_χ^2. Figure A.8 shows observed values of σ_χ^2 plotted against theoretically predicted values of σ_χ^2 using Equation A.19 and known values of k and L and C_n^2 values derived from temperature probes. It can be seen that for all path lengths except the shortest saturation occurs. Over extreme long path lengths a point will be reached were σ_χ^2 starts to decrease. This is called super saturation (see Figure A.8 for $L = 1750$ m).
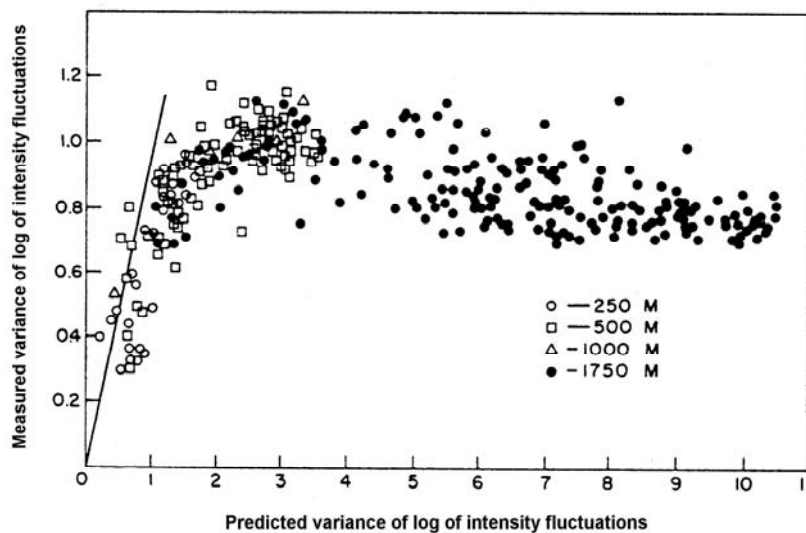

Figure A.8: Measured values of σ_χ^2 (vertical axis) plotted against modelled σ_χ^2 values (horizontal axis) showing the saturation effect, which occurs over long path lengths (reproduced from Strohbehn, 1968). The solid line equals a 1:1 line.

Clifford et al. (1974) explained the saturation effect as follows, which is sketched in Figure A.9. As the wave passes through a strong scattering medium lenses at both sides of the lens F

will distort the wave front resulting in small irregularities in the wave front. When the size of these irregularities is smaller than the size of F the power of lens F will be diminished. Finally, this results in a pattern at $x = L$, which is different in size compared with the pattern for a single scattering situation with an undisturbed spherical wave front. This effect is known as smearing of the pattern and will result in a decrease of σ_χ^2. When the size of lens F becomes smaller and smaller eventually a point will be reached where there can be no irregularities in the wave front than the smallest eddy l_o. This means that if lens F has the size l_o it can no longer be distorted and is effective in producing scintillations. In the case the irregularities in the wave front are larger than the F the pattern at point $x = L$ will not change in size but only its position will shift on the screen (this can be seen as tilting of the wave front). To summarize over longer path lengths the most effective eddies are no longer of the scale size of the first Fresnel zone. Instead smaller scales become dominant. According to the turbulent power spectrum small scale turbulence is less powerful than large scale turbulence resulting in a decrease of σ_χ^2 as is shown in Figure A.8.
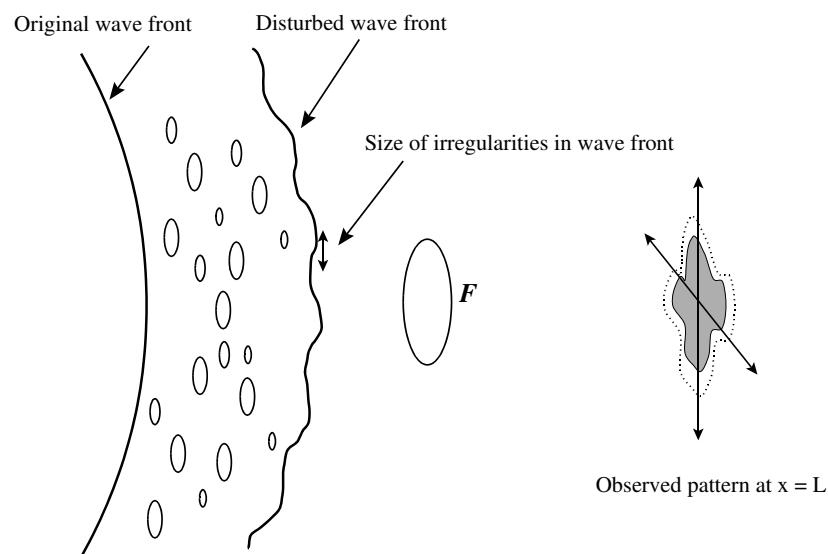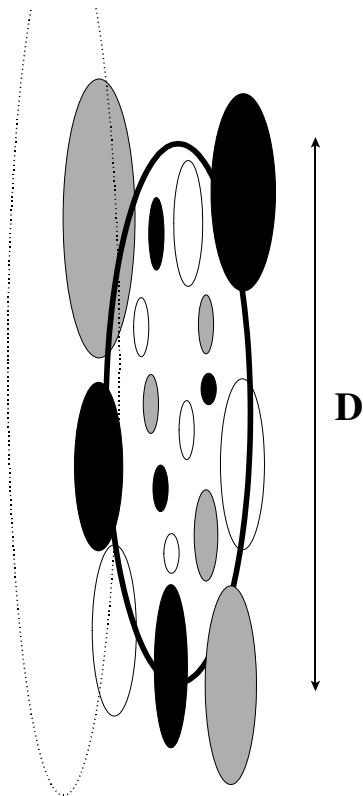

Figure A.9: Schematic representation of the smearing effect caused by irregularities smaller than lens F under strong turbulent conditions.

A.7 The Large Aperture Scintillometer

A simple way to avoid saturation is by limiting the path length. Another way to overcome saturation of the signal is to increase the aperture size (*D*) of the scintillometer (Wang et al., 1978). When the aperture size of the receiver is larger than the scale of the optically most effective eddies (*F*) the receiver will average out fluctuations of the received signal over the aperture area. This process, called aperture averaging leads to reduced intensity fluctuations.

In Figure A.10 a schematic drawing of the averaging effect is shown. Due to the diffraction process in the atmosphere a scintillation pattern, which consists of a wide range of dark and bright structures, will drift over a screen positioned at the receiver side. A very small receiver will be sensitive to all these scales in the scintillation pattern. As the aperture of the receiver increases fine scale structures in the pattern will average out over the aperture, i.e., small dark and bright spots will compensate. As a result σ_χ^2 will decrease. Very large-scale structures in the scintillation pattern, which are larger than the aperture diameter, will not be seen because they don't produce intensity fluctuations. On the other hand structures that are in the order of the aperture diameter will be dominant. Although it is less apparent, the same averaging occurs when the diameter of the transmitter increases (assuming an incoherent source). In this case the aperture of the transmitter can be regarded as a collection of point sources, which filter out fine scale turbulence.

Figure A.10: Schematic drawing of aperture averaging of fine scale turbulence.

For equal transmitting and receiving apertures with diameter D, the expression for σ_χ^2 is as follows (Hill and Ochs, 1978)

$$\sigma_\chi^2 = 4\pi^2 k^2 \int_o^L dx \int_0^\infty d\kappa\,\kappa\,\Phi(\kappa)\sin^2\left(\frac{\kappa^2 x(L-x)}{2kL}\right) \cdot$$

$$\left[\left(\frac{2J_1\left(0.5\kappa D\frac{x}{L}\right)}{0.5\kappa D\frac{x}{L}}\right) \cdot \left(\frac{2J_1\left(0.5\kappa D\left(1-\frac{x}{L}\right)\right)}{0.5\kappa D\left(1-\frac{x}{L}\right)}\right)\right]^2, \qquad \text{(A.26)}$$

where J_1 is the Bessel function. Note that this expression is still based on the first-order scattering theory, which means that a large aperture scintillometer also has saturation point. The term between the brackets accounts for the aperture averaging. For infinite small aperture (i.e. $D \to 0$) this term approaches unity and the resulting equation is valid again for a point source/detector scintillometer (Equation A.19). In Figure A.11 this term is plotted as a function of wave number. At high wave numbers this term goes to zero, i.e., small-scale turbulence is filtered out.
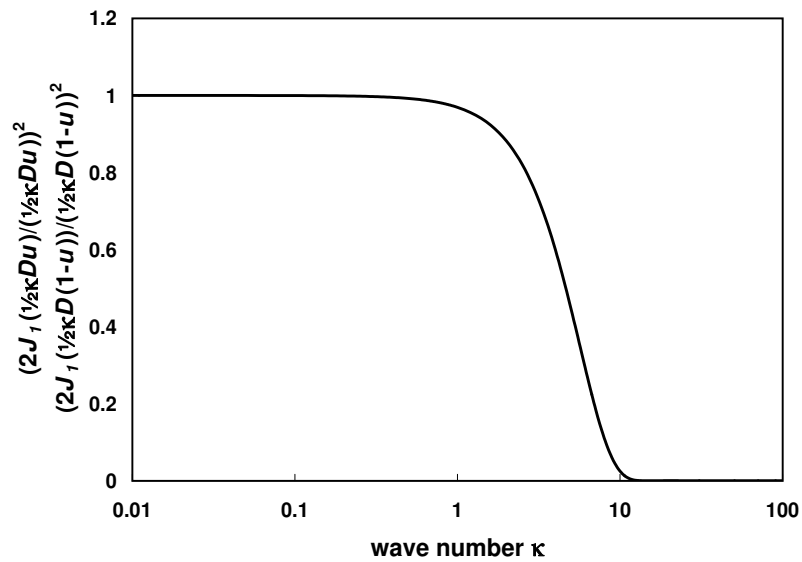

Figure A.11: The 'aperture averaging' term of Equation A.26 as a function of wave number (for $u = 0.5$).

After inserting the spectrum of refractive index fluctuations and integrating Equation A.26 the relation between σ_χ^2 and the path averaged C_n^2 for a large aperture scintillometer can be derived (Wang et al., 1978)

126

$$\sigma_\chi^2 = 0.223 D^{\frac{-7}{3}} L^3 \overline{C_n^2}, \qquad l_o << F << D << L_o. \tag{A.27}$$

Important to note is that aperture size must be sufficiently large. In Figure A.12 the normalized variance σ_χ^2 is plotted as a function of the normalized aperture diameter α (= D/F). It can be seen that σ_χ^2 is only proportional to $\alpha^{-7/3}$ when α is larger than 2, i.e., $D > 2F$. This means that if L becomes too large Equation A.27 is no longer valid.
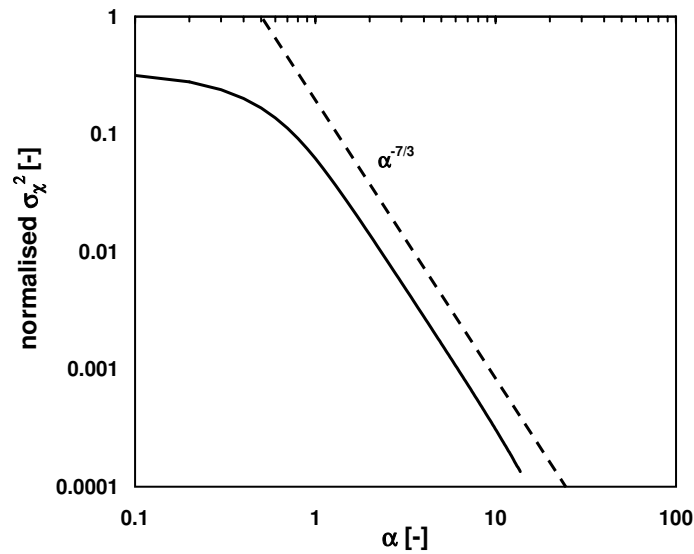

Figure A.12: The normalized σ_χ^2 as a function of α (= D/F). For small α (i.e., small D) σ_χ^2 is no longer proportional to $\alpha^{-7/3}$.

As for the point source/detector scintillometer Equation A.26 can be re-written in a more convenient form to derive the path weighting function $W(x)$ for a LAS

$$W(x) = 4\pi^2 k^2 \int_0^\infty d\kappa \kappa \Phi(\kappa) \sin^2\left(\frac{\kappa^2 x(L-x)}{2kL}\right) \cdot \left[\left(\frac{2J_1\left(0.5\kappa D \frac{x}{L}\right)}{0.5\kappa D \frac{x}{L}} \right) \cdot \left(\frac{2J_1\left(0.5\kappa D\left(1-\frac{x}{L}\right)\right)}{0.5\kappa D\left(1-\frac{x}{L}\right)} \right) \right]^2. \tag{A.28}$$

The path weighting function is depicted in Figure A.13, which shows that a large aperture scintillometer is also most sensitive in the centre of its path.
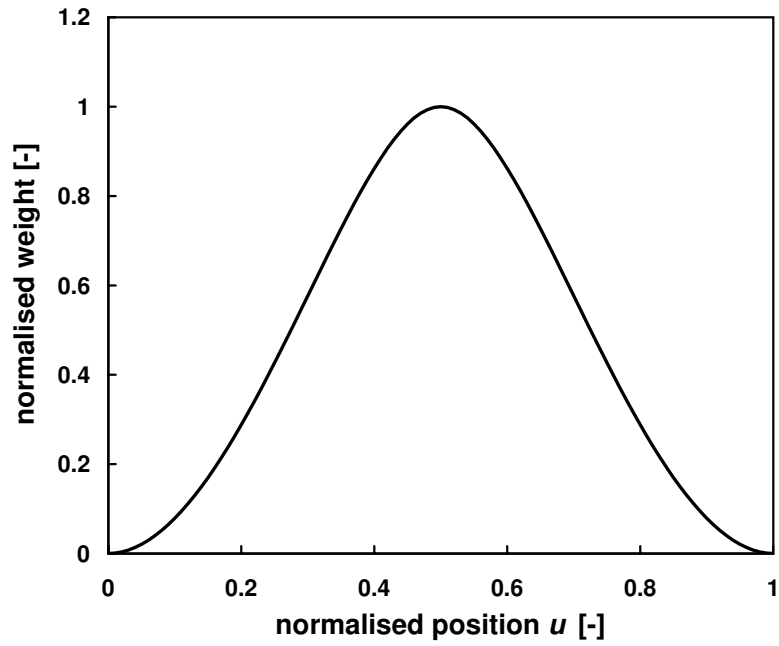
Figure A.13: The path weighting function (W) of a large aperture scintillometer ($\lambda = 930$ nm) as a function of the relative position u (= x/L).

In Figure A.14 the integrand of Equation A.28 is shown. This Figure is similar to Figure A.6 showing the most effective eddy seen by a scintillometer. In Figure A.14 the peak of the integrand lies at a scale of the order of the aperture diameter D instead of the first Fresnel zone for $x/L = 0.5$, showing that a LAS is most sensitive to D sized scales.

Figure A.14: Values of the integrand (normalized to 1) as a function of the size of the inhomogeneity l, which is normalized by the aperture diameter D (for $x/L = 0.5$ and 0.05).

According to Wang et al. (1978) the diameter of the aperture should be sufficiently large in order to avoid saturation. They derived the following criterion
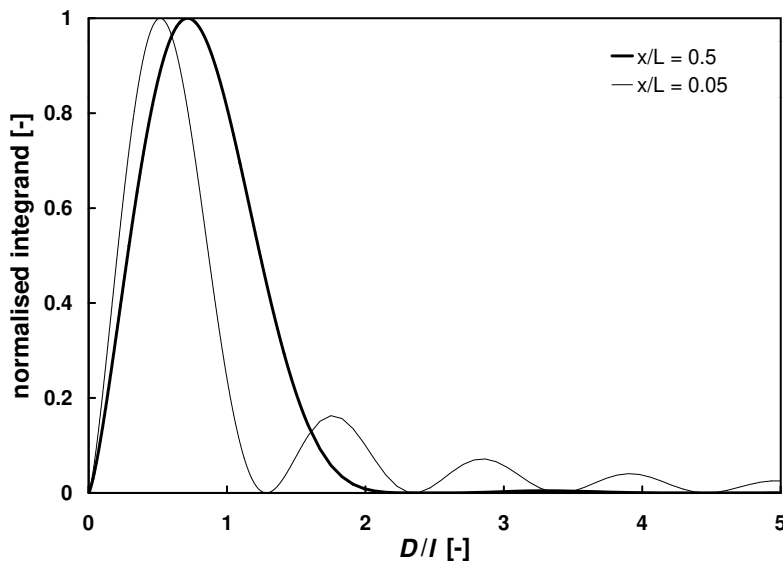
$$\frac{D}{\sqrt{\lambda L}} > 0.98 \left(\sigma_\chi^2 \right)^{3/5} . \tag{A.29}$$

By substituting the latter Equation in Equation A.27 the maximum value for C_n^2 can be derived, which is a function of aperture diameter, the path length and the optical wavelength

$$C_n^2 < 0.93 D^{5/3} L^{-8/3} \lambda^{2/6} . \tag{A.30}$$

Based on experimental measurements Ochs and Hill (1982) found that the restriction given by Wang et al. (1978) was too optimistic. They proposed the following criteria

$$\frac{D}{\sqrt{\lambda L}} > 2.7 \left(\sigma_\chi^2 \right)^{3/5} \tag{A.31}$$

and thus as maximum C_n^2

$$C_n^2 < 0.18 D^{5/3} L^{-8/3} \lambda^{2/6} . \tag{A.32}$$

Their criterion is about 5 times stricter than Wang et al. (1978) proposed. However, it must be noted that Ochs and Hill used dual-aperture tangent detector scintillometers instead of single-aperture detector designs. Frehlich and Ochs (1990) also studied the saturation effect on optical large aperture scintillometers. They found that for σ_χ^2 values of about 0.03 the large aperture scintillometer underestimated the fluxes in the order of 10% (see Kohsiek et al., 2002). Based on the σ_χ^2 value of 0.03 the following criteria can be derived

$$\frac{D}{\sqrt{\lambda L}} > 5.4 \left(\sigma_\chi^2 \right)^{3/5} \tag{A.33}$$

and

$$C_n^2 < 0.057 D^{5/3} L^{-8/3} \lambda^{2/6},$$ (A.34)

which is about 3 times stricter than Ochs and Hill (1982). Frehlich and Ochs (1990) studied the effect of saturation in strong turbulence by comparing observations with theoretically derived predictions of saturation effects. However, a complete analysis could not be done due to missing inner scale measurements. As Frehlich and Ochs noted, further research is required.

Another advantage of the large aperture scintillometer, besides its saturation resistance, is that the effect of inner scale dependence is small (Wang et al., 1978). In Section A.5 it was shown that if the Fresnel size for a point source/detector configuration approaches the size of l_o inner scale effects could no longer be ignored. This means that an exact shape of the spectrum of refractive index fluctuations ($\Phi(\kappa)$) is required in order to derive C_n^2 from σ_χ^2 measurements. The same applies for large aperture scintillometers, i.e., when the diameter of the aperture becomes too small the scintillometer looses its calibration and becomes dependant on l_o. Hill and Ochs (1978) found that aperture diameter should be 20 times larger than l_o to be inner scale independent.

A.8 Related structure parameters

Temperature (T), humidity (Q in kg m^{-3}) and to a lesser extend pressure (P) fluctuations cause fluctuations in the refractive index of air (n). By neglecting pressure fluctuations C_n^2 can be related to the structure parameters of temperature (C_T^2), humidity (C_Q^2) and the covariant term (C_{TQ}) as follows (Hill et al., 1980)

$$C_n^2 = \frac{A_T^2}{\overline{T}^2} C_T^2 + \frac{2 A_T A_Q}{\overline{TQ}} C_{TQ} + \frac{A_Q^2}{\overline{Q}^2} C_Q^2 .$$ (A.35)

A_T and A_Q are functions of the wavelength and the mean values of temperature, humidity and atmospheric pressure (Hill et al., 1980; Andreas, 1989). For visible and near-infrared wavelengths (λ between 0.36-3 μm) A_T and A_Q are defined as follows

$$A_T = -m_1(\lambda)\left(\frac{P}{T}\right) - R_v m_2(\lambda)Q , \qquad\qquad (A.36)$$

$$A_Q = R_v m_2(\lambda)Q , \qquad\qquad (A.37)$$

where R_v is the specific gas constant for water vapour (461.5 J K^{-1} kg^{-1}). In case of a near-infrared wavelength of 930 nm $m_1 = 0.78\times10^{-6}$ K Pa^{-1} and $m_2 = -0.126\times10^{-6}$ K Pa^{-1}. At radio wavelengths ($\lambda > 3$ mm) A_T and A_Q are slightly different (Kohsiek and Herben, 1983; Andreas, 1989)

$$A_T = -\left(\frac{0.776\times10^{-6}P}{T} + \frac{1.723Q}{T}\right) , \qquad\qquad (A.38)$$

$$A_Q = \left(\frac{1.723Q}{T}\right) . \qquad\qquad (A.39)$$

In Table A.1 typical values for A_T and A_Q are given. For a wavelength of 930 nm it can be seen that $A_T \gg A_Q$. This means that at this wavelength temperature fluctuations are dominant. At radio wavelengths (e.g. 11 mm) A_Q approaches A_T, i.e., both humidity fluctuations and temperature fluctuations are important. Table A.2 shows some values of C_n^2 measured with a near-infrared and radio wave scintillometer and the contributions of T and Q.

Table A.1: Typical values for A_T and A_Q for 'normal' atmospheric conditions for $\lambda = 930$ nm and $\lambda = 11$ mm ($P = 1\times10^5$ Pa, $T = 288$ K and $Q = 0.012$ kg m^{-3}).

	A_T [-]	A_Q [-]
$\lambda = 930$ nm	-0.27×10^{-3}	-0.70×10^{-6}
$\lambda = 11$ mm	-0.34×10^{-3}	0.72×10^{-4}

Table A.2: C_n^2 values measured with a near-infrared and a radio wave scintillometer and contributions of C_T^2, C_Q^2 and C_{TQ} to C_n^2 (Flevoland experiment, 1998)

	C_n^2	$\dfrac{A_T^2}{\overline{T}^2}C_T^2$	$2\dfrac{A_T A_Q}{\overline{TQ}}C_{TQ}$	$\dfrac{A_Q^2}{\overline{Q}^2}C_Q^2$
$\lambda = 930$ nm	1.22×10^{-14}	1.09×10^{-14}	1.19×10^{-15}	3.89×10^{-17}
$\lambda = 11$ mm	8.7×10^{-13}	1.7×10^{-14}	-2.49×10^{-13}	1.10×10^{-12}

The problem is to solve Equation A.35. Kohsiek (1982a) suggested measuring C_n^2 at three different wavelengths in order to obtain C_T^2, C_Q^2 and C_{TQ}. However, the problem is that there is no wavelength where only humidity fluctuations are dominant. To some degree temperature fluctuations always play a role at most wavelengths (e.g., see Table A.2). Kohsiek and Herben (1983) proposed as an alternative to use two wavelengths plus an extra relation between T and Q fluctuations instead.

Following the suggestion of Kohsiek and Herben, Andreas (1989) found that a combination of a visible to near-infrared scintillometer and a near-millimetre to radio wave scintillometer, denoted as the 'two-wavelength method', is the best option for measuring the fluxes of H and L_vE. Both Hill et al. (1988) and Andreas (1989) presented a method to solve C_T^2 and C_Q^2 from C_n^2 values measured at a near-infrared ($_{nir}$) and a radio wavelength ($_{rw}$) thereby assuming $R_{TQ}\sqrt{C_T^2 C_Q^2} = C_{TQ}$ in order to eliminate C_{TQ}

$$C_Q^2 = \frac{A_{T\_rw}^2 C_{n\_nir}^2 + A_{T\_nir}^2 C_{n\_rw}^2 + 2R_{TQ}\sqrt{C_{n\_rw}^2 C_{n\_nir}^2}}{\left(\Gamma \overline{T}\right)^2}, \tag{A.40}$$

$$C_T^2 = \frac{A_{Q\_rw}^2 C_{n\_nir}^2 + A_{Q\_nir}^2 C_{n\_rw}^2 + 2R_{TQ}\sqrt{C_{n\_rw}^2 C_{n\_nir}^2}}{\left(\Gamma \overline{Q}\right)^2} \tag{A.41}$$

with

$$\Gamma = \frac{A_{T\_rw} A_{Q\_nir} - A_{T\_nir} A_{Q\_rw}}{\overline{TQ}}. \tag{A.42}$$

R_{TQ} is the correlation coefficient between the temperature and the absolute humidity within the inertial sub range. Because in most cases C_{TQ} is not measured directly, it is customary to assume that R_{TQ} is ± 1 in order to estimate C_{TQ} from C_T and C_Q.

In case C_n^2 is measured at only one wavelength Wesely (1976a) showed that at visible to near-infrared wavelengths Equation A.35 can be rewritten as follows

$$C_n^2 = \frac{A_T^2}{T^2} C_T^2 \left(1 + R_{Tq} \frac{A_Q T}{A_T Q} \frac{C_Q}{C_T} \right)^2 . \tag{A.43}$$

First, it is assumed that R_{TQ} equals ± 1 to get an estimate C_{TQ}. Second, the Bowen ratio is expressed as

$$\beta = \frac{H}{L_v E} = \frac{\rho c_p \overline{w'T'}}{L_v \overline{w'Q'}} = \frac{\rho c_p C_T}{L_v C_Q} , \tag{A.44}$$

which is used to replace (C_T / C_Q). Kohsiek (1982b) experimentally showed that β could be derived from C_T and C_Q measurements. Finally, this leads to the following very practical Equation (using $\rho = 1.2$ kg m^{-3}, c$_p$ = 1005 J kg^{-1} K^{-1} and $L_v = 2.45 \times 10^6$ J kg^{-1})

$$C_n^2 \approx \frac{A_T^2}{T^2} C_T^2 \left(1 + \frac{0.03}{\beta} \right)^2 , \tag{A.45}$$

for deriving C_T^2 from C_n^2 measurements obtained with a visible to near-infrared scintillometer.

A.9 Monin-Obukhov Similarity Theory

In the lowest part ($\approx$ 10%) of the planetary boundary layer (PBL), the surface layer (SL), it is considered that the vertical fluxes of momentum and conservative scalars are nearly constant with height. Within the SL the Monin-Obukhov similarity theory (MOST) makes it possible

to link the structure parameter of temperature (C_T^2) and humidity (C_Q^2) with the surface fluxes H and L_vE. Assuming stationary conditions and a horizontal homogeneous surface MOST describes this relationship as follows

$$\frac{C_T^2(z-d)^{2/3}}{T_*^2} = \frac{C_Q^2(z-d)^{2/3}}{Q_*^2} = f\left(\frac{z-d}{L_{Ob}}\right), \qquad (A.46)$$

with z is the height of the scintillometer above the surface, d the displacement and L_{Ob} the Obukhov length

$$L_{Ob} = \frac{u_*^2 T}{g k_v T_*}, \qquad (A.47)$$

where k_v is the von Kármán constant. The temperature scale T_*, the friction velocity u_* and the absolute humidity scale Q_*, are defined as follows

$$T_* = \frac{-H}{\rho c_p u_*}, \qquad (A.48)$$

$$u_* = \sqrt{\frac{\tau}{\rho}}, \qquad (A.49)$$

$$Q_* = \frac{-E}{u_*}. \qquad (A.50)$$

Wyngaard et al. (1971) proposed the first expression for f between C_T^2 and H, that was based on in-situ measurements done during the Kansas 1968 experiment

$$f\left(\frac{z-d}{L_{Ob}}\right) = c_{T1}\left(1 - c_{T2}\frac{z-d}{L_{Ob}}\right)^{-2/3} \text{ for } \left(\frac{z-d}{L_{Ob}}\right) < 0, \qquad (A.51)$$

with $c_{T1} = 4.9$ and $c_{T2} = 7$. This expression is only valid for unstable atmospheric conditions. Alternative expressions have been proposed (Wesely, 1976b; Andreas, 1988; Thiermann and

Grassl, 1992; Hill et al., 1992a; De Bruin et al., 1993) for both unstable (some examples are depicted in Figure A.15) and stable conditions. Most proposed expressions are based on in-situ eddy covariance observations of the Kansas experiment (Wyngaard et al., 1971; Andreas, 1988). Interesting to note is that it is not known how well the eddy covariance derived fluxes did close the energy balance during these experiments (Kohsiek et al., 2002a), which questions the validity of f.
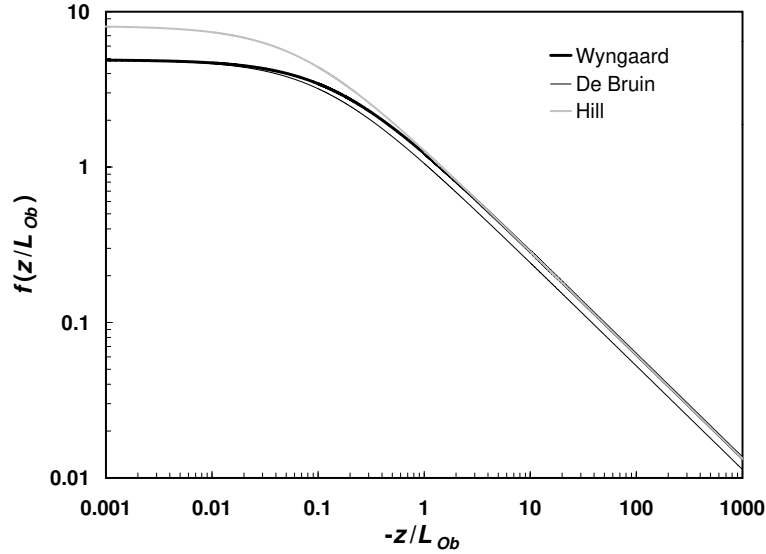

Figure A.15: Stability functions proposed by Wyngaard, De Bruin and Hill for unstable conditions (z/L_{Ob} < 0).

In order to solve H the friction velocity is required. The friction velocity can be determined using different techniques. First, measure the inner scale l_o using a small aperture scintillometer (see e.g., Hill et al., 1992a; Thiermann, 1992; Thiermann and Grassl, 1992). Once the inner scale is known u_* and the fluxes can be derived iteratively. Second, an eddy covariance system can be used to measure the friction velocity ($u_* = \sqrt{-\overline{u'w'}}$). Third, u_* can be derived by applying the C_T^2 - profile method proposed by Hill et al. (1992b) thereby using two large aperture scintillometers installed at two different heights. Finally, the friction velocity can be obtained from wind speed data (u) and an estimate of the surface roughness (z_0)

$$u_* = \frac{k_v u}{\ln\left(\frac{z_u - d}{z_0}\right) - \Psi_m\left(\frac{z_u - d}{L_{Ob}}\right) + \Psi_m\left(\frac{z_0}{L_{Ob}}\right)}.$$

(A.52)

Ψ_m is the well-known Businger-Dyer expression. The main advantage of the first and third method is that path averaged values for u_* can be derived. The second and latter methods are 'traditional' point techniques for estimating u_*. For these cases one can question their representativeness over non-homogeneous areas.

For very unstable atmospheric conditions ($-\dfrac{z-d}{L_{Ob}}>1$) the following simple expression for the sensible heat flux can be derived

$$H = \rho c_p b(z-d)\left(\frac{g}{T}\right)^{1/2}\left(C_T^2\right)^{3/4},\tag{A.53}$$

where $b=\sqrt{\left(\dfrac{1}{c_{T1}}\right)^{3/2}k_v c_{T2}}$ varies between 0.48 and 0.57 (Kohsiek, 1982b; De Bruin et al., 1995). This expression is also known as the free convection limit and provides a simple method to determine H directly from C_T^2 without knowing u_*. In practical applications the free convection approach can provide accurate fluxes when the scintillometer is installed relatively high above the surface (≈ 10 m). Despite its simplicity it must be noted that the measurement height of the scintillometer should be measured accurately because H is linearly related to the measurement height (z-d) (see e.g., Hartogensis et al., 2003). In non-flat areas this can be complicated.

A.10 Summary

In the preceding sections the basics of the scintillation method is explained. Based on the Rytov method it is now possible to describe the propagation of EM radiation in a turbulent medium. This means that we can link the propagation statistics of EM radiation (i.e. the Rytov variance σ_χ^2) with the characteristics of the atmosphere (C_n^2) using a small aperture or point source/detector scintillometer (further denoted as SAS). A scintillometer is considered a SAS when its diameter is smaller than first Fresnel zone (F). However the proportionality between σ_χ^2 and C_n^2 is only valid when σ_χ^2 remains smaller than 0.3. Above this limit the signal

becomes saturated. This means that for near infrared to visible wavelengths the optical path is restricted to short distances of approximately 250 m. In the radio wavelength region saturation is less likely and the distance can be several kilometres. Turbulent scales in the order of the first Fresnel zone (F) primarily cause the scintillations observed by a SAS. Depending on the operational wavelength of the light source F varies between several millimetres (near infrared region) to a few meters (radio wave region). A near-infrared SAS is therefore very sensitive to inner scale effects. Outer scale effects are relevant in the propagation statistics of radio waves meaning that non-isotropic conditions can distort the measurements. Another problem is that at radio wavelengths also absorption fluctuations by water molecules influence the intensity statistics.

The large aperture scintillometer (LAS) and the extended XLAS, which operate in the near infrared region, are designed to overcome the saturation effect of the near-infrared SAS. Due to the increased aperture small-scale structures are filtered out, which lead to a reduction of the amount of scintillations. As a result the LAS can operate over longer distances, i.e., the proportionality between σ_χ^2 and C_n^2 remains valid under strong turbulent conditions. Although the LAS and XLAS also have a saturation maximum, it has not been thoroughly investigated. Another advantage of the LAS is that the instrument is most sensitive to eddy sizes in the order of its diameter (LAS, $D = 0.15$ m; XLAS, $D = 0.32$ m), which lie far from the inner scale and outer scale. As a result the LAS is less sensitive to inner scale and outer scale effects. In Table A.3 an overview is given of different, widely used, scintillometer types; the near-infrared small aperture scintillometer (SAS), the near-infrared large aperture scintillometers (LAS and XLAS) and the small aperture radio wave scintillometer (SA-RWS); their operational regimes, characteristic length scales and sensitivities. The LAS, XLAS and SA-RWS have the potential to obtain surface fluxes over spatial scales of several kilometres.

Once C_n^2 is known, C_T^2 and/or C_Q^2 can be derived depending on the scintillometer configuration (a near-infrared SAS, LAS or a combined LAS - SA-RWS configuration). The final step is to relate C_T^2 and/or C_Q^2 to the surface fluxes of sensible and latent heat applying MOST. The latter step is most sensitive to distortions, especially when C_n^2 is obtained over long path lengths of several kilometres since MOST requires stationary and homogeneous surface conditions. This issue is discussed in the Chapter 2 and 3.

Table A.3: Overview of different scintillometer types: the near infrared small aperture (SAS), the large aperture scintillometer (LAS and XLAS) and the small aperture radio wave scintillometer (SA-RWS).

	SAS	LAS	XLAS	SA-RWS
λ	670 nm	930 nm	930 nm	11 mm
L	20 – 250 m	0.25 – 5 km	1 – 10 km	1 – 10 km
F	≈ 0.01 m	≈ 0.05 m	≈ 0.08 m	≈ 5 m
D	≈ 0.002 m	0.15 m	0.32 m	0.6 m
Most effective eddy	$\approx F$	$\approx D$	$\approx D$	$\approx F$
Restrictions of:				
σ_χ^2 (saturation)	< 0.3	$\dfrac{D}{\sqrt{\lambda L}} > 2.7\left(\sigma_\chi^2\right)^{3/5}$	$\dfrac{D}{\sqrt{\lambda L}} > 2.7\left(\sigma_\chi^2\right)^{3/5}$	< 0.3
D ('inner scale dependence')	-	$D \gg 20 l_o$	$D \gg 20 l_o$	-
D ('aperture averaging')	-	$D > 2F$	$D > 2F$	-
F, D	$l_o \approx F \ll L_o$	$l_o \ll F \ll D < L_o$	$l_o \ll F \ll D < L_o$	$l_o \ll F \ll L_o$

Based on the restrictions of e.g., the LAS given in Table A.3 the operational regime of the LAS can be derived, which is shown in Figure A.16. The minimal height of the LAS is estimated for 6 different surface characteristics ($H = 100$ Wm^{-2} to 600 W m^{-2}) and path lengths using the proposed saturation regime of Ochs and Hill (1982) and applying the free convection approach. The area below the 6 curves represents the area where saturation occurs. It can be seen that for a constant height and path length over wet areas the LAS can be installed at lower heights than over dry areas. The maximum path length of a LAS is approximately 5 km in order to satisfy the criterion that the diameter must be larger than two times the Fresnel zone F. The minimum distance of the LAS is approximately 250 m and depends solely on the signal-to-noise characteristics of its electronics. It has been shown in Section A.9 that in the surface layer (10% of the boundary layer height, h or z_i), when $-\dfrac{z-d}{L_{Ob}} > 1$ the local free convection approach can be applied, and u_* no longer is an important MOST variable. Above the surface layer, inside the mixed layer the structure functions can be scaled as a function of large-scale structures in the order of the boundary layer height (h or z_i) instead of MOST. Experimental data have shown (see e.g., Wyngaard and LeMone, 1980; Kohsiek, 1988) that this mixed-layer-scaling holds only in the lower part of the convectively driven boundary layer ($0.2 z_i \sim 0.3 z_i$), and thus limits the installation-height of the scintillometer.
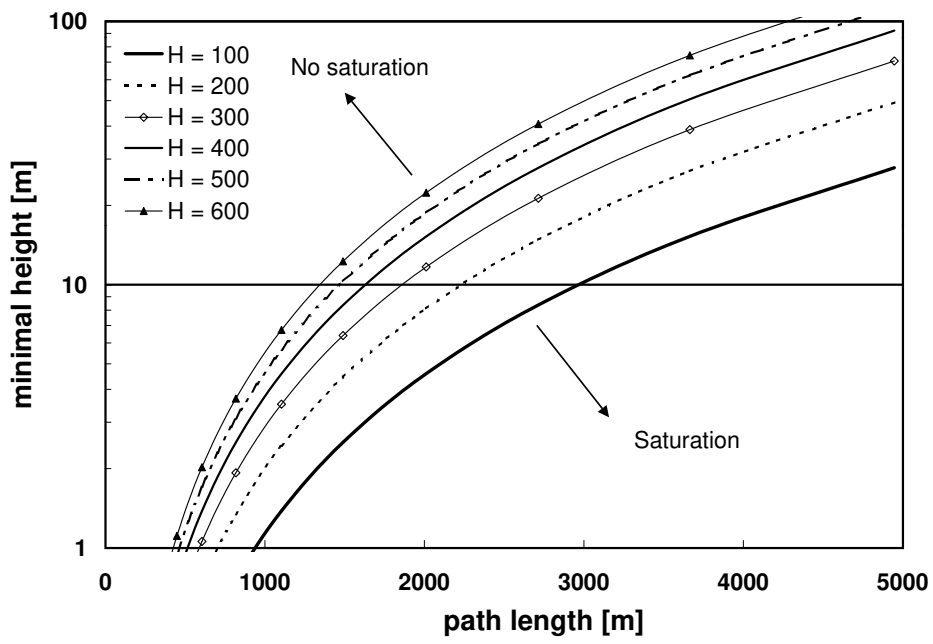
Figure A.16: Operational regimes of the LAS.

Appendix B

Description LAS and XLAS

The LAS (mirror type, $D = 0.15$ m) and XLAS (Fresnel type, $D = 0.31$ m) are almost identical and can be described as follows.

Figure B.1: The LAS (transmitter and receiver).

Transmitter part

The transmitter uses a high power gallium-arsenide infrared-emitting diode (TIES16A, Texas Optoelectronics, Inc., Garland TX, USA) emitting at a wavelength of 930 nm ($\pm$ 5 nm). The diameter of the LED is 1.8 mm and the wavelength is slightly temperature dependant. The first part of the transmitter electronics, called the oscillator, generates a block wave with a frequency of 7 kHz (duty cycle of 0.5), which is used as input signal for the second part, the power-amplifier. Depending on the input voltage, which can be set by an external dial, this amplifier generates a current of maximal 2 A (based on a 0.5 duty cycle the average current is 1 A). As a result the light intensity of the LED can be set, depending on atmospheric conditions and path length. The LED is thus modulating at a frequency of 7 kHz, well above natural ambient fluctuations, in order to distinguish the EM signal from background radiation.

In the LAS mirror type scintillometer the LED is placed in the focal point of a spherical concave mirror (with a diameter of 0.15 m and a focal length of 0.30 m) to construct an incoherent light beam. The optical parts are protected against atmospheric influences by a transparent Plexiglas window. In the XLAS a Fresnel lens with a diameter of 0.32 m (the focal length is 0.61 m) was chosen in order to keep the size and the weight down (e.g. a mirror with a diameter of 0.3 m has a focal length of about 3 m). Because the focal length of the XLAS is 2× larger than the LAS, the improved focal-length/LED-diameter ratio should theoretically lead to a less diverging beam (2×) than the LAS and thus lead to a 4× better signal.

Figure B.2: The XLAS (transmitter and receiver).

Receiver part

In both the LAS and XLAS the same square law detector (i.e. it measures the intensity I) is used (UDT455, UDT sensors, Inc., Hawthorne CA, USA), which is placed in the focal point of a spherical concave mirror (LAS) or Fresnel lens (XLAS) identical to the one used in the transmitter. Note that the LAS (XLAS) uses a square law detector and thus measures intensity I of the incident EM radiation rather than the amplitude A (see Appendix A). Since I is proportional to A^2, the variance of the log intensity is equal to 4× the variance of the log amplitude (χ)

$$\sigma_{\ln I}^2 = 4\sigma_\chi^2 \qquad\qquad (B.1)$$

Therefore expression A.27 (see Appendix A) can be rewritten into

$$\sigma^2_{\ln I} = 0.892 D^{\frac{-7}{3}} L^3 C_n^2 \tag{B.2}$$

The spectral bandwidth of the detector ranges from 350 nm to 1100 nm. An optical filter is placed in front of the detector to narrow the bandwidth to about 800 – 1000 nm (*LEE* filters, Hampshire, England). The electronics of the receiver provide real-time C_n^2 values expressed as a voltage U_{out} [V] (which can be logged by a data logger)

$$C_n^2 = 10^{(-12+U_{out})}, \tag{B.3}$$

or

$$U_{out} = \log\left(10^{12} C_n^2\right). \tag{B.4}$$

The conversion from intensity fluctuations to C_n^2 involves a number of steps (see Figure B.3). First, a feedback circuitry ($\tau = 0.1$ s) removes the slowly varying offset, i.e. ambient light, from the detector signal, remaining a signal that fluctuates around zero. This signal is fed into the demodulation circuitry. In the later versions of the LAS (and XLAS) an extra high pass filter (1600 Hz) is added to remove any offsets that might be caused by variations in cloud cover. These fluctuations in the offset can lead to problems in the demodulation circuitry. After demodulation the 7 kHz carrier wave is removed using a low pass filter (400 Hz). What remains is the demodulated signal, i.e. the amplitude of the carrier wave and its fluctuations (i.e. scintillations). This signal can be monitored by the analogue meter at the back panel of the receiver. Next, the logarithm of the received signal intensity is taken (i.e., conversion from I to $\ln(I)$) using a log-amplifier. After the log-amplifier the signal is amplified or debilitated depending on the path length L, the wavelength and the aperture diameter. Since the wavelength and aperture diameter are constant the amplification (G) is a function only of the path length and can be set by an external potentiometer. Then the signal is band pass filtered between 0.2 Hz and 400 Hz, to remove high frequency noise due to the carrier frequency and demodulator and low frequency fluctuations related to water vapour absorption fluctuations (Nieveen et al., 1998). Finally, the signal passes through a second log-amplifier in RMS

mode, giving the logarithm of variance of its input signal. The output signal of the latter RMS amplifier is the final output signal of the LAS and XLAS and can be logged by an external data logger. Several LAS instruments were equipped with a small data logger (Mirco-G2, Z-World, Davis CA, USA). In general both the C_n^2 signal and the signal strength (i.e. demod) are logged, since the signal strength provides information about the reliability of the C_n^2 measurements.

In summary the output signal U_{out} is as follows (Moene et al., 2000b)

$$U_{out} = 2\log\left(G\sigma_{2\log I}\right)$$

$$U_{out} = \log\left(G^2\sigma_{2\log I}^2\right)$$

$$U_{out} = \log\left(10^{12}1.12D^{\frac{7}{3}}L^{-3}\sigma_{\ln I}^2\right)$$

$$U_{out} = \log\left(10^{12}C_n^2\right), \tag{B.5}$$

where G is the total Gain of the electronics, depending on the path length L. In case of the XLAS the total Gain of the electronics is 0.5× smaller. This is done to modify the range of the external potentiometer to path lengths of 10 km. U_{out} varies between –5.3V (i.e. signal noise ratio, which depends on the signal strength) and 0V, which corresponds to C_n^2 values of 10^{-18} m$^{-2/3}$ and 10^{-12} m$^{-2/3}$, respectively.
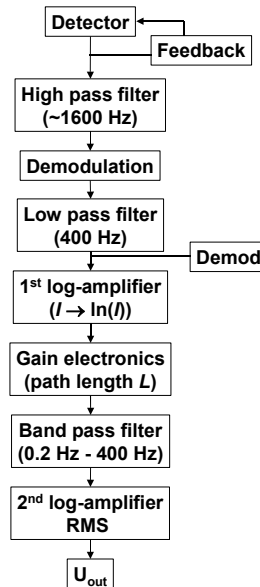

Figure B.3: Overview of steps of the receiver electronics of both the LAS and the XLAS.

Note that the relationship between U_{out} and C_n^2 is non-linear. To correct for this non-linearity the variance of the U_{out} is required:

$$C_n^2 = 10^{\left(-12 + U_{out} + 1.15\sigma_{Uout}^2\right)}.$$ (B.6)

Because the aperture of the XLAS receiver is 2× larger than the LAS receiver the measured intensity should be 4× larger. Meaning, in theory, that when the XLAS and LAS are set-up over the same distance the signal of the XLAS should be in total 16× larger than the LAS. However, Kohsiek et al. (2002a) found a gain of only 2, which can be related to the poor quality of the Fresnel lenses. In Table B.1 some specs of the LAS' and XLAS' are given.

Table B.1: Specifications of LAS and XLAS.

	LAS	XLAS
Aperture diameter [m]	0.15	0.32
Effective diameter [m]	0.149	0.31
Wave length [nm]	930 (±5)	930 (±5)
Path length [km]	0.25 – 5	1 - 10
Band width [Hz]	0.2 – 400	0.2 - 400
Signal noise	-4.0V @ $I = 0.1$V (~$1\cdot10^{-16}$ m$^{-2/3}$)	-4.0V @ $I = 0.1$V (~$1\cdot10^{-16}$ m$^{-2/3}$)
(Pot$_{LAS}$ = 594 (L = 1193m; Pot$_{XLAS}$ = 413 (L = 2000m))	-5.3V @ $I = 0.6$V (~$5\cdot10^{-18}$ m$^{-2/3}$)	-5.3V @ $I = 0.6$V (~$5\cdot10^{-18}$ m$^{-2/3}$)

Appendix C

Spatial filtering of scintillations (ULAS)

In order to derive the sensible heat flux (H) of the C_n^2 signal of the LAS additional wind speed data (u) is required. In most cases wind speed data is taken from standard cup anemometer measurements. Unfortunately, these observations are representative only for small areas. Although the contribution of wind speed to the derived heat flux is relatively small, it limits the applicability of the LAS. Churnside et al. (1988) have demonstrated that using a spatial filtering technique applied to a LAS can yield information on the crosswind (u_{cross}) and its variance (σ_{cross}^2). The spatial filter can be easily generated by applying vertical stripes across the aperture of the incohere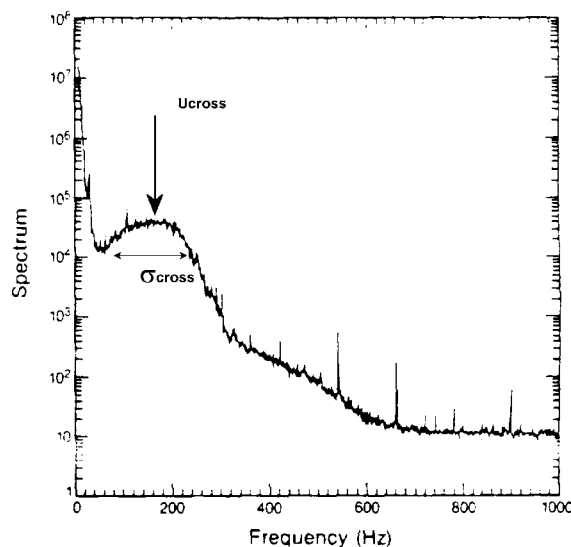nt transmitter and receiver. A typical spectrum of the scintillometer signal, collected by Churnside et al. (1988) using a XLAS type instrument with an aperture diameter of 0.4 m, is shown in Figure C.1. The position of the peak in Figure C.1 lies at around 180 Hz. The observed averaged cross-wind was ~ 2.6 m s^{-1}, which corresponds to a frequency of 205 Hz, lies close to the peak in Figure C.1. The width of the peak depends on the variability of the wind speed (i.e. the variance). Knowing the variance of the cross wind, the sensible heat flux can be derived from the LAS signals (i.e. C_n^2, σ^2_{Cross}) without additional (local) wind speed data.

Figure C.1: Power spectrum of signal fluctuations (reproduced from Churnside et al., 1988).

References

Andreas, E.L., 1988, 'Estimating C_n^2 over Snow and Sea Ice from Meteorological Data', *J. Opt. Soc. Am.* **5**, 481-495.

Andreas, E.L.: 1989, 'Two-Wavelength Method of Measuring Path-Averaged Turbulent Surface Heat Fluxes', *J. Atmos. Ocean. Tech.* 6, 280-292.

Andreas, E.L.: 1990, *Selected Papers on Turbulence in a Refractive Medium*, SPIE Milestone Series 25, SPIE - The International Society for Optical Engineering, Bellingham, 693 pp.

Andrews, L.C., Phillips, R.L. and Hopen, C.Y.: 2001, *Laser Beam Scintillations with Applications*, SPIE PRESS, SPIE - The International Society for Optical Engineering, Bellingham, 376 pp.

Bange, J., Beyrich, F. and Engelbart, D.A.M.: 2002, 'Airborne Measurements of Turbulent Fluxes over Heterogeneous Terrain with Helipod and DO 128 – Error Analysis and Comparison with Ground-Based Systems', *15th Symposium on Boundary Layer and Turbulence*, 15 – 19 July, 2002, American Meteorological Society, Wageningen, The Netherlands, pp. 125-128.

Bastiaanssen, W.G.M., Menenti, M., Feddes, R.A. and Holtslag, A.A.M.: 1998, 'A Remote Sensing Surface Energy Balance Algorithm for Land (SEBAL) – 1. Formulation', *J. Hydrol.* **212-213**, 198-212.

Bastiaanssen, W.G.M. and Bos, M.G.: 1999, 'Irrigation Performance Indicators Based on Remotely sensed Data: A Review of Literature', *Irrigation and Drainage systems* **13**(4), 291-311.

Bastiaanssen, W.G.M.: 2000, 'SEBAL-based Sensible and Latent Heat Fluxes in the Irrigated Gediz Basin, Turkey', *J. Hydrol.* **229**, 87-100.

Batchvarova, E. and Gryning, S.E.: 1991, 'Applied Model for the Growth of the Daytime Mixed Layer', *Boundary-Layer Meteorol.* **56**, 261-274.

Batchvarova, E. and Gryning, S.E.: 1994, 'Applied Model for the Growth of the Daytime Mixed Layer and the Entrainment Zone', *Boundary-Layer Meteorol.* **71**, 311-323.

Beljaars, A.C.M.: 1982, 'The Derivation of Fluxes from Profiles in Perturbed Areas', *Boundary-Layer Meteorol.* **24**, 35-55.

Beljaars, A.C.M., Schotanus, P. and Nieuwstadt, F.T.M.: 1983, 'Surface Layer Similarity under Non-Uniform Fetch Conditions', *J. Climate Appl. Meteorol.* **22**, 1800-1810.

Beljaars, A.C.M. and Holtslag, A.A.M.: 1991, 'Flux Parameterisation over Land Surfaces for Atmospheric Models', *J. Appl. Meteorol.* **30**, 327-341.

Beyrich, F.: 2000, 'LITFASS-98 Experiment 25.5.1998 – 30.6.1998 Experiment Report', Deutscher Wetterdienst Forschung und Entwicklung, Arbeitsergebnisse 62, pp. 78.

Beyrich, F., Richter, S.H., Weisensee, U., Kohsiek, W., Bosveld, F., Lohse, H., De Bruin, H.A.R., Hartogensis, O.K., Bange, J. and Vogt, R.: 2000, 'The LITFASS-98 Experiment: Fluxes Over a Heterogeneous Land Surface', *14th Symposium on Boundary Layer and Turbulence*, 7 – 11 August, 2000, American Meteorological Society, Aspen, CO, USA, pp. 9-10.

Beyrich, F., De Bruin, H.A.R., Meijninger, W.M.L. and Schipper, F.: 2002a, 'Experiences from One-Year Continuous Operation of a Large Aperture Scintillometer over a Heterogeneous Land Surface', *Boundary-Layer Meteorol.* **105**, 85-97.

Beyrich, F., Foken, T. and Herzog, H.J.: 2002b, 'The LITFASS-98 Experiment', *Theor. Appl. Climatol.* **73**(1-2), 1-2.

Businger, J.A., Wyngaard, J.C., Izumi, Y. and Bradley, E.F.: 1971, 'Flux Profile Relationships in the Atmospheric Surface Layer', *J. Atmos. Sci.* **28**, 181-189.

Cain, J. D., Rosier, P.T.W., Meijninger, W. and De Bruin, H.A.R.: 2001, 'Spatially Averaged Sensible Heat Fluxes Measured over Barley', *Agric. For. Meteorol.* **107**, 307-322.

Carlson, T.N., Taconet, O., Vidal, A., Gillies, R.R., Olioso, A. and Humes, K.: 1995, 'An Overview of the Workshop on Thermal Remote Sensing Held at La Londe les Maures, France, September 20-24, 1993', *Agric. For. Meteorol.* **77**, 141-151.

Champagne, F.H., Friehe, C.A. and LaRue, J.C.: 1977, 'Flux Measurements, Flux Estimation Techniques, and Fine-Scale Turbulence Measurements in the Unstable Surface Layer over Land', *J. Atmos. Sci.* **34**, 515-530.

Chehbouni, A., Kerr, Y.H., Watts, C., Hartogensis, O., Goodrich, D., Scott, R., Schieldge, J., Lee, K., Shuttleworth, W.J., Dedieu, G., and De Bruin, H.A.R.: 1999, 'Estimation of Area-Average Sensible Heat Flux Using a Large-Aperture Scintillometer during the Semi-Arid Land-Surface-Atmosphere (SALSA) Experiment', *Water Resour. Res.* **35** (8), 2505-2511.

Chehbouni, A., Watts, C., Lagouarde, J.-P., Kerr, Y.H., Rodriguez, J.-C., Bonnefond, J.-M., Santiago, F., Dedieu, G., Goodrich, D.C. and Unkrich, C.: 2000, 'Estimation of Heat and Momentum Fluxes over Complex Terrain Using a Large Aperture Scintillometer', *Agric. For. Meteorol.* **105**, 215-226.

Churnside, J.H., Lataitis, R.J. and Lawrence, R.S.: 1988, 'Localised Measurements of Refractive Turbulence using Spatial Filtering of Scintillations', *Appl. Optics* **27**(11), 2199-2213.

Churnside, J.H.: 1990, 'A Spectrum of Refractive Turbulence in the Turbulent Atmosphere', *J. Mod. Opt.* **37**, 13-16.

Claussen, M.: 1990, 'Area-Averaging of Surface Fluxes in a Neutrally Stratified, Horizontally, Inhomogeneous Atmospheric Boundary Layer', *Atmos. Environ.* **24a**, 1349-1360.

Clifford, S.F., Ochs, G.R. and Lawrence, R.S.: 1974, 'Saturation of Optical Scintillation by Strong Turbulence', *J. Opt. Soc. Am.* **64**, 148-154.

Davenport, A.G.: 1960, 'Rationale for Determining Design Wind Velocities', *J. Atmos. Soc. Civ. Eng.* **ST-86**, 39-68.

De Bruin, H.A.R.: 1989, 'Physical Aspects of the Planetary Boundary Layer with Special reference to Regional Evapotranspiration', *Proc. Workshop on the Estimation of Areal Evapotranspiration*, Vancouver, BC, August 9 - 22, 1987, IAHS Publ. 177, pp. 117-132.

De Bruin, H.A.R., Bink, N.J., and Kroon, L.J.M.: 1991, 'Fluxes in the Surface under Advective

Conditions', in T.J. Schmugge and J.C. André (eds.), *Land Surface Evaporation; Measurement and Parameterization*, Springer-Report, New York, pp. 157-169.

De Bruin, H.A.R., Kohsiek, W. and Van den Hurk, B.J.J.M.: 1993, 'A Verification of Some Methods to Determine the Fluxes of Momentum, Sensible Heat and Water Vapour using Standard Deviation and Structure Parameter of Scalar Meteorological Quantities', *Boundary-Layer Meteorol.* **63**, 231-257.

De Bruin, H.A.R.: 1994, 'Analytical Solutions of the Equations Governing the Temperature Fluctuation Method', *Boundary-Layer Meteorol.* **68**, 427-432.

De Bruin, H.A.R., Van den Hurk, B.J.J.M., and Kohsiek, W.: 1995, 'The Scintillation Method Tested Over a Dry Vineyard Area', *Boundary-Layer Meteorol.* **76**, 25-40.

De Bruin, H.A.R., Nieveen, J.P., De Wekker, S.F.J., and Heusinkveld, B.G.: 1996, 'Large Aperture Scintillometry Over a 4.8 km Path for Measuring Areally-Averaged Sensible Heat Flux; A Case Study', Proc. *22nd Symposium on Agricultural and Forest Meteorology*, January 28 – February 2, 1996, American Meteorological Society, Atlanta, GA by the AMS, Boston, MA, pp. 153-156.

De Bruin, H.A.R., Van den Hurk, B.J.J.M. and Kroon, L.J.M.: 1999, 'On the Temperature-Humidity Correlation and Similarity', *Boundary-Layer Meteorol.* **93**, 453-468.

De Bruin, H.A.R.: 2002, 'Introduction: Renaissance of Scintillometry', *Boundary-Layer Meteorol.* **105**, 1-4.

De Bruin, H.A.R., Meijninger, W.M.L., Smedman, Ann-Sofi, Magnusson, Mikael: 2002, 'Displaced-Beam Small Aperture Scintillometer Test. Part I: The Wintex Data-Set', *Boundary-Layer Meteorol.* **105**, 129-148.

Droogers, P.: 2000, 'Estimating Actual Evapotranspiration Using a Detailed Agro-Hydrological Model', *J. Hydrol.* **229**, 50-58.

Finnigan, J.J., Clement, R., Malhi, Y., Leuning, R. and Cleugh, A.H.: 2003, 'A Re-Evaluation of Long-Term Flux Measurement Techniques Part I: Averaging and Coordinate Rotation', *Boundary-Layer Meteorol.* **107**, 1-48.

Frehlich, R.G. and Ochs, G.R.: 1990, 'Effects of Saturation on the Optical Scintillometer', *Appl. Optics* **29**, 548-553.

Frehlich, R.G.: 1992, 'Laser Scintillation Measurements of the Temperature Spectrum in the Atmospheric Surface Layer', *J. Atmos. Sci.* **49**(16), 1494-1509.

Garratt, J.R.: 1992, *The Atmospheric Boundary Layer*, University Press, Cambridge, 316 pp.

Gieske, A: 2001, 'Importing NOAA-14 Images from the NOAA/AVHRR Satellite Active Archive (SAA) – A Simple User Interface', ITC-software (*pers. communication*).

Gieske, A: 2003, 'The Iterative Flux-Profile Method for Remote Sensing Applications', *Int. J. Remote Sens.*, in press.

Green, A.E., McAneney, K.J. and Lagouarde, J-P.: 1997, 'Sensible Heat and Momentum Flux

Measurements with an Optical Inner Scale Meter', *Agric. For. Meteorol.* **85**, 259-267.

Green, A.E., and Hayashi, Y.: 1998, 'Using the Scintillometer Over a Rice Paddy', *Jpn. J. Agric. Meteorol.* **54** (3), 225-231.

Green, A.E., Green, S.R., Astill, M.S. and Caspari, H.W.: 2000, 'Estimating Latent Heat Flux from a Vineyard Valley Using Scintillometry', *J. Terres. Atmos. Ocean. Sci.* **11** (2), 525-542.

Green, A. E., Astill, M. S., McAneney, K. J. and Nieveen, J. P.: 2001, 'Path-Averaged Surface Fluxes Determined from Infrared and Microwave Scintillometers', *Agric. For. Meteorol.* **109**, 233-247.

Gryning S.E. and Batchvarova, E.: 1999, 'Regional Heat Flux over the NOPEX Area Estimated from the Evolution of the Mixed-Layer', *Agric. For. Meteorol.* **98-99**, 159-167.

Gutman, G.: 1988, 'A Simple Method for Estimating Monthly Mean Albedo of Land Surfaces from AVHRR Data', *J. Appl. Meteorol.* **27**, 973-988.

Hartogensis, O.K., De Bruin, H.A.R. and Van de Wiel, B.J.H.: 2002, 'Displaced-Beam Small Aperture Scintillometer test Part II: CASES-99 stable boundary layer experiment', *Boundary-Layer Meteorol.* **105**, 148-176.

Hartogensis, O.K., Watts, C.J., Rodriguez, J-C. and De Bruin, H.A.R.: 2003, 'Derivation of an Effective Height for Scintillometers: La Poza Experiment in Northwest-Mexico', *accepted for publication in J. Hydro-Meteorol.*

Hemakumara, H.M., Chandrapala, L. and Moene, A.F.: 2002, 'Evapotranspiration Fluxes over Mixed Vegetation Areas from Large Aperture Scintillometer', *Agric. Water Man.* **1776**, 1-14.

Hill, R.J. and Clifford, S.F.: 1978, 'Modified Spectrum of Atmospheric Temperature Fluctuations and its Application to Optical Propagation', *J. Opt. Soc. Am.* **68**, 892-899.

Hill, R.J. and Ochs, G.R.: 1978, 'Fine Calibration of Large-Aperture Optical Scintillometers and an Optical Estimate of Inner Scale of Turbulence', *Appl. Optics* **17**, 3608-3612.

Hill, R.J., Clifford, S.F. and Lawrence, R.S.: 1980, 'Refractive Index and Absorption Fluctuations in the Infrared Caused by Temperature, Humidity and Pressure Fluctuations', *J. Opt. Soc. Am.* **70**, 1192-1205.

Hill, R.J., Bohlander, R.A., Clifford, S.F., McMillan, R.W., Priestley, J.T. and Schoenfeld, W.P.: 1988, 'Turbulence-Induced Millimetre-Wave Scintillation Compared with Micro-Meteorological Measurements', *IEEE Trans. Geosci. Remote Sens.* **26**, 330-342.

Hill, R.J.: 1989, 'Implications of Monin-Obukhov Similarity Theory for Scalar Quantities', *J. Atmos. Sci.* **46**, 2236-2244.

Hill, R.J.: 1992, 'Review of Optical Scintillation Methods of Measuring the Refractive-Index Spectrum, Inner Scale and Surface Fluxes', *Waves in Random Media* **2**, 179-201.

Hill, R.J., Ochs, G.R. and Wilson, J.J.: 1992a, 'Measuring Surface-Layer Fluxes of Heat and Momentum Using Optical Scintillation', *Boundary-Layer Meteorol.* **58**, 391-408.

Hill, R.J., Ochs, G.R. and Wilson, J.J.: 1992b, 'Surface-Layer Fluxes Measured Using the C_T^2-Profile

Method', *J. Atmos. Ocean. Tech.* **9**, 526-537.

Hill, R.J.: 1997, 'Algorithms for Obtaining Atmospheric Surface-Layer Fluxes from Scintillation Measurements', *J. Atmos. Ocean. Tech.* **14**, 456-467.

Hoedjes, J.C.B., Zuurbier, R.M. and Watts, C.J.: 2002, 'Larger Aperture Scintillometer Used over a Homogeneous Irrigated Area, Partly Affected by Regional Advection', *Boundary-Layer Meteorol.* **105**, 99-117.

Horst, T.W. and Weil, J.C.: 1992, 'Footprint Estimation for Scalar Flux Measurements in the Atmospheric Surface Layer', *Boundary-Layer Meteorol.* **59**, 279-296.

Horst, T.W. and Weil, J.C.: 1994, 'How Far is Far Enough? The Fetch Requirements for Micrometeorological Measurements of Surface Fluxes', *J. Atmos. Ocean. Tech.* **11**, 1018-1025.

Horst, T.W.: 1999, 'The Footprint for Estimation of Atmospheric-Surface Exchange Fluxes by Profile Techniques', *Boundary-Layer Meteorol.* **90**, 171-188.

Jia, L., Su, Z., Van den Hurk, B., Menenti, M, Moene, A., De Bruin, H.A.R., Yrisarry, J.J.B., Ibanez, M. and Cuesta, A.: 2003, 'Estimation of Sensible Heat Flux using Surface Energy Balance System (SEBS) and ATSR measurements', *Phys. Chem. Earth* **28**, 75-88.

Kite, G.: 2000, 'Using a Basin-Scale Hydrological Model to Estimate Crop Transpiration and Soil Evaporation', *J. Hydrol.* **229**, 59-69.

Kite, G. and Droogers, P.: 2000, 'Comparing Evapotranspiration Estimates from Satellites, Hydrological Models and Field Data', *J. Hydrol.* **229**, 3-18.

Kohsiek, W., 1982a, *Optical and In Situ Measuring of Structure Parameters Relevant to Temperature and Humidity, and Their Application to the Measuring of Sensible and Latent Heat Flux*, NOAA Tech. Memor. ERL WPL-96, NOAA Environmental Research Laboratories, Boulder, CO, USA, 64 pp.

Kohsiek, W., 1982b, 'Measuring C_T^2, C_q^2 and C_{Tq} in the Unstable Surface Layer, and Relations to the Vertical Fluxes of Heat and Moisture', *Boundary-Layer Meteorol.* **24**, 89-107.

Kohsiek, W. and Herben, M.H.A.J.: 1983, 'Evaporation Derived from Optical and Radio Wave Scintillation', *Appl. Optics* **22**, 2566-2569.

Kohsiek, W.: 1984, 'Inertial Subrange Correlation between Temperature and Humidity Fluctuations in the Unstable Surface Layer above Vegetated Terrains', *Boundary-Layer Meteorol.* **29**, 211-224.

Kohsiek, W.: 1987, '*A 15 cm Aperture LED Scintillometer for C_n^2 and Crosswind Measurements*', KNMI Scientific Report WR 87-3.

Kohsiek, W.: 1988, 'Observations of the Structure Parameters C_T^2, C_{TQ} and C_Q^2 in the Mixed Layer over Land', *Appl. Optics* **22**, 2566-2569.

Kohsiek, W., Meijninger, W.M.L., Moene, A.F., Heusinkveld, B.G., Hartogensis, O.K., Hillen, W.C.A.M. and De Bruin, H.A.R.: 2002a, 'An Extra Large Aperture Scintillometer for Long Range Applications', *Boundary-Layer Meteorol.* **105**, 119-127.

Kohsiek, W., Meijninger, W.M.L. and De Bruin, H.A.R.: 2002b, 'Long Range Scintillometry', *15th Symposium on Boundary Layer and Turbulence*, 15 – 19 July, 2002, American Meteorological Society, Wageningen, The Netherlands, pp. 125-128.

Lagouarde, J-P., McAneney, K.J., and Green, A.E.: 1996, 'Scintillometer Measurements of Sensible Heat Flux over Heterogeneous Surfaces' in J. B. Stewart (ed), E. T. Engman, R. A. Feddes, and Y. Kerr, *Scaling Up in Hydrol. using Remote Sensing*, John Wiley, Chichester, U.K., pp. 147-160.

Lagouarde, J-P., Bonnefond , J-M., Kerr, Y.H., McAneney, K.J. and Irvine, M.: 2002, 'Integrated Sensible Heat Flux Measurements of a Two-Surface Composite Landscape using Scintillometry', *Boundary-Layer Meteorol.* **105**, 4-37.

Lagouarde, J-P., Jacob, F., Gu, X-F., Olioso, A., Bonnefond, J-M., Kerr, Y., McAneny, K. and Irvine, M.: 2003, 'Spatialization of Sensible Heat Flux over a Heterogenous Landscape', *Agronomie* **22**, 627-633.

Lawrence, R.S. and Strohbehn, J.W.: 1970, 'A Survey of Clear-Air Propagation Effects Relevant to Optical Communications', *Proceedings of the IEEE* **58(10)**, 1523-1545.

Li, F. and Lyons, T.J.: 1999, 'Estimation of Regional Evapotranspiration through Remote Sensing', *J. Appl. Meteorol.* **38**, 1644-1654.

Ma, J. and Daggupaty, S.M.: 1998, 'Stability Dependence of Height Scales and Effective Roughness Lengths of Momentum and Heat Transfer over Roughness Changes', *Boundary-Layer Meteorol.* **88**, 145-160.

Mahrt, L.: 1996, 'The Bulk Aerodynamic Formulation over Heterogeneous Terrain', *Boundary-Layer Meteorol.* **78**, 87-119.

Mahrt, L: 1998, 'Flux Sampling Errors for Aircraft and Towers', *J. Atmos. Ocean. Tech.* **15**, 416-429.

Mahrt, L., Vicker, D., Sun, J. and McCaughey, J.H.: 2001, 'Calculation of Area-Averaged Fluxes: Application to BOREAS', *J. Appl. Meteorol.* **40**, 915-920.

Mason, P.J.: 1988, 'The Formation of Areally-Averaged Roughness Lengths', *Quart. J. Roy. Meteorol. Soc.* **114**, 399-420.

McAneney, K.G., Green, A.E. and Astill, M.: 1995, 'Large Aperture Scintillometry: The Homogeneous Case', *Agric. For. Meteorol.* **76**, 149-162.

McMillan, R.W., Bohlander, R.A., Ochs, G.R., Hill, R.J. and Clifford, S.F.: 1983, 'Millimetre Wave Atmospheric Turbulence measurements: Preliminary Results and Instrumentation for Future Measurements', *J. Opt. Eng.* **22**, 32-39.

Menenti, M. and Choudhury, B.J.: 1993, 'Parameterisation of Land Surface Evaporation by Means of

Location Dependant Potential Evaporation and Surface Temperature Range', In Bolle, H-J., Feddes, R.A. and Kalma, J. (editors), *Exchange processes at the Land Surface for a Range of Space and Time Scales*, number 212 in IAHS Publications, pp. 561-568.

Meijninger, W.M.L. and De Bruin, H.A.R.: 2000, 'The Sensible Heat Fluxes over Irrigated Areas in Western Turkey Determined with a Large Aperture Scintillometer', *J. Hydrol.* **229**, 42-49.

Meijninger, W.M.L., Hartogensis, O.K., Kohsiek, W., Hoedjes, J.C.B., Zuurbier, R.M. and De Bruin, H.A.R.: 2002a, 'Determination of Area Averaged Sensible Heat Fluxes with a Large Aperture Scintillometer over a Heterogeneous Surface – Flevoland Field Experiment', *Boundary-Layer Meteorol.* **105**, 37-62.

Meijninger, W.M.L., Green, A.E., Hartogensis, O.K., Kohsiek, W., Hoedjes, J.C.B., Zuurbier, R.M. and De Bruin, H.A.R.: 2002b, 'Determination of Area Averaged Water Vapour Fluxes with Large Aperture and Radio Wave Scintillometers over a Heterogeneous Surface – Flevoland Field Experiment', *Boundary-Layer Meteorol.* **105**, 63-83.

Meijninger, W.M.L., Gieske, A. and De Bruin, H.A.R.: 2003, 'Satellite, Scintillometer and Variance Based Sensible Heat Fluxes Over an Irrigated Area – An Intercomparsion Study', *submitted to Int. J. Rem. Sens.*

Moene, A.F.: 2000a, A Review of the Relationships Describing the Signal of a Large Aperture Scintillometer, internal report.

Moene, A.F.: 2000b, The Effect of Finite Accuracy in the Manufacturing of Large Aperture Scintillometers, internal report.

Moene, A.F.: 2003, 'Effects of Water Vapour on the Structure Parameter of the Refractive Index of Near-Infrared Radiation', *Boundary-Layer Meteorol.* **107**, 635-653.

Moore, C.J.: 1986, 'Frequency Response Corrections for Eddy Correlation Systems', *Boundary-Layer Meteorol.* **37**, 17-35.

Müller, E., Foken, Th., Heise, E. and Majewski, D.: 1995, 'LITFASS – a nucleaus for a BALTEX field experiment', DWD – GB Forschung und Entwicklung: Arbeitsergebnisse Nr. 33, 17 pp.

Nieveen, J.P., Green, A.E. and Kohsiek, W.: 1998, 'Using a Large-Aperture Scintillometer to Measure Absorption and Refractive Index Fluctuations', *Boundary-Layer Meteorol.* **87**, 101-116.

Nieveen, J.P. and Green, A.E.: 1999, 'Measuring Sensible Heat Flux over Pasture Using the C_T^2 – Profile Method', *Boundary-Layer Meteorol.* **91**, 23-35.

Ochs, G.R. and Cartwright, W.D.: 1980, *Optical System Model IV for Space-Averaged Wind and C_n^2 Measurements*, NOAA Tech. Memor. ERL WPL-52, NOAA Environmental Research Laboratories, Boulder, CO, USA, 31 pp.

Ochs, G.R. and Hill, R.J.: 1982, *A Study of Factors Influencing the Calibration of Optical Cn2 Meters*, NOAA Tech. Memor. ERL WPL-106, NOAA Environmental Research Laboratories, Boulder, CO, USA, 24 pp.

Ochs, G.R. and Wilson, J.J.: 1993, *A Second-Generation Large-Aperture Scintillometer*, NOAA Tech.

Memor. ERL WPL-232, NOAA Environmental Research Laboratories, Boulder, CO, USA, 24 pp.

Oncley, S.P., Foken, T., Vogt, R., Bernhofer, C., Liu, H., Sorbjan, Z., Pitacco, A., Grantz, D. and Riberio, L.: 2000, 'The EBEX 2000 Field Experiment', *14th Symposium on Boundary Layer and Turbulence*, 7 – 11 August, Aspen, CO, USA., 322-324.

Philip, J.R.: 1961, 'The Theory of Heat Flux Meters', *J. Geophys. Res.* **66**, 571-579.

Poggio, L.P., Furger, M., Prévôt, A.S.H., Graber, W.K. and Andreas, E.L.: 2000, 'Scintillometer Wind Measurements over Complex Terrain', *J. Atmos. Tech.* **17**, 17-26.

Poulos, G.S., Fritts, D.C., Blumen, W. and Bach (jr), W.D.: 2000, 'CASES-99 Field Experiment: An Overview', *14th Symposium on Boundary Layer and Turbulence*, 7 – 11 August, Aspen, CO, USA., 618-621.

Rao, C.R.N., and Chen, J.: 1996, 'Post-Launch Calibration of the Visible and Near-Infrared Channels of the Advanced Very High Resolution Radiometer on the NOAA-14 Spacecraft', *Int. J. Rem. Sens.* **17**, 2743-2747.

Roerink, G.J., Su, Z. and Menenti, M.: 2000, 'S-SEBI: A Simple Remote Sensing Algorithm to Estimate the Surface Energy Balance', *Phys. Chem. Earth* **25**, 147-157.

Rosema, R., Verhees, L., Van Putten, E., Gielen, H., Lack, T., Wood, Lane, A., Fannon, J., Estrela, T., Dimas, M., De Bruin, H., Moene, A. and Meijninger, W., *European Energy and Water Balance Monitoring System (EWBMS) project*, Publication of the European Community, ENV4-CT97-0478, 147pp, 2001.

Schmid, H.P.: 1994, 'Source Areas for Scalars and Scalar Fluxes', *Boundary-Layer Meteorol.* **67**, 293-318.

Schmid, H.P. and Bünzli, D.: 1995, 'The Influence of Surface Texture on the Effective Roughness Length', *Quart. J. Roy. Meteorol. Soc.* **121**, 1-21.

Schotanus, P., Nieuwstadt, F.T.M. and De Bruin, H.A.R.: 1983, 'Temperature Measurements with a Sonic Anemometer and its Application to Heat and Moisture Fluxes', *Boundary-Layer Meteorol.* **26**, 81-93.

Schuepp, H.P., Leclerc, M.Y., MacPherson, J.I., and Desjardins, R.L.: 1990, 'Footprint Prediction of Scalar Fluxes from Analytical Solutions of the Diffusion Equation', *Boundary-Layer Meteorol.* **50**, 355-373.

Seibert, P., Beyrich, F., Gryning, S-E., Joffre, S., Rasmussen, A-S. And Tercier, P.: 2000, 'Review and Intercomparison of Operational Methods for the Determination of the Mixing Height', *Atmos. Env.* **34**, 1001-1027.

Shuttleworth, W.J.: 1988, 'MacroHydrol. - The New Challenge for Process Hydrol.', *J. Hydrol.* **100**, 31-56.

Shuttleworth, W.J.: 1991, 'Insight from Large-Scale Observational Studies of Land/Atmsophere Interactions', *Surveys in Geophys.* **12**, 3-30.

Strohbehn, J.: 1968, 'Line-of-Sight Wave Propagation Through the Turbulent Atmosphere', *Proceedings of the IEEE* **56**, 1301-1318.

Stull, R.B., 1988, *An Introduction to Boundary Layer Meteorology*, Atmospheric Sciences. Library, Kluwer Academic Publishers, 666 pp.

Tatarskii, V. I.: 1961, *Wave Propagation in a Turbulent Medium*, Translated from Russian by R. S. Silverman, McGraw-Hill, New York, USA, 285 pp.

Tatarskii, V.I.: 1971, *The Effect of the Turbulent Atmosphere on Wave Propagation*, translated from Russian by Israel Program for Scientific Translation, Springfield, Va, USA, 472 pp.

Thiermann, V.: 1992, 'A Displaced Beam Scintillometer for Line-Averaged Measurements of Surface Layer Turbulence', *10th Symposium on Turbulence and Diffusion*, Portland Oregon, September 29 - October 2, 1992, American Meteorological Society, Boston, MA, pp. 244-247

Thiermann, V. and Grassl, H.: 1992, 'The Measurement of Turbulent Surface Layer Fluxes By Use of Bichromatic Scintillation', *Boundary-Layer Meteorol.* **58**, 367-389.

Tillman, J.E.: 1972, 'The indirect Determination of Stability, Heat, and Momentum Fluxes in the Atmospheric Boundary Layer from Simple Scalar Variables During Unstable Conditions', *J. Appl. Meteorol.* **11**, 783-792.

Valiente, J.A., Nunez, M., Lopez-Baeza, E. and Moreno, J.F.: 1995, 'Narrow-Band to Broad-Band Conversion of Meteosat Visible Channel and Broad-Band Albedo Using Both AVHRR-1 and −2 Channels', *Int. J. Rem. Sens.* **16**(6), 1147-1166.

Van Asselt, C.J., Jacobs, A.F.G., Van Bozel, J.H. and Jansen, A.E.: 1991, 'A Rigid Fast-Response Thermometer for Atmospheric Research', *Meas. Sci. Technol.* **2**, 26-31.

Van de Griend, A.A. and Owe, M.: 1993, 'On the Relationship Between Thermal Emissivity and the Normalised Difference Vegetation Index of Natural Surfaces', *Int. J. Rem. Sens.* **14(6)**, 1119-1131.

Van Dijk, A.: 2001, The Principles of Surface Flux Physics, internal report.

Verhoef, A., McNaughton, K.G. and Jacobs, A.F.G.: 1997, 'A Parameterisation of Momentum Roughness Length and Displacement Height for a Wide Range of Canopy Densities', *Hydrol. and Earth System Sci.* **1**, 81-91.

Vermote, E.F., Tanre, D., Deuze, J.L., Herman, M., and Morcrette, J.J.: 1997, 'Second Simulation of the Satellite Signal in the Solar Spectrum, 6S: An Overview', IEEE Trans. *Geosc. and Remote Sens.* **35**(3), 675-686.

Wang, T.I., Ochs, G.R., and Clifford, S.F.: 1978, 'A Saturation-Resistant Optical Scintillometer to Measure C_n^2', *J. Opt. Soc. Am.* **69**, 334-338.

Watts, C.J., Chebouni, A., Rodriguez, J-C., Kerr, Y.H., Hartogensis, O. and De Bruin, H.A.R.: 2000, 'Comparison of Sensible Heat Flux Estimates using AVHRR with Scintillometer Measurements over Semi-Arid Grassland in Northwest Mexico', *Agric. For. Meteorol.* **105**, 81-89.

Webb, E.K., Pearman, G.I. and Leuning, R.: 1980, 'Correction of Flux Measurements for Density Effects due to Heat and Water Vapour Transfer', *Quart. J. Roy. Meteorol. Soc.* **106**, 85-100,

Wesely, M.L.: 1976a, 'The Combined Effect of Temperature and Humidity on the Refractive Index', *J. Appl. Meteorol.* **15**, 43-49.

Wesely, M.L.: 1976b, 'A Comparison of Two Optical Methods for Measuring Line Averages of Thermal Exchange Above Warm Water Surfaces', *J. Appl. Meteorol.* **15**, 1177-1188.

Wieringa, J.: 1976, 'A Objective Exposure Correction Method for Average Wind Speeds Measured at a Sheltered Location', *Quart. J. Roy. Meteorol . Soc.* **102**, 241-253.

Wieringa, J.: 1986, 'Roughness-Dependant Geographical Interpolation of Surface Wind Speed Averages', *Quart. J. Roy. Meteorol. Soc.* **112**, 867-889.

Williams, R.M. and Paulson, C.A.: 1977, 'Microscale Temperature and Velocity Spectra in the Atmospheric Boundary Layer', *J. Fluid. Mech.* **83**, 547-567.

Wood, N. and Mason, P.J.: 1991, 'The Influence of Static Stability on the Effective Roughness Lengths for Momentum and Heat Transfer', *Quart. J. Roy. Meteorol. Soc*. **117**, 1025-1056.

Wyngaard, J.C., Izumi, Y. and Collins Jr., S.A.: 1971, 'Behaviour of the Refractive-Index-Structure Parameter Near the Ground', *J. Opt. Soc. Am.* **61**, 1646-1650.

Wyngaard, J.C. and LeMone, M.A.: 1980, 'Behaviour of the Refractive Index Structure Parameter in the Entraining Convective Boundary Layer', *J. Atmos. Sci.* **37**, 1573-1585.

Samenvatting

Gemotiveerd door de vraag naar betrouwbare gebiedsgemiddelde fluxen van natuurlijke landoppervlakken wordt in dit proefschrift onderzoek gedaan naar een relatief nieuwe meettechniek, die bekend is als de scintillatie methode. Oppervlaktefluxen van homogene gebieden kunnen met redelijke nauwkeurigheid worden geschat. De fluxen van grote natuurlijke landoppervlakken (gelijk aan de roosterpuntsafstand van numerieke modellen of de pixelgrootte van satelliet sensoren) zijn echter veel moeilijker te bepalen aangezien op deze schaal het landoppervlak meestal heterogeen is. Op dit moment zijn er maar een paar technieken die op een schaal van enkele kilometers fluxinformatie kunnen verschaffen, waaronder de scintillatie methode.

Gebaseerd op de voortplantingsstatistiek van elektromagnetische straling die enkele kilometers door de atmosfeer heeft afgelegd over een horizontaal pad, is het mogelijk om de oppervlaktefluxen van voelbare warmte, waterdamp en impuls te bepalen. In dit onderzoek is een grote openingshoek scintillometer (Large Aperture Scintillometer, LAS) ontwikkeld die over afstanden tot 5 km kan worden gebruikt. De LAS werkt in het nabij-infrarode golflengtegebied en is daardoor voornamelijk gevoelig voor temperatuurgerelateerde scintillaties, waaruit vervolgens de voelbare warmteflux kan worden afgeleid. In dit proefschrift zijn de volgende aspecten van de LAS onderzocht:

- De verrichtingen van de LAS over heterogene landoppervlakken (**Hoofsdtuk 2**)
- De betrouwbaarheid van gebiedsgemiddelde fluxen van waterdamp bepaald met de LAS en in combinatie met een radiogolf scintillometer over heterogene oppervlakken (**Hoofdstuk 3**)
- De praktische toepasbaarheid en bruikbaarheid van de LAS in andere wetenschappelijke gebieden (**Hoofdstuk 4** en **5**)

Bij het afleiden van de voelbare warmtestroom uit het LAS signaal wordt gebruik gemaakt van de Monin-Obukhov gelijkvormigheidstheorie (MOST). MOST stelt echter als voorwaarde een homogeen landoppervlak. De vraag doet zich voor of een LAS kan worden gebruikt over afstanden van enkele kilometers, aangezien op deze schaal het landoppervlak

159

meestal heterogeen is. Om experimenteel de toepasbaarheid van de LAS over een heterogeen landoppervlak en de betrouwbaarheid van de afgeleide fluxen van voelbare warmtestroom te onderzoeken, is in Flevoland (Nederland) een veldexperiment uitgevoerd. De resultaten van dit experiment worden gepresenteerd en besproken in **Hoofdstuk 2**. De algemene karakteristieken van het Flevoland gebied zijn als volgt: een uitgestrekt en volledig vlak gebied bedekt met vier gewassen in velden van 500 m × 250 m gerangschikt volgens een schaakbord. Op basis van de horizontale lengteschaal van de velden is het gebied geclassificeerd als een Type A landschap, dat wil zeggen dat alleen het onderste deel van de oppervlaktelaag is verstoord door onregelmatigheden. Voor het onafhankelijk bepalen van gebiedsgemiddelde oppervlaktefluxen zijn eddy covariantie (EC) metingen gedaan. Uit de EC metingen blijkt dat de heterogeniteit in het Flevoland gebied voornamelijk wordt bepaald door ruimtelijke variaties in de thermische eigenschappen. De fluxen van twee scintillometers, geplaatst op respectievelijk 11.6 m en 20.4 m hoogte, vertonen een goede overeenkomst met de gebiedsgemiddelde fluxen, met name de bovenste LAS. De onderste LAS vertoont een kleine onderschatting van ongeveer 7%. Deze onderschatting wordt verklaard met behulp van een menghoogte benadering en een analytisch footprint model voor het schatten van de brongebieden en de daarbij behorende fluxen. Hierbij is de menghoogte gedefinieerd als het niveau boven het oppervlak waarboven de invloed van de individuele velden langzaam afneemt. Met behulp van een heuristisch model is gevonden dat de menghoogte voor het Flevoland gebied varieert tussen de 9 m en 14 m. Op basis van de gevonden menghoogtes is geconcludeerd dat de bovenste LAS altijd boven de menghoogte meette, wat in overeenstemming is met de gevonden LAS resultaten. Voor de onderste LAS is de situatie gecompliceerder omdat de individuele velden de metingen beïnvloeden, wat suggereert dat MOST waarschijnlijk wordt geschonden. Na splitsing van het Flevoland gebied in 8 windsectoren en herverdeling van de gemiddelde fluxen van het totale gebied en van de 8 brongebieden wordt een betere overeenkomst gevonden. Deze resultaten geven te kennen dat een LAS, die net beneden de menghoogte meet, nog betrouwbare gebiedsgemiddelde fluxen kan leveren en dat de schending van MOST minimaal is.

In **Hoofdstuk 3** zijn de verrichtingen van een LAS in combinatie met een radiogolf scintillometer (LAS-RWS) over een heterogeen landoppervlak onderzocht. Alhoewel deze scintillatie techniek, bekend als de twee-golflengte methode, zowel de voelbare warmteflux en waterdampflux levert is de meeste aandacht gericht op de waterdampflux. Daarnaast wordt de waterdampflux van alleen de LAS geëvalueerd. In de laatste optie is de waterdampflux

160

afgeleid als residu van de oppervlakte energiebalans met behulp van een eenvoudig parameterisatie schema (gebaseerd op globale stralingsdata) voor het schatten van de gebiedsgemiddelde energie beschikbaarheid ($R_n - G_s$). De resultaten gepresenteerd in Hoofdstuk 3 zijn ook gebaseerd op de data van het Flevoland experiment. Zoals beschreven in Hoofdstuk 2 is de heterogeniteit van het gebied voornamelijk het gevolg van ruimtelijke variatie in de thermische eigenschappen van de gewassen en dus in de buoyancy productieterm volgens MOST. Voor de analyse van de fluxen is dezelfde menghoogte en footprint benadering gebruikt als in Hoofdstuk 2. Als eerste worden de waterdamp fluxen van de LAS-RWS combinatie onderzocht. Deze fluxen zijn in goede overeenkomst met de gebiedsgemiddelde fluxen gebaseerd op lokale metingen. Mogelijke verklaringen voor de gevonden spreiding zijn: de niet-sluiting van de EC metingen, de niet-lineariteit tussen de structuurparameter data en de afgeleide fluxen, en laag frequente waterdampabsorptiefluctuaties die de RWS beïnvloeden. Tenslotte is de waterdampflux afgeleid van alleen de LAS besproken. De resultaten laten zien dat een LAS alleen ook betrouwbare gebiedsgemiddelde waterdampfluxen kan aanleveren over heterogene landoppervlakken (type A).

In Hoofdstuk 4 en 5 worden de operationele aspecten van de LAS bestudeerd. Hiervoor waren 2 LAS instrumenten en een klein micrometeorologisch station geïnstalleerd in het stroomgebied van de rivier de Gediz nabij Menemen (Turkije) als onderdeel van een internationaal meetexperiment in 1998. Hoofddoel van dit experiment was het vergelijken van actuele verdampingsfluxen van satelliet remote sensing technieken, hydrologische modellen en veldmetingen. In **Hoofdstuk 4** wordt alleen gekeken naar de veldmetingen, dat wil zeggen de variantie methode en in het bijzonder de LAS. Eén LAS was geïnstalleerd over een vallei in het stroomgebied van de Gediz rivier. Voor het afleiden van de voelbare warmtestroom zijn additionele windsnelheid- en temperatuurgegevens van een nabijgelegen meetstation gebruikt. Daarnaast was een klein micrometeorologisch meetstation geplaatst in een geïrrigeerd katoenveld. De fluxen voor deze locatie zijn bepaald uit temperatuurfluctuatie metingen volgens de variantie methode. Als gevolg van technische problemen met een tweede LAS, die in hetzelfde katoenveld was geplaatst, zijn deze metingen niet gebruikt. De tijdreeks van daggemiddelde fluxen voor de vallei laat duidelijk de seizoenstrend van voelbare warmtestroom zien inclusief de irrigatie periodes. Vanuit een operationeel perspectief laat deze tijdreeks zien dat de LAS, die het gehele groeiseizoen operationeel was, een robuust en betrouwbaar instrument is en weinig onderhoud vergt.

Op basis van de resultaten gepresenteerd in Hoofdstuk 4 is in **Hoofdstuk 5** onderzocht of deze LAS data kan worden gebruikt als 'ground-truth' data in andere wetenschappelijke studies zoals remote sensing. Daarvoor zijn een groot aantal oppervlaktefluxkaarten gegenereerd met het SEBAL remote sensing algoritme en vergeleken met de LAS waarnemingen. In deze validatie studie zijn ook de lokale fluxen en stralingsmetingen van het geïrrigeerde katoenveld gebruikt. De SEBAL fluxen zijn afgeleid uit de matige resolutie AVHRR zichtbare en thermisch-infrarode beelden van de NOAA-14 satelliet. Zowel de instantane en daggemiddelde fluxen voor het hele groeiseizoen zijn bepaald. Uit de resultaten blijkt dat de instantane fluxen redelijk overeenkomen met de lokale fluxen van het katoenveld. Voor de vallei wijken de fluxen van SEBAL en de LAS echter nogal af. De volgende verklaringen voor deze afwijking zijn aangevoerd: het niet overeenkomen van het brongebied van de LAS en de ruwe pixel grootte van de ruwe AVHRR beelden; de mogelijke verstoring door de droge hellingen in de relatief nauwe vallei in vergelijking tot de resolutie van de AVHRR sensor. Hierdoor kan geen overtuigende validatie van SEBAL voor de vallei worden gedaan. Tenslotte zijn de daggemiddelde fluxen voor het katoenveld vergeleken. Er blijkt dat alleen tijdens de irrigatieperiode de daggemiddelde resultaten overeenkomen. Een mogelijke reden voor de afwijking is de afwezigheid van niet-droge referentiepixels die tot een onderschatting van de verdampingsfractie leiden.

Curriculum vitae

Ik, Wiro Maria Liduina (zeg maar Wouter) Meijninger, ben geboren op 3 mei 1973 te Rozenburg. Al vrij kort na mijn geboorte verhuisde ik met mijn familie naar het stadje Brielle. Nadat ik de basisopleiding op de St. Leonardus school had doorlopen begon ik met mijn havo opleiding aan de openbare Regionale Scholengemeenschap te Brielle. Vervolgens haalde ik ook mijn VWO diploma om in 1992 te verhuizen naar Utrecht en in Wageningen aan de studie Bodem-Water-Atmosfeer te beginnen. Na 1 jaar forenzen besloot ik naar Wageningen te verhuizen. Hier heb ik 4½ jaar een onvergetelijke tijd meegemaakt met mijn 2 huisvrienden Lammert en Alwin. Mijn eerste afstudeervak (bij de vakgroep Hydrologie) in combinatie met mijn stage deed ik samen met Arina en vond plaats in Slowakije. Nadat we samen een grote meetcampagne hadden gedaan in een maïsveld hebben we gekeken naar de waterbalans met behulp van het hydrologische model SWAP (Soil-Water-Atmosphere-Plant). Mede dankzij deze ervaringen raakte ik geïnteresseerd in de experimentele meteorologie. Nadat ik 3 maanden in Reading (Engeland) nog enkele colleges had gevolgd begon ik aan mijn tweede afstudeervak bij de vakgroep Meteorologie en ditmaal alleen. Ik heb op basis van verschillende eddy correlatie datasets gekeken naar de similariteit tussen temperatuur en vocht en de invloed op verschillende meetmethoden. Nog voordat ik mijn laatste afstudeervak had afgerond vroeg mijn begeleider Henk de Bruin of ik interesse had voor een promotieonderzoek. Nadat ik nog snel wat vakken had afgerond en een meetexperiment had uitgevoerd in Zweden kon ik in maart 1997 afstuderen in de studie Bodem-Water-Afmosfeer met als specialisatie meteorologie. Op 1 april 1997 begon ik als parttime onderzoeker in opleiding (OIO) bij de vakgroep Meteorologie in dienst van NWO (Nederlands Wetenschappelijke Organisatie) aan een door STW gefinancierde promotiestudie. Door het vrij experimentele karakter van dit onderzoek heb ik heel wat locaties op de wereld mogen bezoeken waar 'scintillometer' experimenten werden uitgevoerd. Naast mijn OIO baan was ik bij de vakgroep 1 dag per week in dienst als vakgroepmedewerker. Ik heb onder andere het practicum veldwaarnemingen voor 2^e-jaars meteorologie studenten gegeven. Dankzij de inventieve ideeën van Henk de Bruin ben ik ook nog 6 maanden in dienst geweest van het 'China' project. Dankzij dit project heb ik het geluk gehad om tot 3 maal toe door China te mogen reizen. Vanaf 1 april 2002 ben ik (parttime) bij het bedrijf Kipp & Zonen te Delft gaan werken als scintillometer-specialist. Per 1 augustus 2003 zal ik als postdoc beginnen aan een door NWO gefinancierd scintillometer onderzoek bij de leerstoelgroep Meteorologie en Luchtkwaliteit.